

Hennie Marie Johnsen

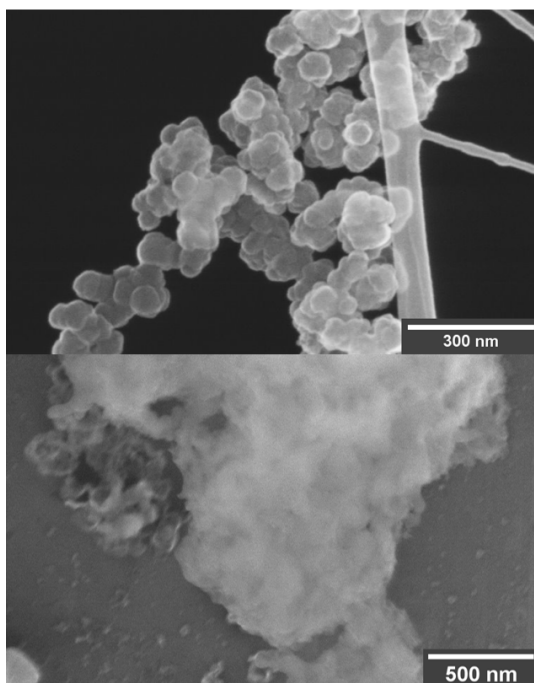
Stability and cell viability studies of silicon nanoparticles for drug delivery applications

Master's thesis in Nanotechnology

Supervisor: Ragnhild Elizabeth Aune

Co-supervisors: Samson Yuxiu Lai (IFE), Alexey Kuposov (IFE)

August 2020



Hennie Marie Johnsen

Stability and cell viability studies of silicon nanoparticles for drug delivery applications

Master's thesis in Nanotechnology

Supervisor: Ragnhild Elizabeth Aune

Co-supervisors: Samson Yuxiu Lai (IFE), Alexey Kuposov (IFE)

August 2020

Norwegian University of Science and Technology

Faculty of Natural Sciences

Department of Materials Science and Engineering



Norwegian University of
Science and Technology

Abstract

The present study aims to assess the potential of porous and non-porous silicon nanoparticles (Si NPs), created by a novel synthesis route, as drug delivery vehicles in terms of stability and biocompatibility. These kinds of nanomaterials can be combined with active pharmaceutical ingredients (API), which then are referred to as nanomedicine. Nanomedicine allows for controlling the *in vivo* destiny of the drug and has tremendous potential in improving treatment for a wide range of patients.

Developing a nanoparticulate drug carrier of non-toxic material that is self-eliminating and easily modified for essential properties like 1) drug release rate, often associated with carrier material dissolution, 2) spatiotemporal control of drug accumulation to reduce off-target toxic effects, and 3) delivery of poorly soluble API that is protected from degradation. Porous silicon has been shown to possess the desired properties for drug delivery such as inherent biodegradability and biocompatibility. A thorough literature review revealed several material properties of Si NPs affecting its dissolution stability, such as size, porosity, crystallinity and surface treatments. The media of NP immersion was also found to affect stability, with increasing stability seen in more acidic environments.

In the experimental part of the present study the pH-dependent stability of porous and non-porous spherical Si NP with a diameter of 80-100 nm (herein referred to as the IFE Si NPs), created by a novel synthesis route by researchers at the Institute for Energy Technology (IFE) is studied. Increasing environmental pH is found to decrease the stability of both particle types observed as increasing hydrodynamic diameter measured by dynamic light scattering (DLS), as well as formation of larger structures seen by scanning electron microscopy (SEM). The pristine particles proved to have superior stability compared to the porous particles with a size increase seen as low as pH 8 and 7 for pristine and porous particles, respectively. Increasing particle size can be explained by particle aggregation or silica deposition of dissolved silicon species, and might affect the performance of the drug delivery system by interfering with the the drug release process *in vivo* as well as giving pre-administration solution complications. On the other hand, pH-dependent degradation might be utilized for stimuli-responsive drug release.

In vitro cytotoxicity studies revealed low toxicity of both the porous and non-porous IFE Si NPs to KPC and PC3 cell lines with a minimum of 50% cell viability of up to 1mg/mL NP exposure over 48 hours. Different toxicity profiles of the two particle types were also observed, with the porous particles generally reported as less toxic. The pristine particles showed concentration-dependent toxicity and porous particles showed a time-dependent toxicity response, emphasizing the sensitive structure-toxicity relationships of NPs for which the cellular mechanisms remain a mystery.

Conclusively, the novel synthesis method is shown to produce pristine and porous Si NPs suitable for use in drug delivery systems in terms of stability and *in vitro* biocompatibility. Porous particles show superior properties in terms of fast dissolution, pH-dependent stability and lower toxicity, in addition to the mesoporous structure being ideal for loading of a variety of API.

Sammendrag

Denne studien har som mål å undersøke potensialet til porøse og ikke-porøse silisium nanopartikler (Si NPs), laget ved en ny syntesemetode, som medisinbærere med fokus på stabilitet og biokompatibilitet. Denne typen nanomaterialer kan kombineres med aktive farmasøytiske ingredienser (API), noe som da blir referert til som nanomedisin. Nanomedisin gjør det mulig å kontrollere legemidlers' skjebne i menneskekroppen og har et enormt potensial for å forbedre medikamentbehandling av en rekke pasienter.

Utvikling av en nanopartikulær medisinbærer av et ikke-toksisk materiale som er selv-eliminierende og enkelt kan modifiseres for essensielle egenskaper som 1) frigjøringshastighet av API, ofte assosiert med nedbrytning av bærer materialet, 2) romlig-temporal kontroll av API akkumulering for å redusere bivirkninger utenfor målvevet, og 3) enkel transport av dårlig oppløselig API som også er beskyttet mot nedbrytning. Det er blitt vist at porøst silisium har de ønskede egenskapene for medisinbærere som iboende biologisk nedbrytbarhet og biokompatibilitet. Et litteraturstudie avdekket flere materialegenskaper til Si NPer som påvirker dens oppløsningsstabilitet, for eksempel størrelse, porøsitet, krystallinitet og overflatebehandling. Mediet som NP blandes i for å måle stabilitet ble funnet å ha sterk påvirkning på stabiliteten, med økende stabilitet observert ved lav pH.

I den eksperimentelle delen av denne studien ble den pH-avhengige stabiliteten til porøse og ikke-porøse sfærisk Si NPer med en diameter på 80-100 nm (heretter referert til som IFE Si NPer), laget i en ny syntesevei av forskere ved Institutt for Energiteknikk (IFE), studert. Økende pH i miljøet ble funnet til å redusere stabiliteten til begge partikkeltypene observert ved økende hydrodynamisk diameter målt ved dynamic light scattering (DLS), samt dannelse av større strukturer sett ved scanning electron microscopy (SEM). De ikke-porøse partiklene hadde overlegen stabilitet sammenlignet med de porøse partiklene med en størrelsesøkning sett ved pH så lavt som 8 og 7 for henholdsvis ikke-porøse og porøse partikler. Økende partikkelstørrelse er blitt forklart ved aggregering av partikler eller deponering av silika fra oppløst silisium. Begge disse prosessene kan påvirke ytelsen til systemet ved å forstyrre frigjørelse av medikamentet i tillegg til å gi komplikasjoner for intravenøs administrasjon av medikamentløsningen. På en annen side kan pH-avhengig nedbrytning benyttes til stimuli-responderende medikamentfrigjøring.

In vitro cytotoxicitetsstudier avdekket lav toksisitet av begge typer IFE Si NPer til KPC og PC3 cellelinjer med et minimum på 50% cellelevedyktighet observert ved opp til 1 mg/ml NP eksponering over 48 timer. Ulik toksisitetsrespons ble observert for de to partikkeltypene. De ikke-porøse partiklene viste konsentrasjonsavhengig toksisitet og de porøse partiklene var mindre giftige og viste en tidsavhengig toksisitetsrespons, noe som understreker den sensitive sammenhengen mellom NP struktur og toksisitet.

For å konkludere er den nye syntesemetoden vist å produsere både ikke-porøse og porøse Si NPer som er egnet for bruk som medisinbærere når det gjelder stabilitet og toksisitet. Porøse partikler hadde overlegne egenskaper når det gjaldt rask oppløsning, pH-avhengig stabilitet og lavere toksisitet, i tillegg til at den mesoporøse strukturen er ideell for transport av en rekke ulike typer API.

Preface & Acknowledgements

This Master's thesis is the final assessment of my five years of studying towards a Master of Science in Nanotechnology at NTNU in Trondheim. I have obtained a specialization in bionanotechnology and nanomedicine, with the work of this thesis.

The work has been carried out during the spring semester of 2020, during the time of the COVID-19 pandemic. Laboratory access was restricted over a longer period and there was uncertainty whether experimental work would be possible to continue at all. Therefore, the project plans were changed a few times and a detailed literature review was conducted during this period. Hopefully, it has not affected the flow of this work.

The work is done at the Institute for Energy Technology (IFE) at Kjeller, where I have been part of the Solar Energy department. All the work has been carried out independently by the author during the spring/summer of 2020, except for particle synthesis and etching and TEM/EDS analysis which has been conducted by researchers at IFE. The project is done on behalf of Nacamed AS, a pharmaceutical company aiming to commercialize porous silicon nanoparticles for medical usage. It was funded by the Oslofjordfondet Regional Research Fund of the Research Council of Norway.

First and foremost, I have to thank the inspiring people in Nacamed, Christina Westerveld Haug and Kjersti Bull Noulund, for letting me work on such an exciting topic and contribute to developing nano drug carrier technology. I am truly inspired by your aspirations in going into the field of nanomedicine with a commercial perspective. Thank you for giving me the opportunity to work as a summer researcher in 2019, which has led to this Master's thesis.

I also have to give my thanks to the competent researchers at IFE. My closest supervisor, Samson Yuxiu Lai, has been of invaluable support, helping with everything from instrument training and understanding of concepts to thesis writing. Co-supervisor Alexey Y. Koposov has contributed with valuable support and insightful discussions. My main supervisor from the Department of Materials Science and Engineering at NTNU, Ragnhild Elizabeth Aune, has been of significant guidance, even from afar. It has been truly inspiring to see you all venturing into a new cross-disciplinary field and learning alongside me. Kristin Grendstad at the Institute of Physics at NTNU provided me with access and the necessary training to do cell studies, and I am grateful for all the help in the cell lab.

Thanks to my family for keeping my hopes up through these uncertain times and always supporting me and my (not always realistic) dreams, and to all the friends I have made in Timini, at NTNUldans and at the revue stage. Finally, a huge thank you to the amazing people of Kull15 that have been a major source of motivation throughout these five years. We have shared so many joyful moments, celebrations and adventurous journeys, as well as stressful exam periods. I believe I have made friends for life.

Hennie Marie Johnsen
MSc/Siv.ing

List of Figures

2.1	Properties of DDS [20]. Copyright 2017, <i>Physiological Reviews</i>	9
2.2	Extra- and intracellular barriers for DDS [20]. Copyright 2017, <i>Physiological Reviews</i>	11
2.3	Drug release from pSi NPs by diffusion out of pores or carrier degradation.	13
2.4	Silicon particle growth in a FSR reactor.	15
2.5	Electrochemical anodization for pSi NP synthesis.	16
2.6	ReEtching chemistry.	17
2.7	Overview of Si surface modifications.	20
2.8	Illustration of cumulative fit of the autocorrelation function measured by DLS.	22
2.9	Illustration of mechanisms giving rise to fluorescence and the Stokes shift.	25
3.1	Two step dissolution of Si.	31
3.2	Si particle dissolution, dependence on porosity from article [76]. Copyright 2013, <i>Biomaterials</i>	33
3.3	Crystallinity dependence on Si dissolution [83]. Copyright 2011, <i>Silicon</i> .	34
3.4	Oxidation dependence on dissolution of Si. Data from several articles [14, 43, 79, 80, 84]	35
3.5	SEM images of oxidized pSi particles during degradation [43]. Copyright 2012, <i>Advanced Functional Materials</i>	36
3.6	Si dissolution dependence on surface PEGylation [14, 75, 77].	36
3.7	Si dissolution dependence on various surface modifications and particle sizes. Summarizing data from several articles [8, 11, 14, 43, 75, 77, 79–82, 84, 85].	38
3.8	Dissolution kinetics of pSi wafers, dependence on pH [13]. Copyright 2003, <i>Physica Status Solidi</i>	39

4.1	Schematic illustration of the synthesis of Si NPs and the etching process creating pSi NPs.	44
4.2	DLS calibration measurements of various Si NP concentrations.	46
4.3	Working principles of the AlamarBlue reagent.	49
5.1	SEM images of pristine IFE Si NPs.	53
5.2	SEM images of etched IFE Si NPs.	54
5.3	TEM micrograph of IFE pSi NPs.	55
5.4	DLS intensity size distribution of pristine and porous IFE Si NPs.	55
5.5	XRD pattern of pristine IFE Si NPs.	57
5.6	EDS mapping of IFE pSi NPs.	57
5.7	Images of pristine IFE Si NPs in aqueous buffer solutions of pH 7 and 10.	59
5.8	DLS measurements of stability test of pristine IFE Si NPs in acidic buffer solutions.	60
5.9	DLS measurements of stability test of pristine IFE Si NPs in alkaline buffer solutions.	61
5.10	DLS stability measurements of pristine IFE Si NPs over pH 4-10 after 8 hours.	62
5.11	DLS measurements of stability test of porous IFE Si NPs in acidic buffer solutions.	63
5.12	DLS measurements of stability test of porous IFE Si NPs in alkaline buffer solutions.	64
5.13	DLS stability measurements of IFE pSi NPs over pH 4-10 after 8 hours.	65
5.14	Z-average values of pristine and porous IFE Si NPs over time and pH range 4-10.	66
5.15	Z-average of porous IFE Si NPs in the pH range 4-10 with linear regression.	67
5.16	PDI values of pristine and porous IFE Si NPs over time and pH range 4-10.	68
5.17	SEM micrographs of pristine IFE Si NPs immersed in acidic and neutral solution for 8 hours and control.	69
5.18	SEM micrographs of pristine IFE Si NPs immersed in alkaline solutions for 8 hours.	70
5.19	SEM micrographs of IFE pSi NPs immersed in acidic solutions for 8 hours.	71
5.20	SEM micrographs of porous IFE Si NPs immersed in alkaline solutions for 8 hours.	72
5.21	Colloid processes taking place in Si NP solutions.	75
5.22	Cell viability of autoclaved IFE Si NPs	79
5.23	Microscopy control images of KPC and PC3 cells.	81
5.24	Microscopy images of KPC cells exposed to autoclaved IFE Si NPs.	82
5.25	Microscopy images of PC3 cells exposed to autoclaved IFE Si NPs.	83
5.26	Optical microscopy images of KPC and PC3 cells exposed to ethanol washed IFE Si NPs.	85
5.27	Filtration attempts of pristine and porous IFE Si NPs.	86
5.28	Assay interference between IFE Si NPs and cytotoxicity assay with and without addition of AlamaBlue assay components.	87

List of Tables

3.1	Dissolution kinetics parameters for untreated porous silicon particles of different sizes [8, 79–82].	32
3.2	Dissolution kinetics of pSi microparticles in pH 6 and 9 [81].	40
4.1	Acidic buffer solutions composition.	47
4.2	Alkaline buffer solutions composition.	48
5.1	Z-average and PDI from DLS measurements of the different IFE Si NP samples.	56
5.2	Comparison of DLS and SEM for stability studies.	78

List of Abbreviations

Abbreviations & Terms

IFE	Institute for Energy Technology
API	Active Pharmaceutical Ingredient
DDS	Drug Delivery System
Si NP	Silicon Nanoparticle
pSi	Porous silicon
FSR	Free Space Reactor
ReEtching	Regenerative Electroless etching
PDI	Polydispersity Index
%CV	%Cell Viability

Characterization methods

SEM	Scanning Electron Microscopy
DLS	Dynamic Light Scattering
EDS	Energy-Dispersive X-ray Spectroscopy
XRD	X-ray Diffraction
TEM	Transmission Electron Microscopy
MBA	Molybdenum Blue Assay
ICP	Inductively Coupled Plasma (spectroscopy)

Chemical compounds and abbreviations

Si	Silicon
SiO ₂	Silica/Silicon dioxide
PEG	Polyethylene Glycol
SiH ₄	Monosilane
HF	Hydrofluoric acid
V ₂ O ₅	Vanadium Pentoxide
H ₂ O ₂	Hydrogen Peroxide
TOPSi	Thermally Oxidized Porous Silicon
TCpSi	Thermally Carbonized Porous Silicon
THCpSi	Thermally Hydrocarbonized Porous Silicon
CO ₂	Carbon dioxide
PBS	Phosphate Buffered Saline
C ₆ H ₈ O ₇	Citric Acid
Na ₃ C ₆ H ₅ O ₇	Sodium Citrate
NH ₄ Cl	Ammonium Chloride
NH ₃	Ammonia

Table of Contents

1	Introduction	1
1.1	Thesis aims	3
2	Theoretical Background	5
2.1	Nanomedicine	5
2.2	Drug delivery systems	7
2.2.1	Opportunities using drug delivery systems	8
2.2.2	Design of drug delivery systems to accommodate physiological barriers	9
2.3	Silicon as biomedical material	11
2.4	Synthesis of porous silicon nanoparticles	14
2.4.1	Silicon nanoparticle synthesis	14
2.4.2	Porosification of silicon	16
2.5	Surface chemistry of silicon	18
2.6	Colloid science	20
2.7	Dynamic light scatterig for particle size measurements	21
2.8	Cell viability studies of nanoparticles	23
3	Silicon Nanoparticle Stability	27
3.1	Methodology of stability studies	28
3.2	Stability dependence on particle properties	30
3.2.1	Particle size	31
3.2.2	Porosity/pore size	32
3.2.3	Crystallinity	34
3.3	Stability dependence on surface modifications	34
3.3.1	Oxidation	35
3.3.2	Polyethylene glycol (PEGylation)	36

3.3.3	Other surface modifications and a comparison between the techniques	37
3.4	Stability dependence on medium pH	39
3.4.1	Mechanism and other applications for pH-dependent Si dissolution	40
3.5	Key findings on silicon stability in literature	41
4	Materials and Experimental Methods	43
4.1	Materials	43
4.2	Synthesis and etching of silicon nanoparticles	43
4.3	Particle characterization	44
4.3.1	Scanning Electron Microscopy	45
4.3.2	Dynamic Light Scattering	45
4.3.3	X-ray Diffraction	46
4.3.4	Energy Dispersive X-ray spectroscopy	47
4.4	Particle stability studies	47
4.4.1	Preparation of buffer solutions	47
4.4.2	Sampling over time and pH range	48
4.5	<i>In vitro</i> cytotoxicity studies	48
4.5.1	Nanoparticle sterilization techniques	49
4.5.2	AlamarBlue assay and optical microscopy imaging methodology	50
5	Experimental Results and Discussion	53
5.1	Particle characterizations	53
5.1.1	Scanning Electron Microscopy	53
5.1.2	Dynamic Light Scattering	55
5.1.3	X-ray Diffraction	56
5.1.4	Energy Dispersive X-ray spectroscopy	57
5.1.5	Stability predictions based on particle characterization data	58
5.2	Particle stability studies	59
5.2.1	Dynamic Light Scattering	60
5.2.2	Scanning Electron Microscopy	69
5.2.3	Possible explanations for stability study observations	73
5.2.4	Implications of stability observations in biomedical applications	76
5.2.5	Comparison of DLS and SEM for stability studies	77
5.3	<i>In vitro</i> cytotoxicity studies	79
5.3.1	AlamarBlue assay	79
5.3.2	Bright field microscopy images	81
5.3.3	Impact of particle sterilization process	84
5.3.4	Nanoparticle - viability assay interference	87
6	Summary and Conclusion	89
7	Further Work	91
	References	93

Appendix	I
A Si NP stability & drug interactions	I
B Supplementary DLS material	III
C AlamarBlue assay results for ethanol washed Si NPs	VI

CHAPTER 1

Introduction

The field of nanomedicine has recently gained attention for the use of inorganic materials such as silicon that display beneficial properties for use in biomedical applications. Development of a highly versatile novel drug carrier platform for *in vivo* transport of a variety of active pharmaceutical ingredients (APIs) can revolutionize the use of drug carriers, improving drug treatment and thereby human health [1]. Advanced formulation strategies, including the use of nanoformulations, is in increasing demand for meeting requirements of therapeutic performance of novel APIs.

Nano- medicine involves the use of materials small enough to pass through the entire circulatory system. Encapsulating APIs in nanomaterials has several major benefits based on its ability to alter the physicochemical properties of the carrier, tuning biological interactions and the *in vivo* handling of the drug, without directly altering the API structure and thereby retaining its therapeutic response. The design of nanomaterial carriers allows for the creation of “*smart*” drug delivery systems (DDS) with several major benefits such as increasing solubilization of drugs, protecting APIs from degradation for increasing circulation time, controlling and sustaining drug release, co-encapsulating multiple drugs in synergistic ratios or with diagnostic agents and reducing off-target toxic effects by exploiting passive targeting and enhanced accumulation due to leaky blood vessels often found in tumor tissue [2].

One major obstacle of conventional systemic drug formulations is side effects caused by the vast majority of the administered drug not reaching its target tissue. The use of drug carrier technology has traditionally been focused on reducing the hideous side effects of chemotherapeutic drugs in cancer therapy. However, nanomedicine has recently shown great potential in increasing therapeutic responses in a vast range of diseases and conditions [3, 4]. Active targeting, as used in *e.g.* drug-antibody conjugates, has shown to improve localized tissue and cell penetration, increasing medical response by sustaining the concentration of API in the therapeutic range over time and reducing side-effects

[5]. Along with the above-mentioned benefits and the large surface area of nanoparticles available for a variety of targeting ligands, as well as other surface functionalities, nanomedicine has been said to display endless opportunities in drug delivery.

Since the discovery of the electrochemical pathway for silicon porosification [6], and the discovery the biocompatibility of porous silicon materials [7], several technological solutions utilizing porous silicon nanoparticles (pSi NPs) as DDS has been developed in research scale [8–13]. Loading of drugs by physical adsorption or via chemical bonds, either inside the porous structure, on the particle surface, or in association with polymers attached to the surface has been explored, proving great versatility for drug, protein and peptide delivery in addition to the high drug payload reported for pSi NPs. Furthermore, nanoporous silicon has self-eliminating *in vivo* properties as it dissolves into the orthosilicic acid in aqueous environments [14]. The inherent biodegradability, along with non-toxicity of the material and its degradation by-products, has raised increasing attention to biomedical applications of the material [8]. Additionally, hydrogen-terminated or native oxidized silicon surfaces are readily grafted by a variety of methods for passivation and bio-interactive purposes.

Challenges associated with scalability and low reproducibility of the traditional synthesis route of pSi NPs, an electrochemical porosification processes, has been a major obstacle for clinical translation of this material as a drug carrier [1]. A recently developed particle synthesis route using a novel reactor technology providing Si NPs of narrow size distribution, with tunable size and geometry, has been developed at the Institute for Energy Technology (IFE) in Norway [15]. Furthermore, a recently developed catalytic porosification process reported in literature [16] is about to be adapted to the IFE particles. This is believed to be a process available for up scaling that is more effective than conventional processes a well as providing more parameters for optimization control.

Commercialization requirements for use of drug carriers in the pharmaceutical industry includes comprehensive characterization of various properties, and are yet to be established for the IFE particles. The design of novel drug carriers for applications in various pharmaceutical products require not only a fundamental understanding of how biodegradation and stability phenomena are affected by NP properties but also of cellular and tissue responses which determine the biocompatibility of the constructs.

Stability can be defined as "*the strength to stand or endure*" and "*resistance to chemical change or to physical disintegration*" [17]. The retention of NP properties, both in terms of dissolution and aggregation, highly depends on the colloid dispersed phase in which the particles are immersed. A pH value of 7.4 is considered "normal" in most tissues in the body as well as in the blood. However, pH is one medium property that varies *in vivo* in different compartments from highly acidic *e.g.* in the stomach and in intracellular endosomal compartments, to slightly acidic in some inflamed tissues, to alkaline, in the intestines [18, 19]. It is a well-known fact that drug release rates, especially for API covalently bound to the carrier, is closely associated with carrier dissolution rate. pH can be a trigger for localized drug release in the case of pH-dependent carrier dissolution, however, the extent of this effect in the IFE particles is useful information for the design of NPs with the desired stability properties. Understanding the mechanism at which instability of Si NPs arise in different pH environment is a crucial step in gaining comprehensive insights in how to control its stability.

In vitro cell viability assays are today the preliminary toxicity studies determining cytotoxicity of NPs to specific cell lines or tissues. These studies are necessary pre-clinical steps for verifying biocompatibility of materials for pharmaceutical purposes as well as for assessing the structure-toxicity relationships of NPs.

1.1 Thesis aims

The overall aim of the present thesis has been to assess the drug carrier potential of the IFE particles (simply referred to as particles hereafter), both porous and non-porous, by characterizing them with an emphasis on the pH-dependent stability and induced *in vitro* cytotoxicity. The following summarizes the different experimental and analytical activities of the project that will be discussed:

- Characterization of the particles using scanning electron microscopy (SEM), dynamic light scattering (DLS), energy dispersive x-ray spectroscopy (EDS), transmission electron microscopy (TEM) and x-ray diffraction (XRD).
- Assessing how stability studies of solid, nanoparticulate and mesoporous silicon is performed in existing literature, including identification of essential Si NP and medium properties affecting dissolution stability.
- Developing a procedure for assessing pH-dependent stability for NPs for biomedical applications, and conduct stability studies of pristine and porous Si NPs.
- Conducting *in vitro* cell viability studies for determining particles toxicity and structure-toxicity relationships.

Theoretical Background

The present chapter introduces the field of nanomedicine and explains the potential in using silicon nanotechnology for biomedical applications, as well as presenting techniques and terms used in the work of this thesis.

2.1 Nanomedicine

Nanotechnology has been said to extend the scope of what is possible with technological interventions in electronics, materials and medicine [4]. The field of nanomedicine explores how nanotechnology can be of use in medicine and medical technology, and provides new approaches for improving healthcare. Overall, nanoscale materials are usually defined by having at least one dimension in the scale of 1-100 nm. Such materials have shown beneficial properties for a wide range of biomedical applications. The use of nanotechnology in biomedical research allows for near-atomic manipulation of materials giving the possibility to tailor its properties for various *in vivo* and *ex vivo* applications. Tuning properties like size, shape, charge and surface functionality of nanomaterials give endless opportunities. As a result, nanomedicine has been assigned tremendous potential with yet unknown future aspirations that can significantly impact human health by improving diagnosis, prevention and treatment of diseases [20, 21].

In addition to the introduction given above, literature presents plentiful definitions of nanomedicine, ranging from nanobiotechnology dealing with structure and function of cells and intra- and intercellular processes, to nanorobots, nanosurgery and nanoparticulate materials used as carriers for pharmaceuticals. The diversity of the field indicates the wide scope of applications for nanomedicine. Nanomedicine is said to contribute to three main areas: drug delivery, diagnosis and regenerative medicine, which are summarized below [4].

- The term nanopharmaceutical is used for any active pharmaceutical ingredient (API) that is combined with nanomaterials for therapeutic purposes, often referred to as a drug delivery system (DDS). Biocompatible nanomaterials like polymers, liposomes, micelles or specific inorganic materials can be used as nanocapsules for transporting a variety of APIs like molecular drugs, vaccines and gene therapies. DDS intend to enhance therapeutic efficiency of the API by altering *in vivo* properties like solubility, stability and toxicity by exploiting chemical, physical and biological engineering of nanomaterials. The surface of such carriers can be equipped with targeting ligands for specific biorecognition and localized delivery to the target tissue with minimal side effects. Furthermore, coencapsulation of APIs in one carrier or combination with diagnostic properties, what is referred to as theranostics, could significantly improve the quality of life of patients. In the early age of nanomedicine localized cancer treatment was the major area of interest. However, there has been a rising interest in nanomedicine-based therapies for drug targeting to non-cancer conditions in the recent years [21]. Drug delivery systems are discussed in further detail in section 2.2.
- Early detection of disease is often said to be the number one measure for improving treatment outcomes. Nanomedicine intend to develop inexpensive, rapid and minimally invasive tests for genetic predispositions and early detection of pathological changes at the molecular level. Nanomaterials like fullerenes and carbon nanotubes increase the performance of contrast media in diagnostic. Quantum dots, small semiconductor crystals ($\sim 2\text{-}50$ nm), can luminesce one thousand times brighter than conventional contrast media [22]. Nanoimaging using quantum dots can therefore precisely determine the presence, size and position of tumors in real-time. Additionally, lab-on-a-chip devices would allow precise and personalized multi-diagnostics from the smallest amount of sample [4].
- Nanomedicine and nanobiotechnology also opens up new possibilities in the field of regenerative medicine. The aid of nanomaterials in tissue engineering could stimulate controlled cell growth and artificially produce or regenerate damaged or absent tissue. Nanoporous materials are already in use in wound healing as a scaffold for cell growth and could potentially be used for *in vitro* growth of entire organs meeting quality requirements for transplant [23]. If targeted growth of nerve cells were to be successful, new possible treatments of incurable neurological diseases like Alzheimer's, Parkinson's and epilepsy could be developed by exploring the wide applicability of nanomaterials.

With these advancements, nanomedicine will have the capability to early detect, specifically diagnose and tailor-make treatments to improve healing prospects in accordance with recent developments in personalized medicine, as well as having the potential to significantly reduce treatment and after-care costs. Other nanotechnological interventions also contribute in creating precise research models such as organ-on-a-chip technology [3, 4]. A number of obstacles, however, contribute to difficulties in clinical translation of nanomedicines, irrespective of whether they are therapeutically beneficial or not. The main challenge with nanomedicine is based on the fact that it is a recently developed field and a lot of research is required for realizing the potential in commercialization and clinical

usage. There is also a lack of consistency in quality testing. Long-term toxicology studies are required with low inter-person and inter-laboratory variations to assess the toxic effects of nanomaterials towards the human body and the environment. Establishing a standard terminology with consistent definitions would contribute in facilitating standardized determination of nanoscale toxicity and aid in clinical translation of nanoscale materials for pharmaceutical applications [24]. Ethical and social questions should also be raised on whether everyone will benefit from nanomedicine. Overcoming these challenges and realizing the possibilities in nanomedicine has the potential to revolutionize medicine and human healthcare in the history of medical technology.

2.2 Drug delivery systems

Emphasized as a major category of nanomedicine, DDS has been subject to a huge amount of research to improve drugs' physicochemical and pharmacokinetic properties upon administration. DDS are micro- and nanosized vehicle materials used for encapsulation, transportation and delivery of therapeutic and/or imaging compounds. Nanosized carriers are ideal for DDS as their size allows for free circulation, deep tissue penetration and uptake by single cells. They are smaller than human cells, but similar in size to large biomolecules and can therefore interact with enzymes and receptors [25]. The *in vivo* circulation time of conventional drugs is typically limited to by renal filtration and elimination through the urine due to their small size (<5.5 nm), which is also true for very small nanoparticles. Particles larger than 200 nm, on the other hand, are more rapidly sequestered by phagocytotic cells of the spleen. The ideal size range for drug delivery purposes is therefore 10-200 nm [26]. These nanoformulations increase the drug circulation time that enables increased interaction with tissue, in turn allowing for increased biorecognition and increased biochemical or physiological effect [3]. Furthermore, the small dimensions of nanomaterials provide an extremely high surface area to mass ratio. The high surface area available allows for a high degree of surface functionalization accessible for tailoring the interactions with tissue.

Little emphasis is given to other aspects than biological response in conventional drug discovery. Bioavailability and biocompatibility is not always considered. Therefore, there are a large number of drugs with proven therapeutic efficiency that are incompatible with biological tissue. Hydrophobic drugs, for instance, may have low efficiency simply due to the low solubility in the aqueous *in vivo* environment. Carrier materials can be used to alter physicochemical properties like stability, solubility and rate of drug release. It also enables control of pharmacokinetic properties like bioavailability increasing cellular uptake of drug, distribution by enabling localized drug release using passive or active targeting and triggered release, and elimination by increasing circulation times compared to naked drugs due to size. In other words, the aim of the drug carrier is to enable control over the drug interactions with healthy and diseased tissue without changing the biological action of the API directly.

2.2.1 Opportunities using drug delivery systems

A 100-year-old concept of the “magic bullet” is one of the main reasons nanomedicine has attracted attention. The “magic bullet” contains active substance and targets diseased tissue to localized release of drugs for specific killing of pathogens or malignant cells. This is a particularly desirable idea because less than 1% of the administered dose of systemic naked drugs normally reach the diseased tissue [27]. With the development of nanocarrier DDS the “magic bullet” realization looks to be possible for the first time. The nanocarriers can be equipped with surface molecules that recognize and bind the desired cell type or pathogen, and subsequently release the active substance to the target without the surrounding tissue being affected. Different targeting ligands like antibodies, proteins, peptides, carbohydrates and other polymers can be used to target extracellular receptors specific for or over-expressed by the diseased cells. This is called active targeting. Using nanocarriers that are not filtered out of the blood, the increased circulation time will allow for increased chance of reaching its target. Three areas that could benefit from active targeting of drugs comprise 1) the use of tumor-homing peptides for cancer treatment, 2) targeting infectious sites to increase antibiotics efficiency and reduce development of resistance, and 3) in using ligands to recognize and bind to immune cells for specific delivery of vaccines with reduced side-effects. These mechanisms are of interest above all during cancer treatment as a controlled release of chemotherapy drugs exclusively into the tumor tissue may heavily reduce the hideous side effects when it is exclusively administered. Cancer treatment based on targeted transport can, moreover, take advantage of the poor vasculature in tumors. Aggressive angiogenesis creates leaky gaps in the endothelial vessel wall. Together with the reduced lymphatic drainage observed in tumor tissue is this phenomenon called the enhanced permeability and retention (EPR) effect. It may be utilized for nanomedicine therapeutics by controlling the carrier size as entities of size <200 nm can passively extravasate through the leaky tumor vessels and stay deposited there due to reduced drainage, promoting localized delivery of chemotherapy drugs. The discovery of the EPR effect resulted in huge promises for nanomedicine in cancer treatment, but the heterogeneity of the effect between cancer types and patient responses have given lower amounts of clinical results than initially anticipated [2, 4].

Additional possibilities that has been explored for nanomedicine include stimuli-responsive release either upon environmental changes internally or externally applied stimuli. For instance, incorporating biologically active polymers or environmental-sensitive moieties, either in the carrier body or as a surface modification, can create stimuli-responsive carrier systems. This includes DDS that are sensitive to internal environmental body changes, such as rising temperature upon infection, reduced pH in tumor tissue or the presence of specific enzymes and proteins in diseased or damaged tissue. When stimuli-responsive DDS encounter these changes will a conformational or chemical change take place allowing localized release of the loaded drugs. Nanocarriers can also be designed to incorporate drugs in a light- or mechanically dependent manner. Externally applied stimuli like ultrasound, light or heat is then applied to activate release of drugs with precision determined by the externally applied stimuli [28].

Controlling the time of drug release can be equally important as controlling the location. Spatiotemporal control is enabled by DDS properties and the mechanism by which a drug is attached to its carrier. Drugs adsorbed onto the surface of a carrier will be quickly

released when entering the body, what we call burst release, while a drug incorporated into the carrier material, encapsulated or covalently bound to the carrier will be released in a slower manner. Some drugs are released as the carrier is degrading, giving a sustained mechanism of release. Controlling release properties could allow for a more natural effect over extended periods, reducing number of doses by increasing amount of active compound per dose and overall increasing patient wellness [3]. Incorporation of targeting and stimuli-responsive moieties and spatiotemporal control can be realized by studying surface chemistry modifications, as well as how these affect other properties like DDS stability and solubility. The possibilities in DDS carrier design and surface modifications are summarized in Figure 2.2.

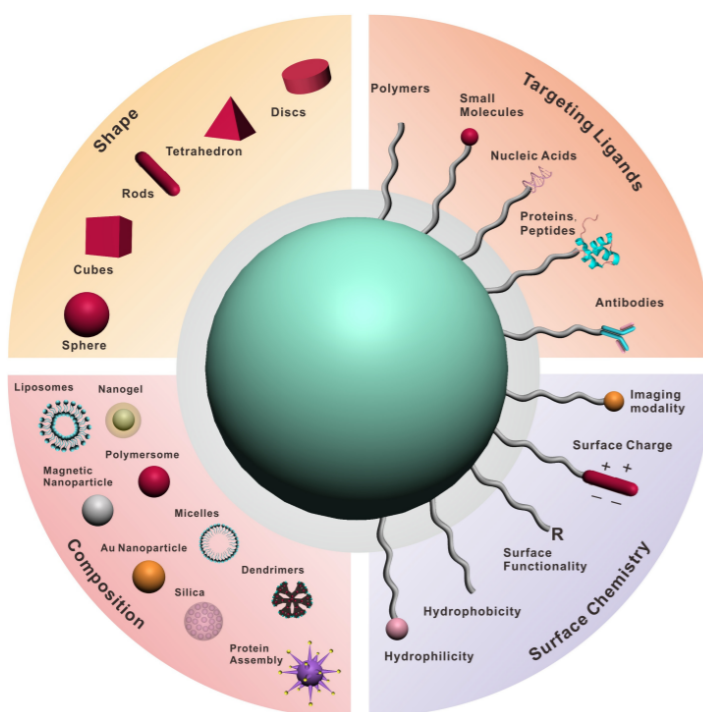


Figure 2.1: Schematic figure illustrating the tunable properties of nanocarrier DDS. Illustration originally appears in [20].

2.2.2 Design of drug delivery systems to accommodate physiological barriers

Several design considerations of drug delivery NPs are critical for accommodating biophysical barriers and for clinical success. In addition to the extraordinary possibilities depicted above, another great advantage of using DDS is, in fact, the possibility to be designed to overcome physiological barriers faced by all drugs formulations. This includes extracellular barriers, before the drug reaches the target cell, and intracellular barriers, which are

encountered as the cell takes up the drug. Both pharmacokinetic and -dynamic properties of drugs controlling *in vivo* absorption, distribution, metabolism and elimination, and how physiological response is related to dose, can be tailored by utilizing DDS with highly tunable properties. Simple control of carrier geometry, size, surface charge and surface chemistry allows for increased drug efficiency in terms of accommodating physiological barriers and improving pharmacological properties.

The main extracellular barrier for circulating drugs is elimination by the immune system. Circulating DDS will rapidly attract a corona of numerous types of proteins adsorbed on the surface, making the particle susceptible for uptake by circulating immune cells. The adsorbed protein corona also prevents eventual targeting ligands from interacting with their target receptors. Significant quantities of systemically administered nanomaterials are cleared by the mononuclear phagocytic system before finding their targets, increasing the likelihood of unintended acute or chronic toxicity. Nanoparticle composition should also be chosen wisely and the possibility to engineer self-destructive non-toxic nanomaterials is studied for giving systemically eliminated products to reduce immunological short and long term effects [8]. Other strategies to decrease immune clearance and increase circulation times include tuning properties that beneficially alter the protein corona composition such as particle size and shape, surface charge, hydrophobicity and biological functionalities [20]. Other extracellular barriers include interactions with blood and endothelial cells in blood vessels, as well as the extracellular matrix (ECM) that surrounds cells. Particularly in tumors is the microenvironment composition distinct from normal ECM which creates opportunities for incorporating mechanisms for triggered release in DDS. The fluid dynamics of the DDS in blood is also significantly affected by their size and geometry [2].

A few portion of drugs exert their biological function on specific cell surface receptors and have reached their target after overcoming the extracellular barriers. However, most drugs need to overcome additional subcellular barriers in order to meet the intracellular target and exert their biological effect. It is a consideration in DDS design, whether the carrier releases the drug prior to internalization or the carrier works as a promoter for internalization of the drug prior to release. For the latter case, carriers can be designed for internalization across the lipid bilayer plasma membrane of cells. Several endocytosis pathways exist and optimizing DDS properties, particularly particle size and geometrical properties, but also surface charge and surface modifications with targeting ligands can promote selective internalization. Contrary to the effects of a negatively charged surface for beneficial protein corona creation are positively charged carriers favorable for endocytosis as they show stronger interaction with negatively charged phospholipids in plasma membranes. Following endocytosis are carriers generally encapsulated inside endosomes (intracellular vesicles) for enzymatic and acidic degradation. This entrapment poses the most critical barrier for intracellular drug delivery and in order to successfully deliver the drug, it must escape. Various carrier materials are proposed for allowing vesicle escape, such as the proton-sponge effect, nanoparticle membrane fusion and photochemical distribution [20].

Design of DDS allows for accommodating endocytosis and endosome elimination, in addition to other intracellular barriers such as cellular resistance mechanisms like drug efflux proteins and the nuclear membrane, for the vast amount of drugs reaching intranu-

clear targets. All these extra- and intracellular barriers pose a complex conundrum for obtaining successful drug carrier design. Besides, as emphasized along the way, controllable drug carrier properties can be tailored to overcome or bypass all of these mechanisms. The *in vivo* fate of DDS is dependent on several properties of the carrier such as shape, geometry, surface properties and stability properties when faced by distinct environmental factors. Spatiotemporal control of degradation of DDS, either for drug release or for meeting physiological barriers, is an extremely valuable property for which nanocarrier composition has to be carefully selected. The majority of nanomedicines generated are based on biomaterials such as liposomes, albumin, polymeric micelles and nanosized polymer-drug conjugates. Such nanomedicines are desired for their biocompatibility and several different variants of these are today approved for clinical use by the FDA [3]. Furthermore, inorganic materials have also shown to be promising materials for biomedical applications, allowing for more precise control and providing intrinsic properties like photoluminescence or magnetic properties for enhanced diagnosis. Drug carriers based on dendrimers, gold, silica, iron oxide, fullerenes and carbon nanotubes are under clinical investigations [3]. One material that has recently gained attention for its highly suitable biodegradation and luminescence properties, which also has the advantage of high accessibility and is therefore widely being used in industrial processes, is mesoporous silicon with a pore size ranging from 2-50 nm (IUPAC classification of pore size) [25].

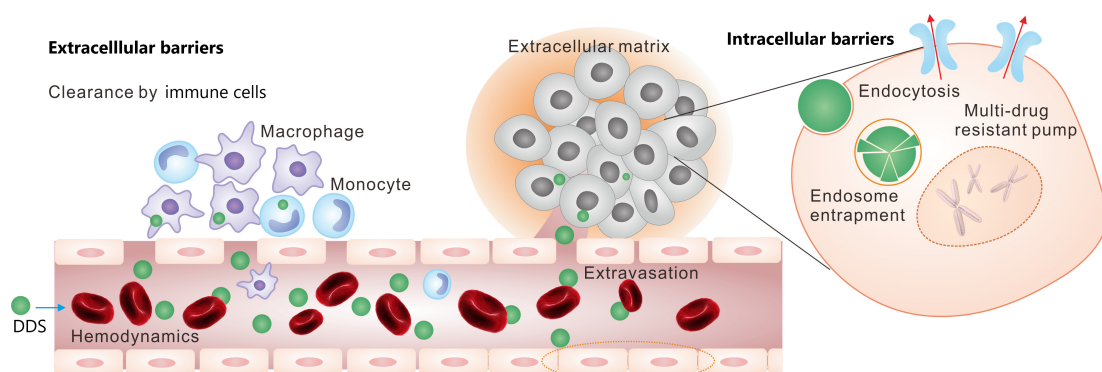


Figure 2.2: Schematic illustration of the extra- and intracellular barriers faced by drug delivery systems (DDS, shown in green) before they reach their target site. Figure adapted from [20].

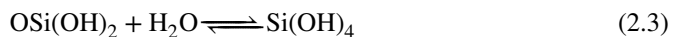
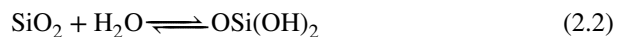
2.3 Silicon as biomedical material

Silicon (Si) is a material with unique properties that is widely utilized in commercial products because of its abundance, low cost and wide applicability. The material is also used in research purposes in a wide range of fields, including for electronics, photovoltaics and biomedical research. This section will give a brief overview of the industrial and research usages of silicon materials, with a focus on biomedical applications and usage in DDS.

Si is the second most abundant element in the earth's crust, after oxygen. With a

high chemical affinity for oxygen, silicon readily form various oxide formations such as silicon dioxide (silica, SiO_2), that can react with metal oxides to form silicates, which is the form of silicon usually found in nature. Crystalline Si is a semiconductor material dominating the microelectronics industry, as well as being widely used as the energy-absorbing material in solar cells. Its conductivity properties can be tuned by doping with other elements, and the material is therefore ideal for use in transistors in electronic devices [29]. The electronics industry has utilized the semiconducting properties in electronic devices for over 60 years, and it has even been given a nickname to present day's society *i.e.* the "*Silicon age*" or the "*Information age*" for the easy access to information realized by the Si-based computer industry [30].

Initially, therapeutic applications of Si comprise implanted microelectronic devices such as biosensors, with research on dosage forms in drug delivery applications emerging. Nanosized Si crystal particles are of widespread interest for their potential usages in drug delivery applications due to its beneficial properties of inherent biocompatibility and biodegradability. Leigh T. Canham [6] pioneered the development of biomedical applications of Si with the discovery of electrochemical etching for Si porosification in 1990. The discovery of this method raised an increasing interest in the material in particular for exploring its luminescence properties. In 1995 he also showed the biocompatibility of mesoporous structured Si [7]. Biocompatibility is a characterization of materials having "*compatibility with living tissue or a living system by not being toxic, injurious, or physiologically reactive and not causing immunological rejection*" [31]. Biodegradability of mesoporous Si means the ability of being self-degrading in aqueous environments, and producing the non-toxic byproduct of orthosilicic acid. The main chemical reactions in this process involve oxidation of the Si crystal structure and subsequent hydrolysis of the resulting silica shell generating soluble Si species, as seen in the following reactions [32].



These steps represent the slow reaction that nanosized Si has in water with increasing reaction rates in basic solutions (this mechanism will be further discussed in Section 3.4). Orthosilicic acid is the bioavailable form of silicon in tissues that can be excreted from the body through the urine. It is a weak acid with low solubility in water, < 2 mM, and is found naturally in several food items including vegetables, whole-grains and beer. It is a vital component for normal bone and connective tissue homeostasis and is even offered as a dietary supplement [13, 27].

The versatility of porous silicon (pSi) has made it functional in various biomedical applications in all the major areas of nanomedicine, as outlined in Section 2.1, *i.e.* regenerative medicine, biosensing and bioimaging for diagnosis and as a carrier for API in drug delivery. Si is a "*universal*" material and can be modified and designed by easily changing surface chemistry as well as size, shape and porosity. Combining the advantageous properties of pSi materials in terms of biocompatibility and -degradability with those of nanoscale vehicles, can greatly benefit the field of drug delivery for which particle geometry is an important factor determining interactions with tissue and degree of

cellular uptake. These properties, as well as the versatility in surface modifications, provide enhanced properties as compared to several other semiconductor materials and other materials used in nanomedicine. Possibly most important, the small size of pSi NPs creates an extremely high surface area available for modification. Surface chemistry of pSi NPs is an important DDS property affecting applications in biomedical devices, which is increasingly important for nanoparticles as they are dominated by surfaces rather than bulk. A range of different processes is developed for Si surface modification using a range of different molecules [33–39]. Conjugation of drugs, diagnostic agents, as well as targeting ligands, are available for tailoring Si vehicles for desired properties suitable for treating a wide range of diseases and conditions. Coating Si NPs with polymers like PEG are possible for further increasing biocompatibility and solubility. Also, conjugating with tumor-homing or disease-recognizing peptides give immense opportunities in localized delivery of therapeutics. A summary of commonly used Si surface modification processes is found in Section 2.5.

Main efforts in the studies of porous materials as DDS have been focused on sustained or controlled drug release, where the drug release rate is determined either by the erosion rate of the material or the diffusion of drug(s) through the carrier material, as illustrated in Figure 2.3. Carrier properties can be tuned to determine which of the two mechanisms dominates, hence how fast diffusion- and dissolution related drug release happens. Porous materials also offer a potential means to increase the dissolution of poorly soluble drugs. By tuning the pore size to only a few times larger than the drug molecule will secure that the drug is kept in a noncrystalline amorphous state due to the confined space of the pores. Keeping drugs

in an amorphous state that exhibit higher dissolution rates, particularly for compounds with high crystal energy, could be an increasingly important strategy in drug development [40]. In this context, pSi NPs provide attractive delivery platforms because of the tunability in pore size to affectively accommodate desired payloads and drug release rates. Furthermore, using mesoporous structures present a great increase in drug loading capacity compared to conventional inorganic nanoparticulate DDS. Tuning of pore size is also useful for tuning the degradation rate of the carrier (which will be discussed in Chapter 3).

Nanomedicine DDS are traditionally developed for loading chemotherapeutic agents

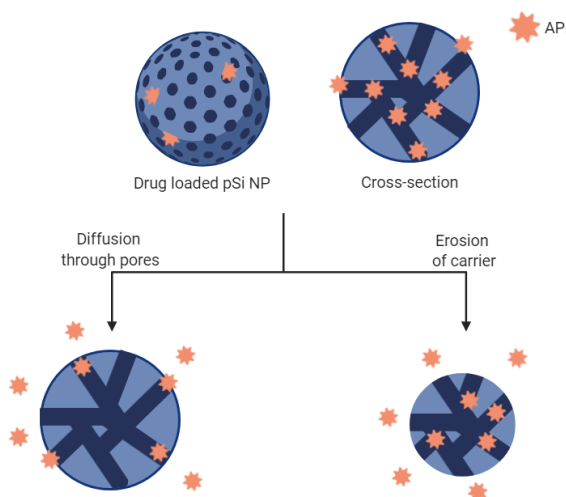


Figure 2.3: Illustration of the drug release routes of pSi NP DDS, showing diffusion of active pharmaceutical ingredient (API) out of pores and release upon carrier material erosion.

for treatment of cancer (as previously mentioned). However, as the perspective of DDS potential has expanded, research on pSi for delivery of different therapeutic compounds and other biomedical applications has also expanded. Several studies are done on loading porous silicon nanoparticles (pSi NPs) with chemotherapeutic agents [8, 10, 14, 32, 41], but mesoporous Si has also been used for instance for *in vivo* gene delivery for treating bacterial infections as an alternative to antibiotics, accommodating the increasing danger of antibiotics resistance. Kim *et al.* [12] and Hussain *et al.* [42] loaded pSi with antibiotics, and the latter demonstrated successful tissue targeting that effectively suppressed infection *in vivo* in mice. Anderson *et al.* [13] studied orthosilicic acid release from pSi wafers with the aim of developing a bioavailable form of Si for supplements. The mesoporous structure of pSi has proven to have a high drug loading capacity optimal for loading of a variety of API, increase the interest in development of alternative strategies using pSi NPs for treating a wide range of conditions. Salonen *et al.* [40] and Nieto *et al.* [11] verified successful loading of a variety of drugs for instance for anti-inflammatory, fungicide and diuretic purposes to pSi. Successful loading of nucleic acids to pSi was demonstrated by Bertucci *et al.* [27]. Engineering pSi particles for spatiotemporal control of the drug has also been explored. Wang *et al.* [9] created multi-functional pSi drug carriers for chemotherapy drug loading with surface grafted ligands for tumor targeting. Herranz *et al.* [10] developed multistage DDS of polymeric coated pSi NPs that are sensitive to changes in pH. Upon exposure to acidic environments, like typically seen in tumor tissue, the PEG-based polymers will disassemble from the NP surface causing localized release of the loaded chemotherapeutic agents. *In vivo* studies in mice have shown that effective drug delivery to tumors can be verified by tracking the intrinsic luminescent properties of pSi, arising from quantum confinement effects [8, 43].

Many benefits and possibilities for using pSi NP in DDS have been identified. It is, however, important to notice that several of these properties are highly dependent on the carrier materials' properties. Research on Si NPs as DDS is sometimes done without critical evaluation of essential properties of the carrier material alone. The inherent particle properties are important and can determine the biocompatibility and stability of the DDS, which are two essential properties in drug delivery.

2.4 Synthesis of porous silicon nanoparticles

2.4.1 Silicon nanoparticle synthesis

Recently, Si NPs are prepared by a variety of chemical and physical approaches including electrochemical etching, ion implantation, thermal vaporization, laser ablation, gas phase decomposition of silanes and reduction of silane-containing compounds. Conventional approaches used for research and industry purposes are gas-phase synthesis such as physical and chemical vapor deposition (PVD/CVD). These techniques use either physical or chemical means to vaporize precursors, or to deposit the precursor material for creation of a thin layer of material. Reduction of silicon tetrachloride (SiCl_4) in solution with lithium aluminium hydride (LAH) and tetraoctylammonium bromide (TOAB) is also reported to produce nanosized Si particles [44, 45]. Common drawbacks with the above-mentioned techniques include multiple production steps, required post-annealing or -etching, exten-

sive reaction times, low yield and complex precursor synthesis. Physical means of size-reduction of materials down to nanoscale can be done by well known industrial mechanical processes like ball grinding in a planetary mill. This method, however, have little processing control and may result in wide particle size distributions [46]. As the Si NPs size, morphology and surface chemistry substantially influence its properties in regards to stability, degradation properties and interactions with cells and tissues, realizing an effective size control and surface engineering is required. Establishing these requirements are sufficient for controlled synthesis in lab-scale. However, a major limitation of the mentioned techniques are associated with scalability to large-scale high throughput production with preserved quality and control of the process [47]. For pharmaceutical applications size control is also extremely important as different sized particles are handled very different by the body. Most of the synthesis methods mentioned above will therefore not meet pharmaceutical requirements of producing particles with a narrow size distribution.

Industrial production of Si feedstock is mainly for micro-electronic and photovoltaic applications. The Siemens Bell Jar reactor and the Fluidized Bed reactor are the two reactor designs usually used for this kind of commercial production. Trichlorosilane (SiHCl_3) is the main gaseous precursor that can be used directly in a Siemens Bell Jar reactor or to produce monosilane (SiH_4) in a redistribution process. The monosilane route, despite requiring more synthesis steps, often present a more efficient process resulting in higher purity silicon [48]. These reactors are based on CVD technology, and for such designs, high quality is related to high costs. CVD/PVD reactors may also be used for Si NP synthesis but today's commercial approaches are not appropriate for production of Si for biomedical applications that require high level of control of size distribution and purity [29, 49].

The IFE Si particles are synthesized by thermal decomposition of monosilane (SiH_4) gas precursors within a free space reactor (FSR). Chemical decomposition of monosilane under elevated temperatures cause Si-Si bond formation and simultaneous removal of hydrogen. Higher order silanes are step-wise created, as illustrated in Figure 2.4, before elemental Si powder is formed and collected from the reactor bottom. The name of the FSR indicates that nucleation occurs absent of a nucleation surface, thus in free space. Silane concentration and reactor pressure determine the number of silane molecules present and the amount of silane collisions. Furthermore, several heating zones and options for temperature increase and hydrogen removal rate determine the amount of silane present in the gaseous state at the different stages of decomposition and growth, promoting defined particle formation. The above-mentioned parameters can be adjusted to produce Si powders of a narrow size distribution with an average size ranging from below 10 nm up to several μm [15]. A monodisperse particle distribution of consequent

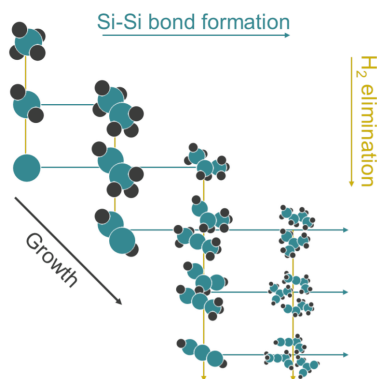


Figure 2.4: Silicon particle growth by silane gas decomposition in a free space reactor. Illustration by Thomas J. Preston.

spherical morphology are properties provided by the FSR that are also highly desirable for pharmaceutical applications.

2.4.2 Porosification of silicon

The conventional approach for synthesizing pSi NPs used in literature includes starting with flat Si wafers, not nanoparticles, porosifying the wafer followed by ultrasonication to break the porous wafer into particles. This process is illustrated in Figure 2.5. Usually, an electrochemical anodization method is used for porosification. This approach includes attaching the Si wafer and a counter electrode (usually platinum) to a power supply, passing a voltage across the wafer while immersed in a solution of hydrofluoric acid (HF). The voltage will inject charge carriers into the Si crystal structure that are susceptible for a nucleophilic attack by fluoride ions in HF. Benefits of using this approach includes the ability to tune the pore sizes by adjusting the applied field strength of the voltage. This is a well-studied and robust approach. However, it will only work for pre-fabricated p-doped Si wafers [50, 51], or by making charge carriers available by a photon source in so-called photoelectrochemical and laser-assisted etching, for which both p-doped and n-doped Si wafers may be utilized. The main limitation of these strategies includes poor scalability for industrial production due to the energy requirements.

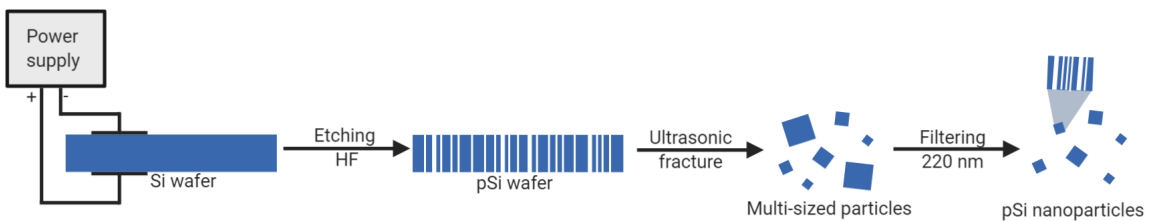


Figure 2.5: Schematic illustration of electrochemical anodization for porosification of Si wafers followed by ultrasonica fracture and filtration to obtain pSi NPs.

Although the method for Si etching using externally applied current is unambiguously the most commonly used, a purely chemical approach could provide a simpler alternative that excludes the need for an electrode setup. For these types of electroless etching, electrochemistry occurs spontaneously without the intervention of a power supply or photon source. It require an oxidant with the ability to introduce electron holes in the silicon structure and fluoride compound, typically HF, that remove the oxidized Si. Electroless etching is typically divided into three categories: chemical vapor etching, metal-assisted etching and stain etching. In chemical vapor etching the Si is set in contact with a vapor that is of a solution of an oxidant and HF rather than the solution itself, but with similar chemistry. In metal-assisted etching, metal NPs with a diameter smaller than the object that is to etched is utilized as catalysts, facilitating transportation of charges. The particles work as catalysts "*digging*" holes in the Si wafers so that the resulting pore size is determined by the size of the metal particles' [50]. Stain etching is another widely studied approach of which various oxidants have been utilized. The predominance of Si stain etching literature is concentrated on the use of HF solutions with a nitroxy oxidant, typically HNO_3

or NaNO_2 . These oxidants are reliable alternatives for only a limited range of films and greater control over morphology and other properties can potentially be achieved by using a wider range of fluoride carriers and oxidants [50].

The described treatments of Si wafers followed by ultrasonification can produce nano-sized particles, however, a wide particle size distribution is often obtained with the particle size varying from 10-20 nm up to μm . The need for filtration to obtain the desired size distribution adds another processing step and generates additional waste material of the particles filtered out. Furthermore, the method gives little control of the particle geometry, which is vital in drug delivery applications, often producing cube-like fragments. Another possibility for synthesis of porous Si NPs is etching of pre-fabricated Si NPs. Ge *et al.* [52] developed a procedure for stain etching commercially produced Si NPs that includes doping with boron (p-doping) before etching with silver nitride (AgNO_3) and HF. These particles show promising characteristics as anode material in lithium-ion batteries and provide an alternative approach for etching of Si NPs.

The IFE solid Si particles from the FSR are porosified using a purely chemical process, *i.e.* a type of stain etching called regenerative electroless etching (ReEtching), described by Kolasinski *et al.* [16]. In ReEtching it is possible to control many different parameters in order to create the carrier with the most desirable properties in regards to the drug and target tissue in question. The process of ReEtching depends on the interplay between two oxidant species, *e.g.* vanadium pentoxide (V_2O_5) and hydrogen peroxide (H_2O_2). In the case of V_2O_5 and H_2O_2 , it is V_2O_5 that is the catalyst of the etching process and H_2O_2 that is the driver of the catalytic process. V_2O_5 dissolves into VO_2^+ ions with a vanadium oxidation state of +5 (V) when put in an acidic solution of HF. VO_2^+ ions react with crystalline silicon by taking an electron, thus leaving a positive charge, an electron hole, in the silicon valence band resulting in the reduced VO^{2+} ion with vanadium oxidation state of +4 (IV). The injected electron hole makes Si susceptible for a nucleophilic attack from HF that dissolves the Si surface atoms in the form of H_2SiF_6 species in a ratio of 1:1 of electron hole:Si dissolved.

The described process is a basic stain etching reaction and has limitations in that the vanadium amount and its concentration cannot be controlled independently. Large amounts of vanadium is necessary to etch sufficient Si and thereby create a highly porous structure, whereas low concentration is desirable to achieve a low etch rate to avoid chemical polishing of the particle surface and particle size reduction. This dilemma is overcome by slow continuous addition of H_2O_2 . The reduction potential of H_2O_2 exceeds the one for vanadium oxide. Not being able to inject holes in the Si structure, H_2O_2 is able to oxidize the vanadium(IV) species to regenerate the vanadium(V) species, as schematically illustrated in Figure 2.6. This is a highly efficient process as vanadium is regenerated and the only element that is consumed in the process is peroxide.

Using this regenerative reaction allows for higher precision control of pore formation by being able to control the concentration and the amount of oxidant separately. The concentration of vanadium is controlled by the injection rate of peroxide, as well as the amount

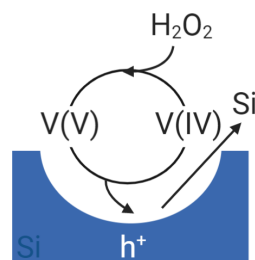


Figure 2.6: ReEtching chemistry. h^+ represents an electron hole.

of Si etched by the time of etching, giving more opportunities in controlling the etching process and thereby allowing for continuous pore etching instead of electropolishing.

The described formation of pSi NPs for biomedical applications presents a revolutionary approach in precision medicine, allowing for synthesis of biocompatible and fully biodegradable materials. The synthesis process gives versatility in size and geometry of the resulting particles. Combined with the chemical means of etching pores, this process gives ultimate opportunities in tuning the pore size, the particle size and the geometry allowing fully versatile carrier materials with tunable properties to be designed for the desired therapeutic agents to be transported and to their targets.

2.5 Surface chemistry of silicon

There are two main purposes for modifying the surface of Si in biomedical devices: 1) to stabilize the surface and protect from chemical and physical degradation of the material, and 2) to enable attachment of molecules and polymers that enhance the biological interactions, including bioconjugation and attachment of targeting ligands and responsive materials. Understanding of the behavior of Si surfaces in ambient air and other environments give valuable information on its modification possibilities. This section will briefly review a handful of the established routes for modification of Si surfaces, for tuning stability and compatibility of the material.

The intensive use of Si in the electronics industry as well as the downscaling of electronic devices, has requested feasible methods for high-precision control of Si surface passivation techniques. Over the years, native surface oxide has served as the main passivation route. A vast amount of alternative thermal, catalytic and wet chemistry routes have, however, been developed (*e.g.* carbonization, hydrocarbonization, hydrosilylation, capping with alkyl-, alkoxy- and chloro-silanes as well as grafting of functional moieties [30]). While most of these methods are initially developed for flat Si wafers for the electronics industry, they can be adapted to pSi and nanosized materials for biomedical purposes.

Passivation of Si-based microdevices, lab-on-a-chip technology and sensors for biological usage have similar functionality as in the electronics industry, whereas drug delivery devices require an increasing level of surface chemistry control *in vivo* in which the pharmaceutical industry possess rigorous quality standards, with an additional focus on biocompatibility and toxicity aspects [51, 53]. A need to passivate and functionalize reactive surfaces to create stable biocompatible materials that are un-reactive and non-toxic in physiological environments and temperatures, as well as being stable during storage over an extensive period of time, arise for biomedical usages. Surface chemistry of drug carriers is essential for increasing stability in physiological conditions and contributing in determining the *in vivo* suitability of the drug by tuning interactions with cells and tissue. It also affects the release kinetics of the API, either by creating steric hindrance for diffusion of drugs that are entrapped inside pores or by altering degradation rate that reduce release of covalently bound drugs. These principles have been used to create stimuli-responsive DDS by grafting of surface moieties that change their chemical or physical properties upon encountering specific environmental triggers, causing release of the API [54]. Furthermore, active targeting is accomplished by conjugation of bio-interactive ligands. Surface chemistry can also be modified to control protein corona formation and escape clearance by the

immune system (opsonization) for prolonged circulation time, for which surface PEG is often used.

Chemical surface modification of pSi NPs requires an understanding of the behavior of pristine Si materials. Hydrogen-terminated silicon surfaces, as usually produced by electrochemical or chemical synthesis, are highly reactive. Si-H bonds are only stable for short periods in air and readily oxidize in aqueous media. Various surface treatments are utilized to stabilize pSi surfaces, often involving the formation of either Si-O or Si-C surface bonds using thermal and chemical processes, for which a range of chemistry has been proposed in the literature. Grafting of silane molecules is also a widely studied approach giving multiple possibilities in functionalization.

Si slowly oxidize in ambient air depending on environmental conditions like humidity, temperature and composition of the air, forming a few nm thick native oxide layer [51]. Moreover, controlled thermal oxidation provides one of the most straightforward passivation methods. Thermally oxidized pSi (TOPSi) has a hydrophilic surface which is beneficial for solubility in blood and tissue, but it has low chemical stability often not desirable for pharmaceutical usages [40]. Alternative techniques to oxidize pSi include anodic oxidation, photo-oxidation and chemical oxidation in the presence of inorganic or organic agents. Besides, thermal oxidation is utilized as the first step in a wide range of functionalization processes as the resulting Si-O and hydroxide bonds readily react with various reactive molecules [24].

Creation of Si-C bonds is another passivation approach, often used to attach aliphatic or aromatic hydrocarbons to the Si surface. Several different routes have been studied for this purpose, including thermal carbonization, hydrosilylation of unsaturated organic species, electrochemical coupling (reductive or oxidative) of alkyl halides, diazonium salts, alkyl-lithium reagents, or Grignard reagents [55]. The resulting surface is chemically and thermally very resistant with hydrophilicity highly dependent on the nature of the functional groups added. Such functional groups provide the opportunity for further modification of the surface using standard organic chemistry strategies for creating advanced DDS. Thermally carbonized pSi (TCpSi) or thermally hydrocarbonized pSi (THCpSi) are created by thermal deposition of gaseous hydrocarbon sources at temperatures below and above approximately 700 °C, respectively. THCpSi have a hydrophobic hydrocarbon-terminated surface with ability for further chemical modification, while TCpSi have a hydrophilic carbide-like surface layer with superior chemical resistance [33, 34]. These methods give effective coating of porous silicon materials due to rapid diffusion of relatively small molecules into the pores.

Various alternative modification strategies have also been adapted for Si NPs as DDS. Hydrosilylation describes addition of Si-H bonds across unsaturated organic molecules; meaning THCpSi synthesis is a form of hydrosilylation [24, 51]. Other examples of organic molecules grafted to Si surfaces by hydrosilylation include 1-dodecene and undecylenic acid. Undecylenic acid has two reactive terminal ends and is used as a linker to conjugate other biomolecules. In addition to presenting an effective way of stabilizing the surface, hydrosilylation of undecylenic acid has also been used for its tumor-recognizing properties [11, 35]. Silanization is covalent bonding of pre-functionalized organosilanes, commonly alkoxy- or chloro-silanes, which occurs only by condensation reactions with surface silanol groups (Si-OH) found at oxidized surfaces. Commonly used alkoxy-

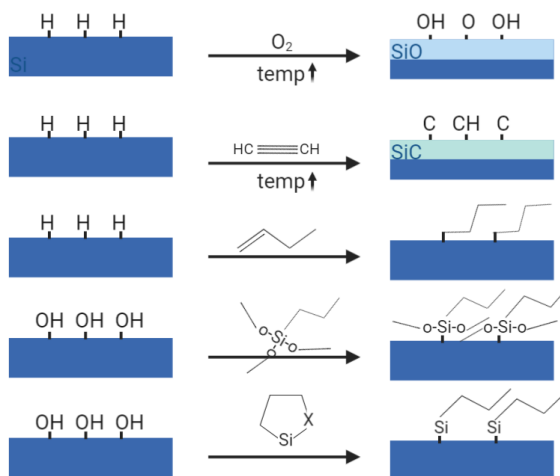


Figure 2.7: Illustration of various chemical routes for Si surface modification using different precursors. From top: thermal oxidation, thermal carbonization, hydrosilylation, silanization and ring-opening.

lane molecules used for Si surface modification in biomedical applications include 3-aminopropyl trimethoxysilane (APTES), (3-mercaptopropyl)triethoxysilane (MPTES) and 3-aminopropyl-dimethyl-ethoxysilane (APDMES) [36–38]. Silylation, not to be confused with silanization, involves the conjugation of a substituted silyl group (R_3Si) onto Si surfaces [39].

Other novel alternative approaches for pSi functionalization, developed specifically for biomedical applications, include thermally induced silane dehydrocoupling, providing reduced possibility of oxidative side-reactions of surface Si-H bonds compared to hydrosilylation [38]. Another approach using cyclic silanes that undergo a ring-opening "*click-reaction*" is also newly developed for simple grafting of organic species. Benefits using this approach includes a relatively mild chemistry giving a fast and more efficient reaction than hydrolytic condensation of trialkoxysilanes on similar hydroxyl-terminated surfaces under room temperature conditions [56]. Similar to silanization approaches, this method will also require pre-functionalized species, and in this case cyclic silane species.

2.6 Colloid science

Colloid science is the study of particles of one phase, typically sizing from 1 nm to 1000 nm, forming suspensions in another phase. Colloids are defined by consisting of two separate phases, as opposed to solutions that has a solute dissolved in a solvent forming one phase. They are also classified by the states of matter making up the particle and medium phase. Combining gas, liquid and solid phases, this makes nine theoretically possible colloid systems. The most common are liquid-liquid (emulsion), solid-solid (solid sol) or solid particles in liquid medium (sol). Colloid systems containing dispersed particles that display an affinity for the dispersant medium are referred to as lyophilic, whereas systems

of particles that repel the medium are referred to as lyophobic. When the dispersant is water, this is referred to as hydrophilic or hydrophobic colloids, respectively [57].

Particles in a liquid solution undergo random translational diffusive motions due to thermal energy in the absence of a concentration or physicochemical gradient, which is referred to as Brownian motion. These thermal motions cause particles to collide and interact, resulting in a range of colloid phenomena. According to DLVO theory, particle-particle interactions are determined by electrostatic double-layer repulsion and van der Waals attraction [58]. These are additive forces of similar range and can be schematically expressed as a potential energy versus separation curve where a positive result corresponds to an energy barrier and repulsion while a negative result corresponds to attraction and hence aggregation. It is generally considered that the DLVO theory provide a sound basis for understanding aggregation stability of colloidal systems [59], however, it is in practise only applicable for highly specified colloidal systems and is not always descriptive for ionic concentrations at 1M and above for the medium phase [60].

Stability is an important property of colloidal solutions, referring to retention of the properties of the two phases. Upon interactions between particles in the dispersed phase, several phenomena might occur as a result of instability, *i.e.* aggregation, agglomeration, coalescence, coagulation and flocculation of the dispersed phase (which are described by others elsewhere [61]). The other major side of colloid stability is chemical stability and dissolution, which would require other means of identification and quantification. Dissolution stability of Si NPs in various mediums will be discussed in detail in Chapter 3.

2.7 Dynamic light scatterig for particle size measurements

Dynamic light scattering (DLS) is a technique used to measure size distribution of particles typically in the sub-micron region, dispersed in a liquid. Its uses are limited to the study of particles of such small dimensions and a theoretical perspective is given to explain the reliability of the technique and its results. Particles of these sizes show light diffraction and other optical effects such as the Tyndall effect of light scattering making some colloid solutions seem translucent [57]. Random Brownian motions of particles in solution depend on the temperature and viscosity of the dispersion medium, as well as the size of the particles. A monochromatic beam of light encountering a colloid solution will scatter light in all directions due to reflection from the particles. The light scatters as a function of the size of the particles and in DLS measurements it is the scattering pattern that is detected and analyzed to deduce the particle size [62]. The smaller the particle, the faster it moves and the faster it causes fluctuations in the scattered light. This is an indirect method giving the size of a hypothetical sphere that has the same diffusion velocity in the liquid as the understudied particle. This technology allows for identification of particle size lower than the wavelength of the light used to measure it, and is a simpler technique than visualization by electron microscopes, which is normally used for these purposes.

DLS measures the time-dependent fluctuations in the intensity of scattered light and these fluctuations can be used to determine the translational diffusion constant, D , by calculating the autocorrelation function. The autocorrelation function predicts how fast a signal is changing by showing the probability of the signal to be the same after a time delay, τ . The normalized autocorrelation function can be expressed as follows

$$g(\tau) = \frac{\langle I(t)I(t + \tau) \rangle}{\langle I(t) \rangle^2} \quad (2.4)$$

where $I(t)$ is the intensity at time t and the brackets indicate the ensemble over t . Assuming a monodisperse sample with a very narrow size distribution, $g(\tau)$ can be written as

$$g(\tau) = 1 + \beta e^{-2D\mu^2\tau} \quad (2.5)$$

where μ is a sinusoidal expression with amplitude $\frac{4\pi}{\lambda}$ and frequency $\frac{\theta}{2}$, β the signal amplitude of the correlation function and D the translational diffusion coefficient. λ is the wavelength of the incident light and θ the detection angle in reference to the incident light beam.

The autocorrelation function is dependent on the translational diffusion coefficient, which is also related to the hydrodynamic radius, R_h as described by the Einstein-Stokes equation, as follows [62]:

$$R_h = \frac{k_B T}{6\pi\eta D} \quad (2.6)$$

The raw signal output of DLS is a cumulant analysis of the light intensity, which is a single exponential fit, applied to the autocorrelation function assuming a single particle size mode. D is proportional to the lifetime of the exponential decay and the size distribution can be graphically interpreted on the basis of the decay, as illustrated in Figure 2.8, with smaller sized particles giving rise to a faster decay due to more rapid diffusive movements. In case of a polydisperse sample, there will be multiple decays of the autocorrelation function. These different decays can then be used to make a size distribution for the sample. In addition to the monodispersity assumption, DLS measurements also assume perfectly spherical and symmetrical particles. This may pose problems as the velocity of diffusion may vary depending on the direction of movement for non-symmetrical and non-spherical particles.

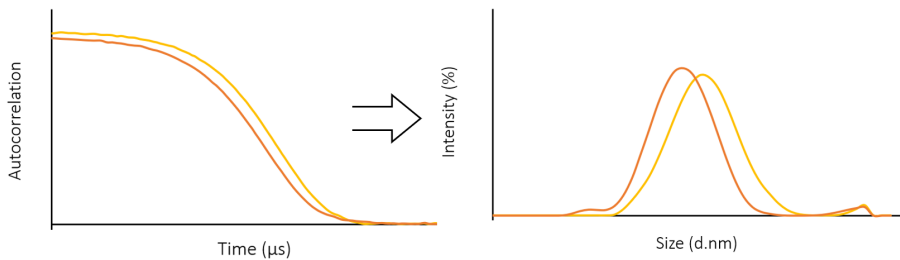


Figure 2.8: Illustration of cumulative fit of the autocorrelation function (left) measured by DLS and conversion to the intensity weighted size distributions (right). A faster decay of the autocorrelation function (orange), the raw data obtained by DLS, converts to a size distribution of smaller particle peak size.

The most stable parameter to be reported from DLS measurements is the Z-average, also known as the cumulative mean. The Z-average is the "harmonic intensity averaged

particle diameter" and is a hydrodynamic parameter that is only applicable to particles in solution. The size of the particle with an outer hydration layer is measured and the resulting Z-average is therefore always higher than the actual size and cannot be compared to direct size measurement data, such as in the case of microscopy. The Z-average can be sensitive to small portions of agglomerates and is the most precise when the size distribution only has one peak with a narrow width.

The polydispersity index (PDI) is another robust DLS output parameter. Polydispersity describes the width of the size distribution, assuming a Gaussian distribution. PDI is a dimensionless value between 0 and 1 where $PDI < 0.05$ represents a perfectly monodisperse distribution and $PDI > 0.7$ a very broad size distribution that is probably not suitable for DLS.

DLS instruments often provide three different size distributions. The intensity distribution is naturally weighted according to the scattering intensity of each particle fraction or family, and is the closest to the raw intensity fluctuation signal. Depending on the particle nature, it might be proportional to the square of the molecular weight which makes it sensitive to small amounts of agglomerates. Conversion into volume and number distributions is done using Mie theory which assumes that all particles are spherical and have a homogeneous and equivalent density, that the optical properties of the particles (refractive index and adsorption) are known, and that there is no error in the intensity distribution. Small errors in intensity distributions may, however, give misleading volume and number distributions. The latter ones should therefore only be used to report relative percentages in samples with multiple peaks. The size of a peak should be interpreted from the intensity distribution as this is the most fundamental, even though the number distribution would be tempting to use when comparing to microscopy data [63].

2.8 Cell viability studies of nanoparticles

Cellular cytotoxicity assays are methods useful for quantification of the toxic effects of polluting or toxic substances, the biological effects of new drug formulas and pre-clinical testing of other pharmaceutical products. Such cytotoxic effects can be studied in *in vitro* experiments using cell cultures, in which cells are grown outside the body under controlled conditions. These conditions include temperature, humidity, microbial contamination control and nutrition. Cell culture mediums are used to ensure cell line specific needs for nutrition by providing vital amino acids, vitamins and inorganic salts. Environmental factors such as humidity, temperature and oxygen content is controlled by the storage inside a CO₂ incubator, made to simulate *in vivo* conditions and reduce experimental variability. Built-in filtration of airborne contamination and sterile cell culture handling techniques are required for contamination control. Antibiotics can also be added to the growth medium to prevent bacterial contamination [64].

In vitro cell viability studies are an important first step for determining the biocompatibility of NPs. In drug delivery it is desirable that the carrier material alone show low toxicity to the majority of cells and tissues, enabling design of a versatile drug carrier. Previous studies have attempted to address structure-activity relationships between the physicochemical properties of NPs and cell death. Particle properties like size, shape and surface chemistry have been identified as key regulators of cell death modalities and

related signaling pathways [65]. Positively charged particles and hydrophobicity have been shown to increase interactions with cell membranes, which make them more likely to be internalized and induce oxidative stress, autophagy (cellular self-degradation) and apoptosis (programmed cell death) compared to negatively charged and hydrophilic NPs. Negatively charged particles, however, has shown to increase protein adsorption while PEG decorations to alleviate these cytotoxicity-related bioeffects. The observed effects may vary in different cell lines and multiple cell lines should therefore be used to investigate toxic effects [66]. Understanding these structure-cell death relationships for Si NPs, including how native surface oxidation and porosity affects cell death, makes it possible to predict NP-induced cell death which is a powerful tool in guiding the design of future NPs for nanomedicine. It is worth noting that NP concentration, as with any bioresponsive agent, is expected to be a major factor in determining cell death.

A wide range of cell viability assays are developed using various techniques for measuring marker activity associated with viable cell number in a population. Viability tracers are used to measure cellular metabolism, enzyme activity, mitochondrial membrane potential, oxygen consumption and/or glycolysis as health indicators often measured by protein-detection, colorimetric or fluorometric biochemical assays. Several fluorescence-based assays rely upon reactions seen in viable cells to change. An increase or decrease of the fluorescence intensity has proven to give reliable and robust cell viability outputs [67]. Fluorescent dyes are molecules with appropriate electronic states that will emit photons at a particular wavelength within the visible range when exposed to light at appropriate wavelengths. The energy difference in the light required for excitation and the emitted light, caused by vibrational relaxation, is called the Stokes shift and makes it easier to distinguish emitted light from the excitation light source. This mechanism, illustrated in Figure 2.9, is utilized in fluorescent-based viability assays in which fluorescent emission intensity, measured by a spectrophotometer, is assumed to be proportional to the number of either live cells or dead cells [68].

There are a few phenomena to be aware of when assessing toxicity of nanomaterials, particularly inorganic material, which is not normally seen when testing biological or molecular drugs. Due to the high surface area to volume-ratio, nanomaterials are used as catalysts in various chemical reactions. A potential reactivity between the nanomaterial and assay components may result in either substantial over- or under-estimations of toxicity. Intrinsic absorbance or fluorescent properties may also interfere with the viability output signal by quenching or increasing fluorescent intensity. Such interference is reported for a number of viability assays when assessing carbon-based nanomaterials, in particular, which are documented to bind to dyes. Also silicon, cadmium selenide and titanium dioxide NPs have shown to interfere with at least one conventional viability assay. Undecylenic acid functionalized Si NPs are shown to interfere with the BCA protein assay and the lactate dehydrogenase (LDH) assay due to intrinsic absorbance and protein binding [69].

Sterilization of nanomaterials, which is required for pharmaceutical usage, is another factor that can alter the outcome of cell viability studies. This phenomenon is probably due to alteration of particle properties [70]. Si is thought to be suitable for most forms of sterilization techniques within the three main categories, exposure to (1) heat, (2) irradiation and (3) various chemicals. Appropriate sterilization techniques and assay types for bio-

logical studies should be carefully selected for specific nanomaterials. As structure-assay components relationships are not always predicted, using controls and doing multiple assays as a quality control would improve assay reliability.

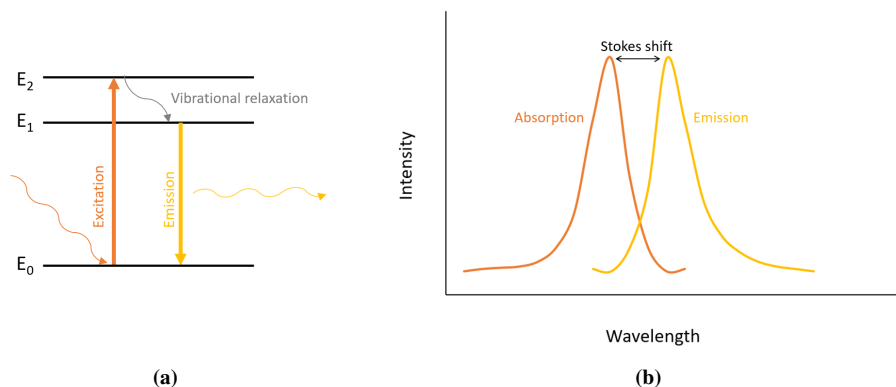


Figure 2.9: Illustration of mechanisms in a fluorescent molecule's electron states giving rise to the Stokes shift. A fluorescent molecule absorbs energy, E_2 , and gets excited when exposed to a light source. An amount of that energy is lost to vibrational relaxation, $E_2 - E_1$, before releasing the rest, E_1 , as emitted fluorescence, as seen in (a). (b) shows the emission and absorption spectra of a fluorescent molecule with the Stokes shift representing the difference in peak intensities of absorbed and emitted wavelengths.

Bright field optical microscopy can be used as an additional quality control when doing biological studies with nanoparticles. The most widely used light optical microscopic technique is called widefield microscopy where lenses are used to focus light onto a sample to magnify structures poorly seen with the naked eye. The entire sample is exposed to light, and contrast methods like phase contrast are used to distinguish morphological features from background intensity. The theoretical resolution obtained using light optical microscopy is as low as 200 nm, roughly half of the wavelength of the light used to image the specimen. However, in practice, this is limited by background fluorescence from regions above and below the focal plane [71].

Silicon Nanoparticle Stability

The stability of silicon materials is an important parameter for all commercial and research applications. In industry, Si stability is measured with regards to the applications in microelectronics and photovoltaics. However, no standard technique for measuring stability is established for Si NP used in biomedical applications. Such stability tests should be part of the material quality assurance, which is a high priority focus in the pharmaceutical industry.

In the present chapter are the findings of a literature survey on the topic of Si NP and pSi stability presented. The methodology of the identified stability studies is described and parameters affecting stability are discussed. An elaboration of pH-dependent stability and possible mechanisms behind, to serve as guidelines for the following chapter on experimental stability studies of Si NPs, is then presented. The methodology for this literature review is described in Appendix A.

The stability of a material describes its ability to retain its inherent properties which will often be disturbed upon dissolution of the material. However, dissolution describes a process in which the atoms of the material release their bonds and is no longer part of the material. These are two concepts that are tightly dependent, yet describe slightly different approaches. As an example: upon dissolution of an atomic layer of a crystalline structure, the material might still retain its physical characteristics, thus its stability. Furthermore, modification of for instance the crystallinity of the material might not be due to dissolution of the material. Therefore, stability and dissolution are not mutually dependent. In the subsequent literature review is NP dissolution the main focus as it is expected to be the dominating factor in the drug delivery process. However, agglomeration is also an important contributor when assessing NP properties and might affect the material performance in several applications, including those in the biomedical field.

3.1 Methodology of stability studies

The performance of biodegradable Si-based DDS is critically dependent on the degradation behavior of the material scaffold in *in vivo* environments, both in terms of drug release and tissue interactions over time. Dissolution of Si is attributed to the water-soluble surface hydride or hydroxyl groups, which are hard to quantify. Real-time monitoring of administered Si would give the most accurate performance data. Furthermore, *in vitro* measurements can serve as a model for predicting dissolution kinetics inside the human body and gives a measure of the nanostructured Si stability performance. Several things are to be kept in mind for the creation of accurate models such as medium composition, salt content, pH, temperature and content of biological factors such as proteins. Blood flow and other forces are also to be considered as they can influence the dissolution behavior to a great extent, in addition to the medium composition. These medium parameters can be altered to simulate different *in vivo* environments to predict degradation behavior in distinct tissues or organs, and in the cases of malignant or inflamed tissue.

No conventional method of studying Si NP stability and quantifying degradation was identified in literature (several different media were used for the stability studies and different methods for measuring the degradation of nanostructured Si). A review of the most commonly used media for Si NP stability studies are summarized below.

- **Simulated physiological conditions**

De-ionized water, buffer solutions and cell culturing media are often used to simulate physiological conditions in the human body with relatively simple solutions. Phosphate-buffered saline (PBS), often used in biological research having a physiological pH and composition of salts, is a widely used buffer for this purpose. PBS in the pH range of 6.8-7.4 was observed used in the open literature. Tris buffers and fasted state simulated intestinal fluid (FaSSIF), with a varying pH from 6.5-7.4, were also used to simulate normal or slightly acidic conditions. Simulated body fluid (SBF), a solution with an ion concentration similar to human blood, was also used in these studies. The mentioned medias are often heated to 37°C to simulate the human body temperature. The main advantage of using the simple medias/solutions is the simplicity in changing one property, *e.g.* pH, without considering other changes at the same time. The drawback, however, is the low translational degree to *in vivo* environments.

- **Blood plasma**

One step closer to mimicking *in vivo* conditions is using human blood plasma. Blood plasma is the liquid part of the blood remaining after the blood cells are excluded by centrifugation. This is more similar to the physiological conditions compared to the simulated medias above. However, the complexity of this media make it difficult to alter single parameters without affecting other properties (altering the viscosity and complex composition of plasma proteins and coagulation factors could make it difficult to conduct particle dissolution measurements). Yet another way of measuring Si NP stability in blood plasma is to measure the degree of particle agglomeration and protein corona adsorption. This can be quantitatively detected by changes in the hydrodynamic diameter, the zeta potential and the polydispersity index over time

in plasma immersion. These measurements give important information about how the particles behave in physiological conditions and give strong indications of the immune clearance rate.

A variety of techniques for measuring Si degradation were identified in literature, which further complicates the inconsistency of the NP stability studies. Three main methods established for this purpose are summarized below (other methods were also used in some of the studies reported in literature, but not included herein).

- **Molybdenum blue assay (MBA)**

The MBA technique is used for the quantification of dissolved silicon. It is a widely used technique in analytical chemistry for colorimetric determination of phosphorus, arsenic, silicon and germanium. The molybdate form blue colored complexes with Si (or another trace element). The amount of blue ions, which is proportional to the amount of Si present, can be measured by absorption using a colorimeter. This is a simple method for quick determination of the dissolved Si content. One limitation is, however, that as the method is also used to determine phosphorus content it is incompatible with the PBS media [72]. The main drawback with this colorimetric analysis method is that it has a limited calibration range where absorption and concentration is linearly related, giving a lower and upper trustworthy detection limit. MBA detection limits for Si are reported to be 5 and 50 mg/L, respectively [73].

- **Inductively coupled plasma (ICP) spectroscopy**

The ICP spectroscopic technique is a widely used element analysis technique with a few variations: ICP-OES (optical emission spectroscopy), ICP-AES (atomic emission spectroscopy) and ICP-MS (mass spectrometry). In all variations, a plasma, an ionized gaseous mixture, of silicon tetrafluoride is created. The ionized gaseous mixture emits photons that are collected by a lens which contain a fingerprints of the species present in the mixture. ICP-AES and -OES are effectively the same method with their names used interchangeably. Both methods also have a linear range for measurement with the advantage that the lower detection limit is very low, down to 9.8 ng/100 μ L. In ICP-MS, plasma is also generated, but it differs from the other two methods presented in that it uses a mass spectrometer system to separate atoms or ions based on their mass-to-charge ratios. In addition to elemental analysis, it also provides isotopic information. The limitations using ICP-MS is that it is a fragile and costly instrument that requires expertise to operate effectively [74].

- **Fluorescence/luminescence intensity**

Fluorescent ligands like fluorescein isothiocyanate (FITC) can be loaded onto pSi NPs and the intensity signal from the solution can be used as an indicator of the amount of particles left in solution during degradation. The intrinsic luminescence of pSi may be used similarly. These methods have been used for quantification of Si dissolution over time, however, it involves many risk parameters like varying photostability and binding affinities. Weak correlations between fluorescence intensity and Si NP content have also been identified [75].

- **Morphological change**

For assessing the remaining material, rather than just the amount of dissolved Si,

certain studies also investigate the morphological changes of the pSi material over time. Electron micrographs of partly dissolved particles are frequently used for this purpose [43, 76, 77]. Such techniques, including SEM and TEM, are appropriate for examination of micro- and nano-sized materials, providing qualitative information about changes in shape, size and pore structure upon dissolution. Other techniques for measuring size distribution, like DLS, are also used for obtaining quantitative size distribution data [78]. It may give information about the homogeneity of the particles and how it is affected upon degradation. All particles may dissolve simultaneously with a reduction in average particle size, or some particles, depending on other properties like size and crystallinity, might completely degrade before others, causing little change in the average size but a wider size distribution. Such data would benefit not only the biomedical industry but can reveal something about how the material is dissolving, rather than only how fast. Such studies on nanosized materials represent a clear knowledge gap in the open literature, as previous literature have only been concerned with micro-sized particles (as far as the present author has been able to establish).

A term frequently used to compare dissolution kinetics is the time at which 50%, 90% or 100% material dissolution is observed, denoted t_{50} , t_{90} and t_{100} . These terms are used in this chapter for comparing data from several studies.

3.2 Stability dependence on particle properties

Several particle properties are expected to affect their stability. In this section, trends in Si stability for particle crystallinity, size and pore size will be discussed, looking at each property individually, aiming to identify patterns or trends in their degree of affecting stability. It should, however, be noted that to get a full understanding of particle stability, that is determined by a complexity of properties, one should regard this information together with particle characterization and surface modification data.

The rate of dissolution consists of two components: 1) the rate of Si dissolution into silicic acid which is determined by the reactivity of the surface, and 2) the rate of diffusion of silicic acid molecules away from the Si surface, which is affected by steric hindrance. An illustration of the two steps of dissolution is shown in Figure 3.1. In other words, the dissolution of pSi NPs is hence reliant on the particles' total surface area and the surface area exposed to the solution. The higher the surface area, the greater the contact with fluid, and the higher the dissolution rates of component one. The diffusion of the dissolved Si, the second component, is affected by steric hindrance such as polymer chains attached to the porous structure or simply by being entrapped inside narrow pores. In addition, surface passivation methods (to be discussed in Section 3.3) may introduce steric hindrance, and also decrease the rate of the Si surface dissolution by altering the reactivity. Lastly, it was established from the open literature that the effect of pH on pSi NP degradation is of importance (to be discussed in Section 3.4).

Comparing the stability of particles with varying surface area is not directly studied in the open literature. However, two common measures affecting the surface area are particle size and porosity, which have been studied for their impacts on stability. Some of these

studies are summarized in the following sections.

Etching Si into mesoporous structures leave hydrogen-terminated surfaces that are highly reactive and will readily form a native oxide in air even though this is a slow process. When assessing stability in a water-based media, *e.g.* in a buffer solution, the surface of the untreated Si particles will also undergo oxidation, creating a thin silica shell. Therefore, few studies are performed to assess the stability of hydrogen-terminated Si. As a result, pSi NPs often undergo surface modifications to enable control of the surface reactivity. Herein, untreated silicon with a low degree of oxidation is regarded as an untreated particle and can be used for studying other particle properties.

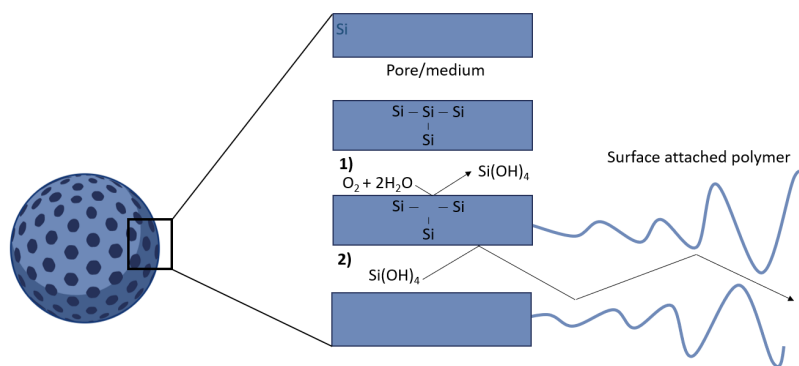


Figure 3.1: Degradation of a pSi NP, depending on two components: 1) the rate of Si dissolution upon reacting with aqueous solution to create orthosilicic acid, and 2) diffusion of orthosilicic acid out of the porous structure and past surface attachments.

3.2.1 Particle size

The effect of the particle size on the dissolution of pSi is not a property specifically investigated in literature. However, different studies use differently sized carriers and comparing their results might give an indication of the size distribution trends impacting the stability.

Untreated particles of different sizes from nano- to micro-sized along with their t_{50} , t_{90} and t_{100} from several studies [8, 79–82] are shown in Table 3.1. It is observed that particles with increasing size generally show an increasing time for dissolution even though the data gives highly variable numbers. As one can see from the table, the $49 \mu\text{m}$ particles showed more similar kinetics to the smaller particles than the $50 \mu\text{m}$ particles. This deviation to the trend might be due to variations in other properties that are also affecting the dissolution kinetics, *e.g.* the degree of crystallinity, as well as slight variations in the testing environment in view of temperature and pH. The $50 \mu\text{m}$ particles were assessed in a medium of pH 6 at RT compared to the pH 7.2 at $37 \text{ }^\circ\text{C}$ (pH is shown to have a great impact on Si dissolution, as discussed in Section 3.4).

Increased surface area per volume for smaller particles is thought to be the main contributor to increased dissolution rates. In addition to the absolute size of the particles, as presented herein, the size distribution may play an important role in the observed degradation kinetics.

3.2.2 Porosity/pore size

The effect of pore size and porosity on the stability of pSi has been studied widely [13, 32, 76, 77]. It was established that a greater pore size and a greater porosity lead to a greater surface area exposed to the surrounding media, thus resulting in a greater dissolution rate. However, the extent of this effect has been hard to quantify experimentally as several other variables like crystallinity and surface modification in addition to porosity also affect the stability.

Table 3.1: Dissolution kinetics parameters for untreated pSi particles of different sizes. The particles are made by electrochemical anodization of porous wafers and are of similar fragmented geometry. RT = room temperature.

Average size	t_{50}	t_{90}	t_{100}	Medium	Reference
100 ± 20 nm	10 min	30 min	3 h	PBS pH 7.4 37°C	[80]
133 ± 12 nm	10 min	2 h	4 h	PBS pH 7.4 37°C	[8]
49 μm	5 min	1 h	7 h	Tris buffer pH 7.2 37°C	[79]
50 μm	1.3 days	5.2 days	7 days	NaCl pH 6 RT	[81]
38-75 μm	9 days	-	-	DI water pH 7 37°C	[82]

Martinez *et al.* [76] investigated how the pore size (and porosity) affects the dissolution kinetics of oxidized and APTES modified photolithography-synthesized pSi discs. Similar particles of 2 μm size with different levels of porosity were immersed in PBS over the course of 24 hours, and the dissolved Si content was measured with ICP-AES at pre-determined time points. They found that porous particles dissolve about ten times more than non-porous particles. A near-linear correlation between the time of 50% and 95% dissolution and pore size was identified, see Figure 3.2b. SEM micrographs were also secured in the study to investigate the size, shape and pore structure transformation of the particles during degradation, see Figure 3.2a. A pattern for degradation was observed with the outer porous ring being dissolved leaving a central core with vertically aligned pores. The porous structure shows a degradation pattern with widening of the pores over time, for both small sized (10 nm) and extra large sized (51 nm) pores, although smaller pores require more time to widen than larger pores according to these images.

Godin *et al.* [77] also studied the affect of the pore size on APTES modified pSi particles. Microparticles of 3.2 μm with either large pores of 30-50 nm or small pores of 10 nm were immersed in PBS at 37 °C. The t_{50} for the particles were found to be 38 and 14 hours for small and large pores respectively. These numbers does not correlate with the linear fit extrapolated by Martinez *et al.* [76] and presented in Figure 3.2. What correlates better with this fit is the t_{95} for large pores after 30 hours, whereas particles with small pores were only degraded at most to 70% after 48 hours [77]. The deviation in the two studies may be due to other distinctions, *e.g.* the distinct surface modification procedures and/or the distribution and number of pores.

Hon *et al.* [80] suggests a non-linear relation between pore size and dissolution rate.

They imply that for pSi particles of a diameter in the order of 100 nm, commonly with 5-20 nm sized pores, the stability does not strongly depend on the pore size within that range. As pore size is decoupled from the degradation rate, it allows for engineering the pore size for beneficial drug loading and release properties without affecting stability [80].

A possible reason for faster degradation of pSi with larger sized pores, despite the fact that smaller pores would increase surface area, is that small pores present a barrier for dissolution due to the steric hindrance of dissolved Si. This would also explain the non-dependence on pore size for pores below a certain size, because once the pores are large enough for sufficient diffusion of dissolved Si away from the pSi surface the dissolution is no longer dominated by diffusion but by surface area effects.

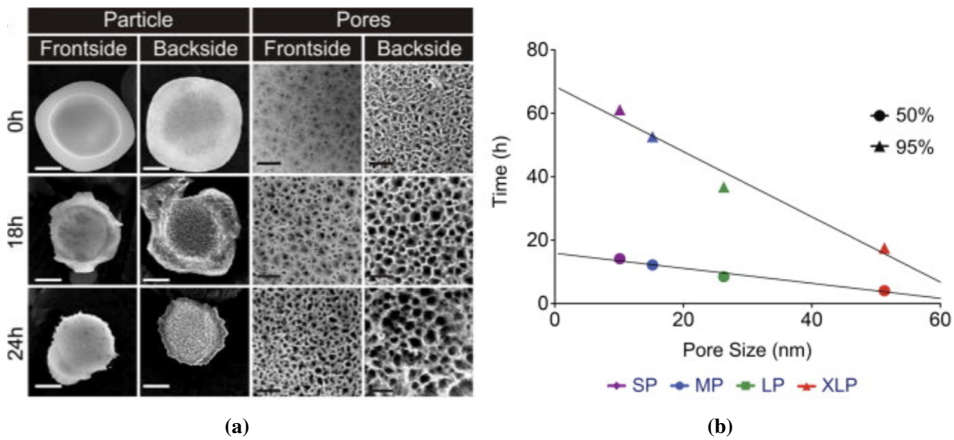


Figure 3.2: Degradation of 2 μm pSi discoidal particles in PBS at 37 $^{\circ}\text{C}$. (a) SEM micrographs showing structural changes for particles with small pores (SP, 10 nm, 46% porosity) over 18 and 24 hours. The left images show changes in particle size and morphology (scale bar = 1 μm) and the right images show changes in pore structure (scale bar = 100 nm). (b) Linear regression of the t_{50} and t_{95} values of dissolved Si measured by ICP-AES versus pore size. Red, green, blue and purple represent particles with extra large pores (XLP, 51 nm, 82% porosity), large pores (LP, 26 nm, 66% porosity), medium pores (MP, 15 nm, 51% porosity) and SP [76].

Salonen *et al.* [33] argue that tunability in pore size of pSi can alter several properties of the material, giving Si a unique position among mesoporous materials. By tuning the porosity, and thus also the degradation rate, the material's biocompatibility may also be tuned. pSi with low porosity is bioinert, meaning it has minimal interaction with the surrounding tissue. Medium porosity makes pSi bioactive while medium to high porosity makes it bioresponsive. To create soluble drug delivery systems or other biomaterials that upon placement within the human body start to dissolve and slowly be replaced by advancing tissue it is desirable with a porosity in the bioresponsive range [33].

In Table 3.1 measured t_{50} , t_{90} and t_{95} have been compared for varying size, and in Figure 3.2 for varying porosification. As can be seen from this table and figure varying particle size, within the nm- μm range, seems to have a larger influence on dissolution kinetics compared to varying pores from 10 to 51 nm.

3.2.3 Crystallinity

The present literature review reveals that the degree of crystallinity has a great impact on the dissolution of porous and non-porous Si NPs. Due to the increased amounts of defects, increased degradation rates in amorphous compared to crystalline Si is expected. Similarly, polycrystalline Si is expected to dissolve faster than monocrystalline Si. This is an important variable to consider, however, pSi NPs are commonly derived by electrochemical anodization of single crystal or polycrystalline wafers and largely retains the crystallinity of such feedstocks.

A central research study [83] reporting the biodegradability of Si makes a point of the considerable differences in dissolution kinetics of amorphous and crystalline (non-porous) Si particles of diameter 0.5-5 μm produced by CVD techniques. In this study it was established that crystalline Si particles are ten times less degraded than amorphous Si particles after four (up to ten) days in a pH 7.4 buffered media kept at 37 $^{\circ}\text{C}$, see Figure 3.3. Using the MBA chemical method for measuring the accumulation of biodegradable products resulted in 80% versus 8% dissolved of amorphous and crystalline Si particles, respectively. It should be noted that this result is for non-porous structures, and the study makes a point about amorphous particles being biodegradable in the same way as porous crystalline Si particles. Non-porous crystalline microparticles are shown not to have these properties [83].

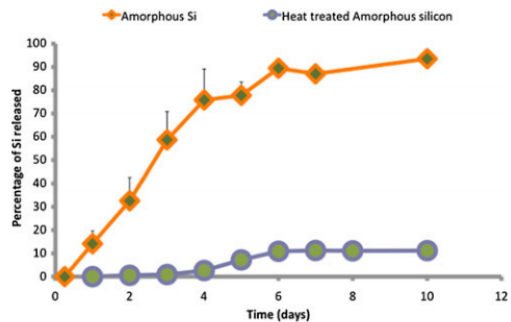


Figure 3.3: MBA assay measurement of dissolution of amorphous and crystalline (heat-treated) Si microparticles in pH 7.4 buffered media at 37 $^{\circ}\text{C}$ [83].

3.3 Stability dependence on surface modifications

The properties of DDS in different environmental conditions, like temperature and pH, are highly susceptible for tunability by chemical surface modifications. The dissolution rate, however, is highly dependent on the presence of surface hydrogen bonds and is reduced upon removal of these bonds, which can be done by surface treatments. Therefore, several post-processing methods are developed for both industrial and research applications of porous Si (some of these methods are described in Section 2.5). The following section aims to compare the dissolution stability of surface modified Si NPs for the breadth of the modification processes available in literature. This information is of utmost importance in understanding how to develop pSi DDS with highly specific stability properties, as well as desired degradation and drug release rates.

3.3.1 Oxidation

Oxidation of Si NPs is reported in literature, using several different procedures. Temperature and duration of oxidation treatment are the most important process parameters determining the silica surface layer thickness which is expected to increase when increasing these two variables ultimately increasing stability and decreasing dissolution rates of the material. Thermal oxidation is the most common surface modification technique for stabilizing pSi NPs and many studies have documented the stability of thermally oxidized particles. Figure 3.4 show an increase in the stability of particles for higher oxidation temperatures and oxidation times. These data presented in the figure summarize data collected from multiple research studies that all studied dissolution of thermally oxidized pSi NPs by either MBA or ICP techniques [14, 43, 79, 80, 84]. A 1-2 hours oxidation time was used for all the indicated oxidation temperatures (horizontal axis) in Figure 3.4a, while for the data in Figure 3.4b a rapid thermal process under 800 °C for 90 seconds was used before a post-processing step at 60 °C during the indicated oxidation times. These dissolution studies are all done in PBS at 37 °C and with a pH close to 7.

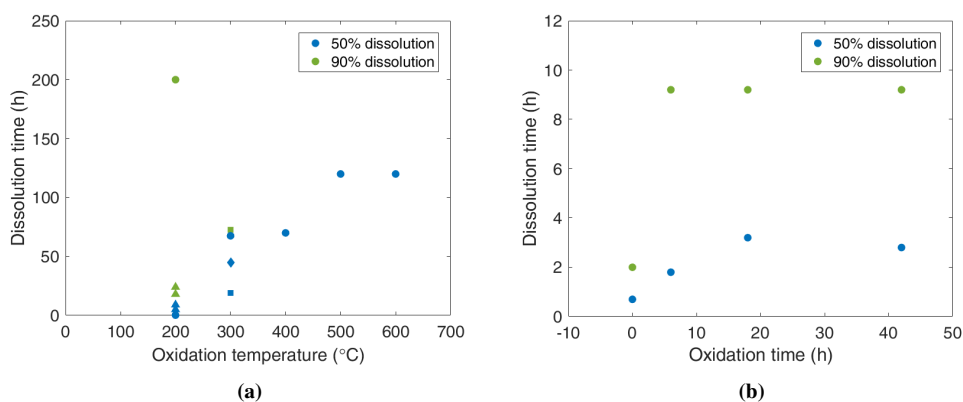


Figure 3.4: Dissolution of pSi NPs as function of (a) oxidation temperature (1 or 2 hours oxidation time) or (b) oxidation time (for 60 °C oxidation temperature, of pSi NPs preoxidized by rapid thermal treatment at 800 °C for 90 sec). The dissolution rate was measured by establishing the amount of dissolved silicon using MBA or ICP-OES/MS. The data presented in (a) in squares, triangles, circles and diamonds are taken from [14, 43, 79, 84], respectively. Data in (b) is taken from [80].

Godin *et al.* [43] have monitored the morphological changes of oxidized nanodiscs upon dissolution in addition to quantification of dissolved Si. SEM images from this study, shown in Figure 3.5, indicate that the pSi particles maintain their general shape during degradation over 8 h. It can also be seen that the non-porous film, forming the bottom of the porous structure, is working as a mechanical enhancement layer that maintains the structure and is retained upon preferable degradation of the porous structure [43]. As mentioned above, this is an expected behavior as the porous structure has a high surface area for dissolution compared to a solid film.

3.3.2 Polyethylene glycol (PEGylation)

PEGylation is a common way of stabilizing biomedical materials for *in vivo* applications as PEG polymers have shown great biocompatibility and an ability to shield the drug carrier particles from immune clearance. There are several different types of PEG with chemical formula $H-(O-CH_2-CH_2)_n-OH$, with different lengths (n) giving different molecular weight (MW). Godin *et al.* [77], Nakki *et al.* [14] and Kang *et al.* [75] have studied the degradation rates for pSi NPs coated with PEG of different MW in PBS at pH around 7.2. Kang *et al.* measured Si degradation by simultaneous release of a conjugated fluorescent probe (FITC) over 2 hours and used a mathematical model for predicting the t_{50} value, while Godin *et al.* [77], Nakki *et al.* [14] and Kang *et al.* [75] used empirical ICP measurements. The data collected from these studies are summarized in Figure 3.6.

As can be seen from Figure 3.6, the stability of PEG-modified particles is not strongly related to PEG MW below 1.4 kDa. For 50% degradation, it is seen that higher MW PEG has a clear lower dissolution rate. This is also true for the t_{90} data as the maximum detected erosion of particles with 3.4 and 5 kDa PEG were identified to 55% and 65% respectively over the duration of the experiment, *i.e.* over 72 hours.

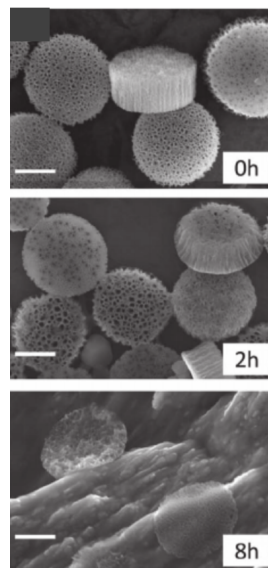


Figure 3.5: SEM of 1000x400 nm pSi disks during degradation [43]. Scale bars are 500 nm.

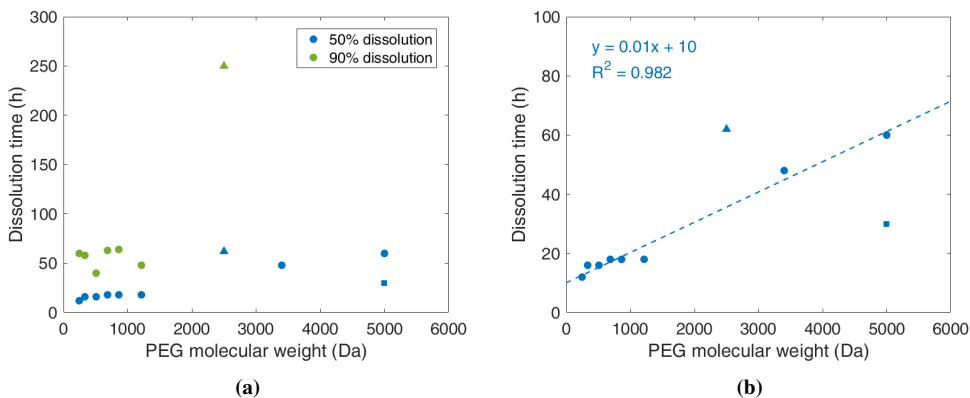


Figure 3.6: Dissolution of pSi NPs as function of PEG surface coating molecular weight. (a) Yellow markers show t_{90} values while blue markers show t_{50} values. Triangles, squares and circles indicate data taken from [14, 75, 77], respectively. (b) t_{50} values (same as in a) and a simple two-variable linear regression of data from [77].

The t_{90} data from Godin *et al.* [77] seems to follow a linear trend with PEG MW. The data from the other studies, however, does not seem to follow this trend, indicating that the measurement techniques, as well as the other variables, also impact the results. Furthermore, these effects are limited as the data points are within a similar range. The data in Figure 3.6 also seems to be independent of particle size as particles of size 3.2 μm , 162 nm and 190 nm were used by Godin *et al.* [77], Nakki *et al.* [14] and Kang *et al.* [75], respectively. This shows that coating particles with PEG may be done to create a surface chemistry-dependent erosion rate, rather than one that is bulk-properties dependent.

Godin *et al.* [77] argue that the dissolution rate of PEG-coated particles is associated with a diffusive release of silicic acid from the pSi matrix into the surrounding solution. Conjugating with PEG of higher MW will increasingly hinder the diffusion of dissolved silicic acid from the pores due to increased steric interactions with the polymer chains [77]. This argument supports the increased dissolution rates seen for lower MW PEG.

3.3.3 Other surface modifications and a comparison between the techniques

UnTHCpSi is another widely used effective surface modification approach with thermally conjugated undecylenic acid species on the Si surface. Tzur-Balter *et al.* identified a t_{50} of 7 days and a t_{100} of 20 days for UnTHCpSi particles of 2-18 μm in PBS at pH 7.4 and at 37°C [85]. Another study done by Nieto *et al.* [11] demonstrated superior stability of about 50 μm UnTHCpSi particles with only 20% of the total amount of Si dissolved after 30 days' immersion in a syringe flow chamber with a PBS solution. The Si erosion of UnTHCpSi microparticles was detected as dissolved oxides of Si by ICP-AES/OES in both studies. A major difference in these studies is, however, the particle size that shows that undecylenic acid modification alone may not be able to nullify the size effect of the particles.

Carbonization is yet another widely used technique for silicon surface passivation. As a comparative study, Nieto *et al.* [11] investigated the effect of surface carbonization and the undecylenic acid functionalized particles described above. Similar particles of 50 μm size modified by hydrosilylation of 1-dodecene (pSi-C12) or by mild oxidation followed by silanization of an 8-hydrocarbon chain (pSiO₂-C8) were immersed in a similar PBS solution and dissolution was recorded similarly. Increased stability compared to UnTHCpSi was observed for both modification strategies, with 5% and 17% dissolution over 30 days of the pSi-C12 and pSiO₂-C8, respectively [11].

Alkoxysilane surface modifications are often used for their versatility in conjugating various hydrocarbon or secondary functionalized species onto Si surfaces, in addition to adding stability to the Si material. APTES, MPTES and APDMES are some examples of alkoxysilane species used for surface modification of pSi in literature. Godin *et al.* [77] reported t_{50} and t_{100} values for surface oxidized followed by APTES modified 3.2 μm particles to be 10 and 48 h. Kang *et al.* [75] studied the degradation of MPTES and APDMES modified particles, which were previously modified with maleimide and PEG, of 210-240 nm in PBS media at physiological conditions. The t_{50} for the MPTES modified particles was recorded as 9.6 h while for APDMES it was 8.9 h [75], which is quite similar to the corresponding value for APTES modified particles. Both studies used ICP-AES to

study the Si dissolution over time. The great difference in particle size seems to have little effect in this case, which might be due to the alkoxy silane functionalization's ability to nullify size effects, or it might be because size effects dominate for larger particles above 40-50 μm so that particles below this range will not be affected by size effects to the same degree as those of the modifications above.

To compare the ability of different surface modifications to increase stability, averages of the identified t_{50} and t_{90} values of various surface modified Si NPS found in literature (along with average sizes) are shown in Figure 3.7. It should be noted that these averages does not account for crystallinity, porosity, or other particle properties that has been shown to have a great impact on the dissolution kinetics. It also does not account for the variations in the number of data points behind the averages (in the case of thee oxidation treatments there are several data points whereas for carbonization there is only one). However, these numbers are meant as a rough overview of the stability trends for the various surface modifications available in literature. Generally it can be seen that t_{50} and t_{90} are higher for all the surface modified particles than for the untreated particles.

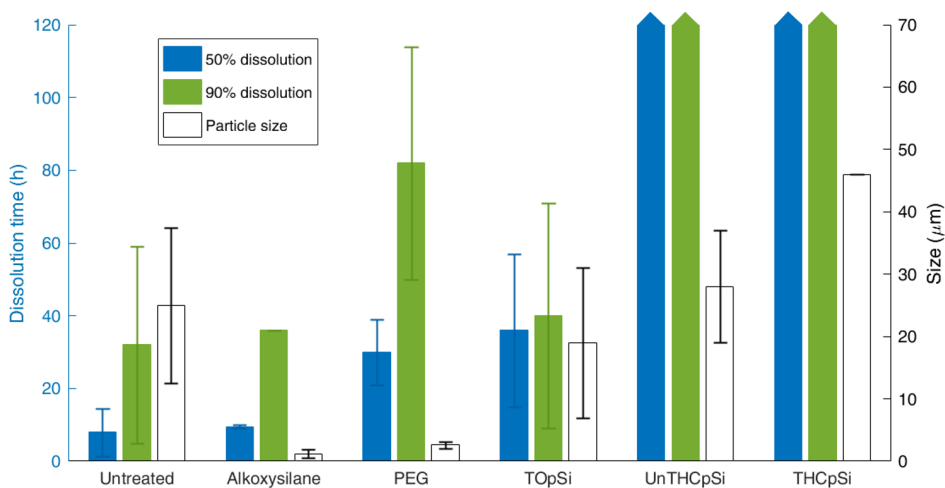


Figure 3.7: The present plot represents the average of dissolution parameters together with sizes of the particles studied with standard deviations. Averages estimated from data found for untreated Si particles [8, 79–82], alkoxy silane [75, 77], PEG [14, 75, 77], thermal oxidation [14, 43, 79, 80, 84], undecylenic acid (UnTHCpSi) [11, 85] and thermal carbonization (THCpSi) [11] surface modified Si particles.

In the present review of the open literature, particle size is identified as one of the major contributing factors to dissolution. As a result, the average particle size was used in Figure 3.7 to investigate whether there is a size-dependent trend for the modified particles. UnTHCpSi and THCpSi seem to have superior stability with t_{50} and t_{90} far exceeding the other surface modifications. However, pSi particles of larger sizes are used as starting material for functionalization in these studies. With increasing size, there seems to be a clear trend towards lower dissolution rates. However, the stability after certain modifications, *e.g.* after PEGylation, show increased stability despite small sized particles. This might be

explained by certain surface modifications having the ability to nullify size effects or have an increasing ability to stabilize the pSi particles.

3.4 Stability dependence on medium pH

Testing behavior of newly developed drugs over a pH range could give valuable information about interactions in various tissues. Furthermore, DDS can be tailored for specific responses to several environmental factors, including pH, to control the behavior of the loaded drug. This is of specific interest since different compartments of the human body have different pH values. The blood has a near-constant pH of 7.4, the stomach is acidic with pH down to 1.5-2 while the intestines are slightly basic with pH up to 8.5 [86]. In other words, it is important to understand how the drug will act in these environments upon both oral and intravenous administration, and pH differences can even be exploited for targeted drug release with increased dissolution for instance in the basic intestines compared to the acidic stomach upon oral administration. This phenomena is also exploited in development of stimuli-responsive carriers for specific delivery to tumors, inflamed tissue or endosomal release that often have slightly acidic environments compared to the "normal" physiological pH of 7.4 [86–88].

The dissolution of pSi NPs is, as previously mentioned, particle size, porosity and pH-dependent, which will have an impact on the use of pSi as a drug delivery vehicle. Particle size and surface chemistry can therefore be used to tailor pSi dissolution rates. In low pH environments, *e.g. in the stomach*, pSi has reduced dissolution which protects the loaded molecule against degradation and release, while at higher pH (neutral to alkaline, *i.e. in the intestines*) the pSi dissolution will occur thereby releasing the loaded API.

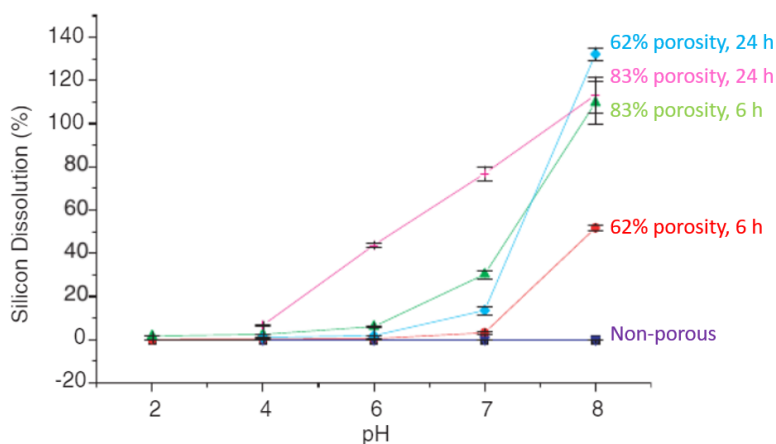


Figure 3.8: Effect of pH on the dissolution of porous and non-porous Si wafers that are oxidized by storage in ambient air over one week. Wafers with 62 and 88% porosity were immersed in five aqueous buffer solutions and ICP-OES was used to measure the dissolved Si content at each pH after 6 h and 24 h, respectively. The figure is adapted from [13].

Most pSi stability studies are performed under standard physiological conditions at

pH near 7 and this can explain why pH-dependent dissolution is not a widely documented property for NPs in literature. Anderson *et al.* [13] studied the pH medium dependence for dissolution of mesoporous Si wafers. They found a strong dependence on pH with acidic solutions having evident lower erosion ability than neutral and basic solutions. The wafers were stored in ambient air for one week before exposure to buffer solutions with different pH, leading to a native oxidation layer formation but otherwise unmodified. The results from the study are presented in Figure 3.8. As can be seen from the figure, a negligible dissolution was observed at pH<6 for the Si wafers with up to 88% porosity. At pH 7, the dissolution rates were increased for wafers of both 62 and 83% porosity, and 100% dissolution was observed at pH 8 over a period of 24 hours [13]. This study also generally underpins the claim that higher porosity demonstrate higher dissolution rates as previously discussed in Section 3.2.2.

Table 3.2: Dissolution kinetics of 50 μm pSi microparticles produced by ultrasonification of electrochemical anodized Si wafers. Buffer solutions of pH 6 and 9 were used to study pH-dependence of dissolution kinetics. Data taken from [81].

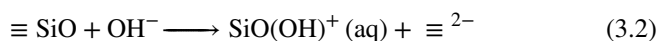
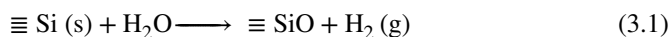
	Unoxidized	TOpSi 400 °C	TOpSi 800 °C
pH 6	$t_{50} = 31 \text{ h}$ $t_{100} = 7 \text{ days}$	3% dissolved at 7 days	3% dissolved at 7 days
pH 9	$t_{50} = 7 \text{ h}$ $t_{100} = 4 \text{ days}$	$t_{50} = 19 \text{ h}$ $t_{100} = 7 \text{ days}$	35% dissolved at 7 days

For pSi NPs we can also expect higher dissolution rates in alkaline solutions similar to the observations for pSi wafers by Anderson *et al.* [13]. Furthermore, the dissolution rate of particles is expected to be higher due to higher surface area exposed to the media, with higher dissolution rates for smaller particles. Jarvis *et al.* [81] studied pH-dependence on dissolution of 50 μm porous Si particles at pH 6 and 9. Both untreated and oxidized particles at 400 and 800°C was studied. The results from the study have been summarized in Table 3.2. As can be seen from the table, the surface oxidation heavily decreased the dissolution rates with less dissolution at higher oxidation temperatures. The pH 6 solution showed no difference between the two coating procedures with negligible dissolution, while the pH 9 solution showed a much higher dissolution of the 400°C treated wafers than the 800°C treated ones [81]. This indicates that oxidation at higher temperatures will create a thicker coating for increased dissolution resistance, as discussed in Section 3.3.1, in addition to the pH-dependent stability.

3.4.1 Mechanism and other applications for pH-dependent Si dissolution

The findings in the open literature for pSi wafers and microparticles support the idea that Si has a pH-dependent dissolution mechanism [13, 81]. This is in accordance with knowledge on conventional Si etching procedures. Potassium hydroxide (KOH) is often used for anisotropic etching of Si wafers, with increased etch rate for certain crystallographic planes. Other sources of hydroxide ions are also used for this purpose, supporting the

idea of pH-dependent dissolution mechanism [89]. It is believed that it is the high content of OH^- ions that cause the rapid Si degradation in alkaline solutions. These negatively charged ions have the ability to react with surface oxide groups upon nucleophilic attack. A proposed reaction route suggests that it is soluble orthosilicic acid and hydrogen gas that is produced through three reaction steps: oxidation of surface Si (3.1), a hydroxide attack forming a soluble Si intermediate $\text{SiO}(\text{OH})^+$ compound (3.2), and formation of silicic acid from the intermediate compound in an alkaline environment (3.3) [90]. It has been proven that the higher the concentration of OH^- ions, the higher the rate of silicic acid by-product formation resulting in faster Si crystal structure dissolution.



The symbols in reactions 3.1 and 3.2 are defined as follows: $\equiv\text{Si}$ and $\equiv\text{SiO}$ represent a Si site and an oxidized Si site at the surface, respectively, while \equiv^{2-} represents a vacancy site at the Si surface.

The pH-dependent dissolution mechanism of pSi NPs has also been studied for applications related to the by-products produced in the process. The oxidation of Si into SiO_2 is in other words a step in the dissolution which produces hydrogen gas as shown in reaction 3.1 above. It has been reported that porous Si produces hydrogen gas under reaction with water with an increase in hydrogen evolution rate in the presence of higher hydroxide concentration as well as when using nanosized Si [91, 92]. This is likely due to higher dissolution rates of Si at higher pH, making underlying layers in the Si structure available for oxidation. Hydrogen gas is useful for a variety of applications and the rapid dissolution of nanostructured Si in water or alkaline solutions provide an alternative approach for producing hydrogen. This might be useful as a technique to measure Si dissolution, as an alternative to both the MBA and ICP techniques, for energy-dense energy carrier applications [93] and for health-related applications as hydrogen is shown to eliminate stress- and disease-related hydroxyl radicals in the body [91]. The latter is another benefit of developing DDS of pSi materials.

3.5 Key findings on silicon stability in literature

The degradation profile of Si and pSi NPs in biorelevant medium is a valuable tool for predicting *in vivo* stability properties. The importance of choosing appropriate media for studying desired environmental impacts should not be underestimated. Furthermore, the dissolution kinetics of these particles are highly dependent on the various particle properties, making it hard to draw conclusions regarding individual particle properties in isolation. However, several trends for Si NP stability are identified in this review. Surface modifications will stabilize the particles due to surface passivation, and larger polymer molecules may have an increasing impact on the diffusion of dissolved Si species. The endless possibilities in Si surface modification may be used for tailoring dissolution kinetics for different *in vivo* applications. Except for the surface modifications, the factors

most likely to accelerate the dissolution behaviour of pSi NPs are decreasing size and crystallinity and increasing porosity. Increasing medium pH is found to be a major contributor to increasing dissolution rates of pSi. An interesting feature of pSi is the biodegradation property which is a major advantage in the drug delivery applications of the material. The pH-dependent stability is another interesting feature that can be exploited for various applications in drug delivery. An interesting approach is to study how this pH-dependent stability affects the remaining DDS material and its properties.

Materials and Experimental Methods

The materials used for the three experimental parts: characterization, stability testing in buffer solutions of different pH and cytotoxicity studies of the pristine and porous IFE particles, are presented in the present chapter. The methodology of the three parts are explained in Section 4.3-4.5, respectively. A description of the Si NP synthesis and etching process is also included in Section 4.2.

4.1 Materials

In the present study, the pristine Si NPs used in the characterization, etching, stability and cytotoxicity studies, as well as the etched porosified particles, were provided from IFE (from here on referred to as the IFE Si NPs). The chemicals used for preparation of the buffer solutions, *i.e.* citric acid monohydrate, sodium citrate dihydrate and ammonium chloride in powder form, and ammonia in 32% solution, were also provided by IFE and obtained from Sigma-Aldrich.

The materials required for cell culturing and for the viability studies, including disposables, were provided by the Department of Physics at the Norwegian University of Science and Technology (NTNU). The cell culture media and the required supplements were obtained from Gibco, the black 96 well plates with transparent bottoms from Corning Inc., and the AlamarBlue reagent was obtained from Invitrogen, Thermo Fisher Scientific.

4.2 Synthesis and etching of silicon nanoparticles

The synthesis and etching of the IFE Si NPs was performed outside the framework of the present work. However, as it can give valuable information about the behavior of the

material during the characterization, stability and cell viability studies, the different steps of the synthesis and etching procedures will be summarized below.

The IFE Si NPs were produced in a direct process in a Free Space Reactor (FSR) using monosilane (SiH_4) gas precursors. Amorphous Si was produced in this process and heat treatment was conducted to form crystalline Si NPs.

For etching 500 mg of the IFE Si NPs, synthesized by the above-mentioned method, were suspended in 10 mL of ethanol using probe ultrasonication conducted during 60 minutes. The etching of the IFE Si NPs to create nanosized pores was done by a ReEtching method, as elaborated in Section 2.4.2. In this step, hydrofluoric acid (48% HF) was used with electron hole injection mediated by continuous supply of hydrogen peroxide (30% H_2O_2) and catalytic amounts of vanadium pentoxide (V_2O_5) in an ice-bath to manage the heat development. The etching solution was made of 10 mL HF and 20 mL glacial acetic acid, and 150 mg of V_2O_5 was dissolved in the mixture. The etching reaction was initiated as the IFE Si NP ethanol solution was added to the etching solution. Continuous stirring with a magnetic stir bar at 450 rpm as well as argon gas bubbling was used to retain a homogeneous dispersion. The reaction was carried out for 1 h with continuous injection of H_2O_2 from a syringe pump at a rate of 0.8 mL/h. The synthesis and etching process of the IFE Si NPs is schematically illustrated in Figure 4.1.¹

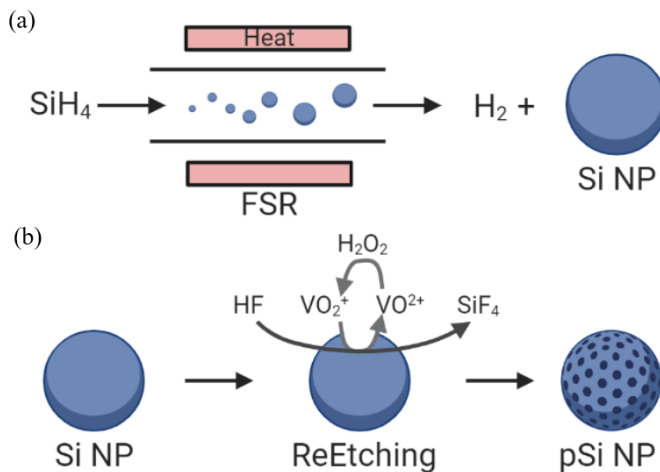


Figure 4.1: Schematic illustration of synthesis and etching process of the IFE Si NPs. (a) Synthesis of Si NPs in a Free Space Reactor (FSR) using monosilane (SiH_4) gas precursors. (b) Porosification of the Si NPs was obtained by using a vanadium-based catalytic reaction called Regenerative Electroless Etching (ReEtching).

4.3 Particle characterization

Characterization of the pristine and porous IFE Si NP powders was performed by several different methods to understand how the etching affected their morphology, and to deter-

¹Particle synthesis and etching experiments were conducted by researchers at IFE.

mine if the morphology has an effect on the stability and cell viability results. The methods used for particle characterization were scanning electron microscopy (SEM), dynamic light scattering (DLS), x-ray diffraction (XRD) and energy dispersive x-ray spectroscopy (EDS), in combination with transmission electron microscopy (TEM) data. Structural and morphological characterization was performed using SEM, the hydrodynamic size distribution was measured by DLS, the crystal structure verified by XRD, and elemental composition of the particles obtained by EDS. In this regards it should be mentioned that several IFE Si NP batches were analyzed, but only two particle batches were systematically used in the different analyses and for stability and toxicity studies.

4.3.1 Scanning Electron Microscopy

During SEM analyses a high-energy electron beam is focused onto an electrically conductive sample by electromagnetic coils. The beam scans across the sample surface and electron beam-specimen interactions produces a variety of signals. Backscattered and secondary electrons, which arise from the inelastic and ionization interaction, are detected to create a topological image of the specimen. Using electrons makes it possible to distinguish features smaller than those seen in light optical microscopy, with a theoretical maximum resolution determined by the electron wavelength [94].

A field emission scanning electron microscope (Hitachi, model S-4800) was used to secure SEM micrographs of the two IFE Si NP samples, as well as for assessing morphological changes in stability studies.

Sample preparation on aluminum stubs was performed by diluting a few mg of Si NPs in deionized (DI) water (18.2 M Ω) at an appropriate concentration, ultrasonicing the solution to create a homogeneous dispersion before using a pipette to add a few drops of the solution onto the stub and letting it dry on a 60-70°C hot plate. An accelerating voltage of 15-30 kV and a working distance of 5-10 mm was used, adjusted for optimal image resolution. The SEM was also used in transmission mode, using a detector measuring the intensity of the electrons transmitted through the sample, to try to identify porous structures in the etched IFE Si NPs. For SEM imaging in transmission mode, copper TEM grids were used. The sample preparation was carried out in a similar fashion as described above.

4.3.2 Dynamic Light Scattering

DLS analyses were performed using a *Zetasizer Nano ZSP* (Malvern) and the accompanying Malvern software. The samples were maintained in a water solution and ultrasonicated for approximately 3 min before the measurements was performed. The sample concentrations were adjusted to give an attenuation coefficient between 2-11 for accurate measurements. A theoretical introduction to the technical principles of DLS in regards to particle size measurements is presented in Section 2.7.

Three repeated measurements with 6-14 scans of 10 seconds were taken and an average of the three measurements was then created. If insufficient quality of the data was obtained, an automatic setup was used instead to obtain an indicator stating "*good quality*" of the data. Statistical analysis is embedded in the number of scans done for each sample in addition to taking the average of the three measurements as the final data for each sample.

The viscosity of water was set as the sample viscosity and was heated to a temperature of 25 °C. Backscattered intensity was measured at an angle of 173°.

Calibration measurements of various Si particle concentrations were conducted by diluting one stock sample of 1 mg/mL to 1:4 using DI water. Dilution was repeated three times, resulting in concentrations varying between 0.0156-1 mg/mL. In Figure 4.2 the variation in concentration is presented. As can be seen in the figure, the concentration had little effect on the resulting hydrodynamic diameter measured and that higher concentrations may result in higher statistical credibility by smaller standard deviations. Thus, a sample concentration of approximately 1 mg/mL was aimed at for all DLS size measurements.

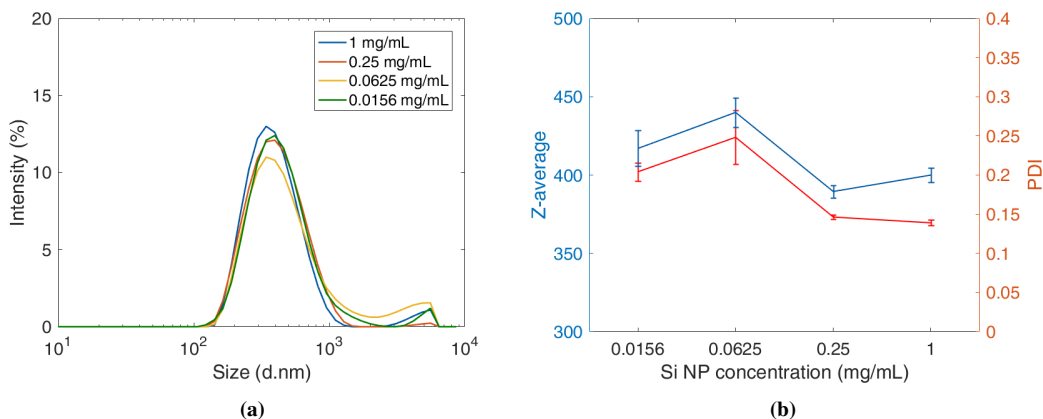


Figure 4.2: Calibration data for the DLS measurements of the IFE Si NPs at different concentrations. (a) Intensity weighted size distribution and (b) corresponding Z-average (blue) and PDI (red) values of several concentrations plotted as averages with standard deviations of $n=3$ measurements.

The particle size distributions presented herein are given in terms of intensity, but number and volume weighted distributions were also calculated by the software.

4.3.3 X-ray Diffraction

Phase identification of the IFE Si NP samples as well as the degree of crystallinity was examined by XRD. When a beam of x-rays strikes a structure that has long-range orders, *e.g.* a crystalline solid, the beam is scattered in different directions and interfere to create diffraction patterns. Detecting the intensities of the diffracted beam at different angles give information about the crystal structure of the sample. The position of the peaks is related to the elements and crystal structure of the material, and the sharpness of the peaks to the size of the crystalline domains. Sharp peaks indicate a crystalline material, while broader peaks and background signal indicate an amorphous material [95].

The XRD analysis was performed on dry IFE Si NP powder using a Bruker-AXS D8 Advance with a CuK_α source and LynxEye detector. The analysis was carried out at an angle from 20° to 60° at 1.33° min⁻¹.

4.3.4 Energy Dispersive X-ray spectroscopy

EDS is used for chemical characterization of a sample by detecting x-rays produced by electron beam-specimen interactions. The energy of these x-rays provides compositional information, as they are characteristic for the electromagnetic emission spectrum of the atomic species present [96]. High resolution EDS data was acquired in parallel with topographic information obtained by transmission electron microscopy (TEM), using a high angle annular dark field (HAADF) detector and an acceleration voltage of 300 kV. HAADF TEM images were also taken to confirm particle porosity ².

4.4 Particle stability studies

Particle stability studies were performed by assessing the particle size distributions, as well as the morphological changes upon dispersion in different pH solutions. The intention was to study both dissolution and aggregation stability of colloid particle solutions as they are both important for overall *in vivo* performance.

Both pristine and porous IFE Si NPs were immersed in water-based buffers over a period of 24 hours and changes in morphology and size distribution were then observed using SEM and DLS. Two buffer systems were utilized to cover a pH range of 4-10.

4.4.1 Preparation of buffer solutions

Citric acid ($C_6H_8O_7$) and sodium citrate ($Na_3C_6H_5O_7$) was used to create buffer solutions of pH 4, 5, 6 and 7. The mass of each compound for each pH solution is presented in Table 4.1. For each solution the compounds were first dissolved in 50 mL DI water and pH paper was used to verify the solution pH (Tritest, Macherey-Nagel and Universal indicator, Merck). The solutions were later diluted to a total of 125 mL using DI water to obtain approximately 100 mM solutions.

Table 4.1: Amount of each compound used to create the citric acid-sodium citrate buffer solutions at the given pH values.

pH	Citric acid monohydrate (g)	Sodium citrate dihydrate (g)
4	1.72	1.27
5	1.08	2.17
6	0.50	2.98
7	0.11	3.40

Ammonium chloride (NH_4Cl) and ammonia (NH_3) solutions were used to prepare buffer solutions of pH 8, 9 and 10. The ammonia solution was diluted to 3.2% by adding 2 mL of 32% ammonia to 18 mL of DI water. For making the pH 8 solutions the 3.2%

²TEM imaging and EDS analysis of Si NPs was conducted by IFE researchers at a TEM facility at the University of Oslo.

ammonia solution was further diluted to 0.32% by adding 1 mL of ammonia 3.2% solution to 9 mL of DI water. The mass of ammonium chloride and the volume of ammonia (3.2% or 0.32%) used for each pH solution are presented in Table 4.2. For each solution the ammonium chloride was first dissolved in 50 mL of DI water. The desired amount of ammonia was then added and the pH was verified using pH paper before the solution was diluted to a total of 125 mL using DI water to obtain approximately 100 mM solutions.

Table 4.2: Amount of each compound used to create the ammonia-ammonium chloride buffer solutions at the given pH values.

pH	Ammonium chloride (g)	Ammonia 3.2 wt% (mL)
8	0.64	4.0 (0.32 wt%)*
9	0.43	2.7
10	0.10	6.5

*3.2 wt% solution was diluted x10 to obtain a more appropriate concentration

4.4.2 Sampling over time and pH range

The pristine Si sample (20 mg) was immersed in 15 mL of each buffer solution with a distinct pH, giving an initial concentration of the colloid solution of 1.3 mg/mL. This concentration was assumed to decrease over time as some of the particles dissolve. Before storage at room temperature, the solution was ultrasonicated for a few minutes to disperse the NPs in the liquid to get a homogeneously distributed solution through rapid oscillation of agglomerated particles using ultrasonic frequency waves.

Aliquots of 2 mL were taken out at the time points 10 min, 30 min, 1 h, 2 h, 4 h, 8 h and 24 h after start of the experiment. The samples reaction was immediately quenched by dilution with DI water and subsequently centrifuged for 40-60 min (depending on how fast the particles settle) at 4400 rpm with an exchange of water followed by ultrasonication in between dilutions for washing out the buffer salts. The final samples were kept in approximately 1 mL of DI water and stored for maximum a couple of days before DLS measurements were performed. The same procedure was repeated for all the pH buffer solutions, and for the porous IFE Si NP sample.

DLS was performed on all sample aliquots following the protocol described in Section 4.3.2 to examine changes in size distribution and hydrodynamic diameter over immersion time in different buffer solutions. Certain samples from the stability studies were prepared for SEM analyses following the protocol described in Section 4.3.1 for assessing changes in morphology during degradation. The samples were removed from the buffer solutions after 8 hours immersion in pH 4 and pH 7-10, and SEM samples were prepared by letting a few drops of the 1:10 diluted stability samples (in DI water) dry on SEM stubs at 60-70°C.

4.5 *In vitro* cytotoxicity studies

The AlamarBlue cell viability reagent was used to determine *in vitro* cytotoxicity as function of IFE Si NP type (pristine and porous), particle concentration, incubation time and

cell line. Viability assay results were supplemented by light optical microscopy images.

The AlamarBlue assay is a conventional assay for measuring cell viability and proliferation of mammalian and microbial cells. It functions as a cell health indicator by using the reducing power of living cells to quantitatively measure the proliferation of various mammalian and microbial cell lines. When the cells are alive, they maintain a reducing environment by active maintenance of high levels of various reducing components of the biological respiration chain within the cytosol of the cell. Continued growth maintains a reduced environment while inhibition of growth maintains an oxidized environment. Resazurin, the active ingredient of AlamarBlue, is a non-toxic cell-permeable compound that is virtually non-fluorescent. Upon entering the reducing environment in viable cells, resazurin is continuously reduced to resorufin, which is a highly fluorescent compound as schematically illustrated in Figure 4.3. Larger fluorescence emission intensity values thus correlate to increased resorufin amounts which are proportional to the number of viable cells [97].

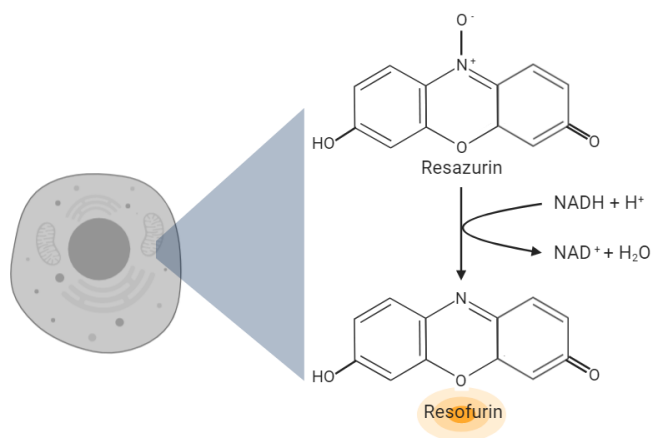


Figure 4.3: The AlamarBlue reagent interacts with the reducing environment of live cells by reacting with key players of their metabolism, such as nicotinamide adenine dinucleotide (NADH). The non-fluorescent compound resazurin is reduced to the fluorescent compound resorufin when permeating into live cells.

4.5.1 Nanoparticle sterilization techniques

Initially, the IFE Si NPs were tested using the cell viability assay without sterilization. However, inaccurate results were observed, possibly caused by microbial infection in the samples due to non-sterilized particles. To try to improve the results, particle sterilization was added as another preparation step prior to the cell viability studies. As there are requirements for sterilization of materials intended for pharmaceutical usage, it is also interesting to study the influence of particle sterilization techniques on cell viability.

Three different methods for sterilization of pristine and porous IFE Si NPs were attempted prior to cell viability studies. Their methodologies are described in the list below.

- Exposure to heat by autoclaving at 121°C for 15 minutes. 50 mg of IFE Si NPs (pristine and porous separately) were immersed in 5 mL phosphate-buffered saline (PBS) and ultrasonicated for 3 minutes before autoclaving. Glass vials were covered by autoclavable paper for steam exchange without disturbing the colloid solution.
- Ethanol wash of pristine and porous IFE Si NPs was done by immersing 50 mg particles in 5 mL 70% ethanol for 30 minutes. Afterwards, 20 minutes of centrifugation at 5000 rpm followed by additional 20 min of centrifugation at 6000 rpm was used to create a Si pellet. The ethanol supernatant was drained and PBS was added for washing the remaining ethanol followed by 20 min centrifugation at 7000 rpm before draining and resuspending in 5 mL PBS.
- Filtering of 50 mg IFE Si NPs suspended in 5 mL PBS was attempted using various filters. The colloidal solutions were ultrasonicated for 10 min prior to filtering. The pristine particle solution was filtered using filters of pore size 0.45 μm and 0.8 μm , while porous particles using filters of pore size 1.2 μm and 5 μm .

4.5.2 AlamarBlue assay and optical microscopy imaging methodology

PC3 and KPC cell lines were maintained in cell culture medium Dulbecco's Modified Eagle Media (DMEM) containing 4.5 g/L D-Glucose supplemented by 10% fetal bovine serum (FBS), 1% Penicillin-Streptomycin and 0.5% L-glutamine. The cell culture was regularly splitted to maintain a critical cell concentration. For viability studies, PC3 and KPC cells were seeded at a density of 4000 and 3000 cells/well, respectively, in black 96 well plates with transparent bottom³. Two cell lines were used for comparative reasons as different cell lines often have different treatment responses. 48 hours after seeding, the growth media was replaced by a growth medium containing either the pristine or porous IFE Si NPs, and incubated at 37 °C with 5% CO₂. To study how cytotoxicity is related to incubation time, three separate plates incubated for three distinct periods for of both cell lines were used. Incubation times of 3, 24 and 48 hours were tested. For both porous and pristine samples, concentrations between 0.063 and 1 mg/mL IFE Si NPs, created by serial dilutions in a cell culturing medium, were prepared. Incubation was stopped by rinsing the cells twice with PBS, after which the growth medium in each well was replaced by 100 μl of AlamarBlue (1:10 dilution with the growth media). After two hours of incubation with AlamarBlue, fluorescence was measured with the spectrophotometer *SpectraMax i3x* (Molecular Devices) with excitation wavelength at 560 nm and a detection of emission at 590 nm. Cell viability was calculated by dividing the fluorescence intensity of the treated wells (FI_{NP}) by the fluorescence intensity of the control wells with cells incubated with only growth medium (FI_C). In the case of background intensity of the growth media (FI_B), it is subtracted from both the control and the NP treatment intensities, resulting in the following expression for cell viability (CV):

$$\%CV = \frac{FI_{NP} - FI_B}{FI_C - FI_B} \times 100 \quad (4.1)$$

³Cell culturing and seeding of cells in well plates was done by the Chief Engineer at the cell lab at the Institute of Physics, NTNU.

For each IFE Si NP sample, and in the case of each incubation time and cell line, the cell viability was plotted against the corresponding particle concentration. The mean of the %CV of at least 4 replications was plotted with standard deviations. P-values were calculated using the student t-test and statistical significance was set at $p < 0.05$.

Immediately after assessing the AlamarBlue assay, optical bright field microscopy images were taken of each cell line, particle type and concentration sample for assessing visual changes in cell density and morphology. An inverted light optical microscope (*Eclipse TS100* (Nikon)) and a camera (*Zyla 4.2 sCMOS* (Andor, Oxford Instruments)) were used for imaging. A 40x magnification lens was used and background light was adjusted for each sample.

Assay interference tests were conducted to assess the possibility of the IFE Si NPs interfering with the AlamarBlue reagent or the fluorescence signal. Pristine and porous particles sterilized by ethanol and prepared as above were added to well plates containing only cell culture media (no cells) and incubated for 24 hours at 37°C in an atmosphere with 5% CO₂. Then the wells were washed once with PBS and AlamarBlue at a 1:10 concentration diluted in cell culture media was added. The same NP concentrations as above, *i.e.* 0.063-1 mg/mL, were used. A spectrophotometer (*SpectraMax i3x*) was used to measure the fluorescence emission at 590 nm with excitation at 560 nm after 24 hour incubation.

Experimental Results and Discussion

In the present chapter, the experimental results from the three parts: the IFE Si NP characterization, stability studies and cytotoxicity studies, are presented and discussed in Section 5.1-5.3, respectively. Section 5.1 describes characterization results of the IFE particles, as well as some predictions on how the particle characteristics observed affects their stability.

5.1 Particle characterizations

5.1.1 Scanning Electron Microscopy

Micrographs of pristine IFE Si NPs were secured using SEM, and the results are shown in Figure 5.1. As can be seen from the figure the primary particles have a spherical shape.

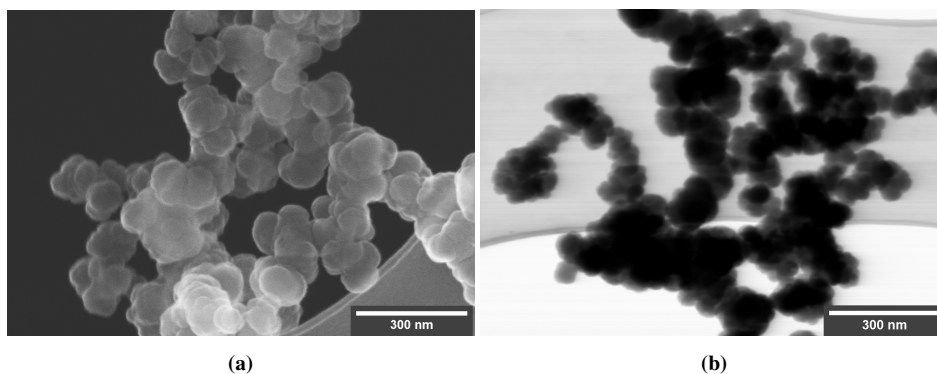


Figure 5.1: SEM micrographs of pristine IFE Si NPs used as base for the following experiments. (a) Secured with the instrument in scanning mode, while (b) in transmission mode.

Particle size analysis of Figure 5.1b was performed using ImageJ software system. Particles with a diameter ranging from 70 nm to 120 nm with an average size of $100.8 \text{ nm} \pm 19 \text{ nm}$ ($n = 30$) were identified.

In Figure 5.2 SEM micrographs of etched particles, also with mostly spherical shape, is presented. Image analysis of Figure 5.2b was even in this case performed using the ImageJ software and resulted in an average particle diameter of $80.3 \text{ nm} \pm 21.9 \text{ nm}$ ($n = 35$). The measured diameters varied from about 50 nm to 120 nm and the average particle diameter was smaller and the size distribution wider for the particles after etching compared to the pristine particles.

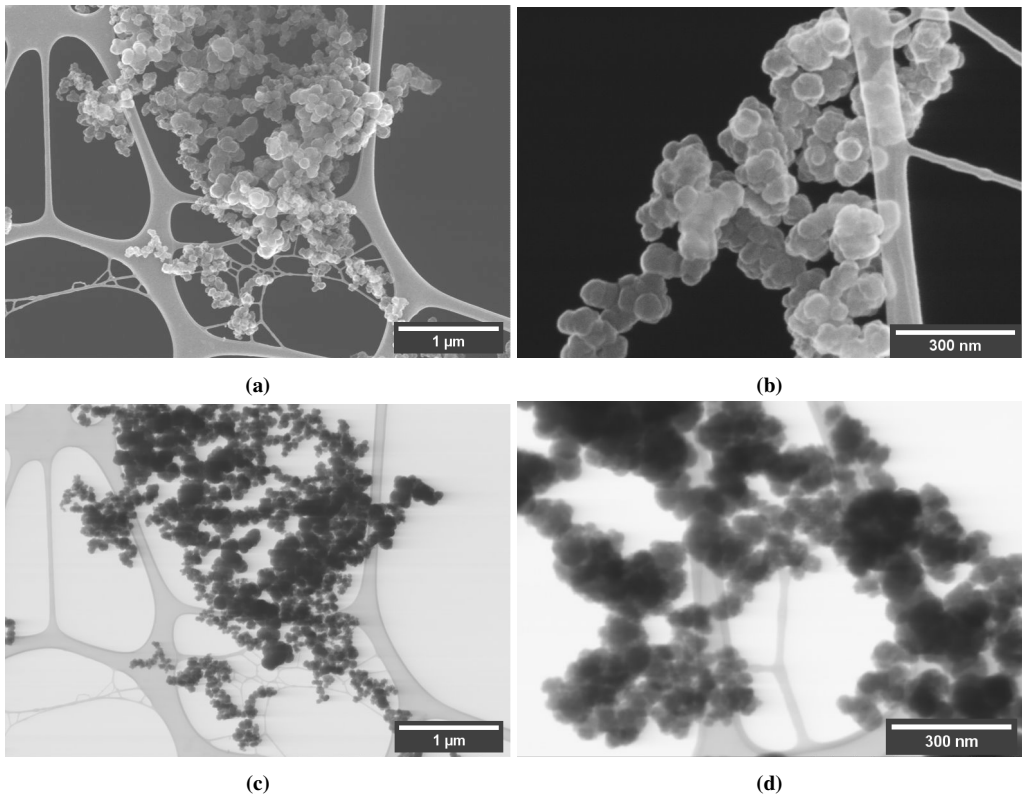


Figure 5.2: SEM micrographs of etched IFE Si NPs. (a) and (b) secured with the instrument in scanning mode with different magnification, while (c) and (d) in transmission mode.

Furthermore, the scanning mode micrographs show a low degree of porosity in the etched particles. Pores of a small size might be difficult to capture by SEM due to the resolution and focus limitations. The transmission mode micrographs, like Figure 5.2d, show signs of porosity in the light grey colored regions, even though not extensive. A high-resolution TEM image, seen in Figure 5.3, of another IFE pSi NP batch confirms porous structure created by the ReEtching process, using the same Si NP base material as studied herein. A standard etching process that allows for pore size and porosity control is

a desired tool from an application point of view.

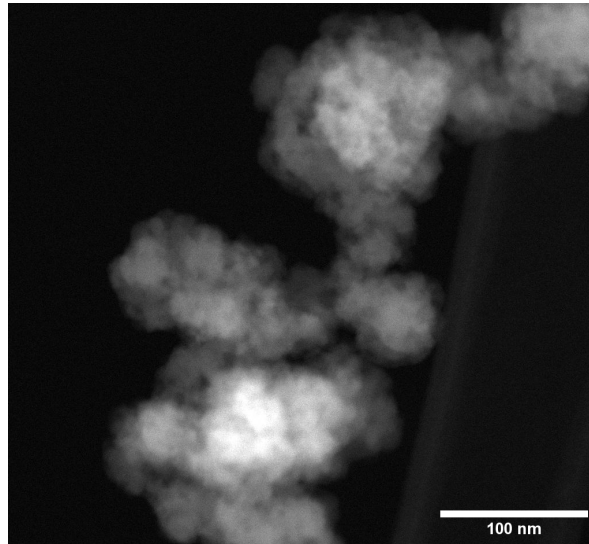


Figure 5.3: TEM micrograph of IFE pSi NPs. Taken with a HAADF detector.

5.1.2 Dynamic Light Scattering

DLS measurements of pristine and porous IFE Si NPs were conducted to obtain their size distributions and hydrodynamic sizes as shown in Figure 5.4 and Table 5.1, respectively.

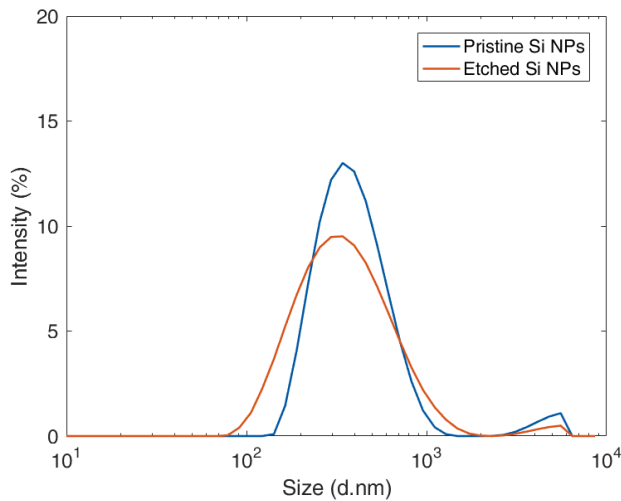


Figure 5.4: Size distribution of pristine and porous IFE Si NPs by intensity measured by DLS. Corresponding volume and number distributions are included in Appendix B, Figure B1.

Table 5.1: DLS results for the IFE Si NP samples dispersed in DI water. Z-average and PDI are given as averages with standard deviations of 3 measurements.

Silicon NP sample	Z-average (nm)	PDI
Pristine	369.5 ± 1.8	0.20 ± 0.01
Porous	305.9 ± 5.4	0.24 ± 0.01

It is notable that hydrodynamic size (Z-average), measured by DLS, and core size, as for instance observed by SEM, have two different definitions, and distinguishing between them is necessary for interpretation of the results of this study. The hydrodynamic diameter is the hypothetical diameter of a hard sphere with the same translational diffusion coefficient as the observed particles. It estimates the size of the hydrated particle in liquid solution; hence the hydrodynamic size will always be larger than the one observed in SEM. In the present study IFE Si NPs of around 100 nm in diameter results in a hydrodynamic diameter above 370 nm.

The Z-average of the particles decrease after etching, which is similar to observations made by SEM, indicating that electropolishing might take place simultaneously as etching pores. The porous particles are, furthermore, not hard spheres but rather porous shells with a decreased mass, compared to the pristine particles. Similar to decreasing size decreasing mass may result in an increase in translational diffusion and a decreased resulting Z-average. Such a change would not be similarly observed in SEM data. In other words, the observed result are likely a mix of the two phenomena.

Both the pristine and porous Si size distributions proved to have a small peak at about 3-4 μm , probably due to agglomerates at this size, in addition to the main peak at about 306/370 nm for the individual particles.

It should be mentioned that the intensity size distributions are slightly different with a broader distribution, thus larger PDI, for the porous particles. This may be due to inhomogeneous etching where smaller particles are more extensively porosified, resulting in an even smaller hydrodynamic diameter and a broader size distribution. It is a well known fact that PDI is an important variable for quality assurance of NPs intended for pharmaceutical use. Polydispersity requirements are set to $\text{PDI} < 0.3$, giving a sufficient precision size control [98]. The PDI values for both the pristine and porous particles are below 0.3, which meets the standards set in the pharmaceutical industry.

5.1.3 X-ray Diffraction

In Figure 5.5 an XRD diffractogram of pristine IFE Si NPs is presented. Narrow peaks indicate the presence of a material composition that is mostly crystalline (polycrystalline). The level variations in the background intensity also state that there is a portion of amorphous structures present, even after the particles have been heat treated. The Bragg peaks identified at $2\theta = 28^\circ$, 47° and 56° verify the material composition as they match the crystalline Si peaks for the crystallographic planes (111), (220) and (311), respectively [99]. Porous IFE Si NPs were not analysed using XRD and the crystallinity of the particles is

expected not to be affected by etching to a notable degree.¹

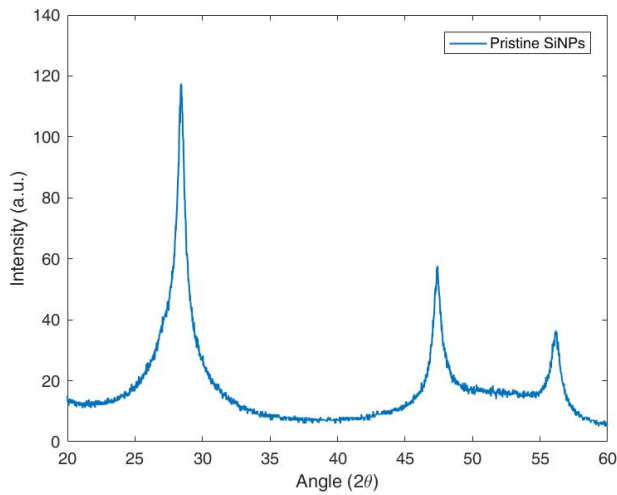


Figure 5.5: XRD pattern of pristine IFE Si NPs.

5.1.4 Energy Dispersive X-ray spectroscopy

EDS analysis was performed to study the surface elemental composition of the particles. In Figure 5.6 the elemental mapping of the porous IFE Si NPs is presented, and as can be seen the presence of a partly surface oxide coating is confirmed.

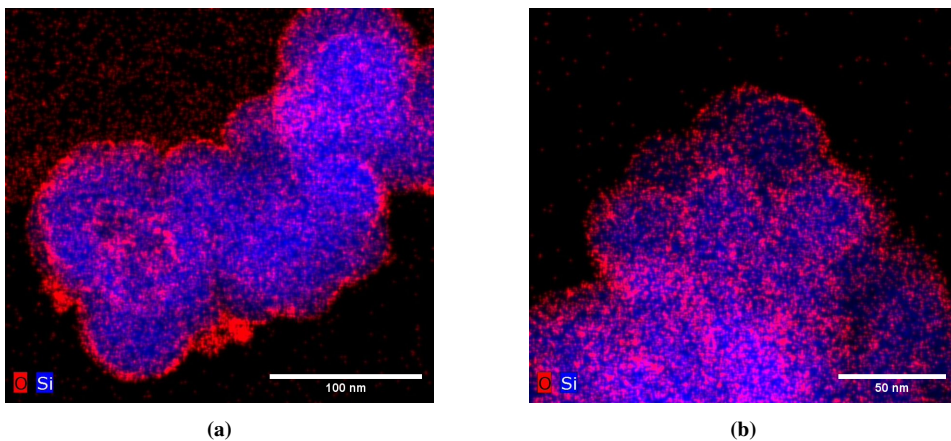


Figure 5.6: EDS mapping of the elemental composition of IFE Si NPs porosified using the same ReEtching process as the particles used for the stability and cell viability studies. Scale bars show (a) 100 nm and (b) 50 nm.

¹Not enough porous Si material for XRD.

The depth of the oxidation layer is estimated to be 1-4 nm, which is similar to previously observed oxidation depths of Si material after air exposure in room temperature [100]. Higher level of surface oxide formation is expected for the porous particles due to the higher surface area, compared to the pristine. It should be noted that the mappings are based on results from another batch of porous particles than the once used otherwise in the present study, however, the etching and post-treatment is the same and it can be expected that the surface oxidation will be similar for the porous particles used for the stability and cell viability studies.

5.1.5 Stability predictions based on particle characterization data

Comparing the obtained particle characterization data to the findings in the open literature on how particle properties affect the Si NP stability could give an indication on the stability properties of the IFE Si NPs. The smaller particle size identified for the IFE Si NPs, *i.e.* 80-100 nm, indicate low stability and fast dissolution with t_{50} in the range of minutes and t_{100} within hours for porous particles. Even though a different particle size is observed in DLS comparing to the SEM data, the actual size is thought to be closer to the once identified in SEM as this is a direct measurement method. The porous particles have a smaller diameter and are therefore expected to dissolve faster than the pristine particles. The porosity is also thought to have a great impact as non-porous particles are much more stable comparing to porous. The high degree of crystallinity and the native surface oxide observed for the IFE particles are properties likely to slow down the dissolution process. The dissolution kinetics could therefore be similar to mildly oxidized particles, with a t_{50} closer to hours. However, it has been reported in the open literature that the native surface oxide do not have the same effect as thermal oxidation procedures, with the latter further increasing stability (see Chapter 3).

5.2 Particle stability studies

A procedure for performing atability studies was developed and executed to assess both dissolution and agglomeration stability. Visual examination and DLS measurements of colloidal solutions and SEM imaging of particle samples after immersion in buffer solutions at different pH were conducted.

By visual examination of pristine IFE Si NPs suspended in buffer solutions of pH 7 and 10, see Figure 5.7, it is clear that these particles dissolve quickly in the pH 10 buffer solution as the colloid color changes from deep brown to transparent over 24 hours. In the pH 7 solution there is very little color change, indicating that the particles maintain long-term stability over a period of 68 days. These test vials contain a concentration of 0.4 mg/mL pristine IFE Si NPs in buffer solution, which is a lower concentration than in the solutions used in the remaining stability-studies where an initial concentration of 1.33 mg/mL was used.



Figure 5.7: Colloid buffer solutions at pH 7 (left vial) and pH 10 (right vial) with pristine IFE Si NPs, (a) at the time of immersion, (b) after 1 day and (c) after 68 days. The present pristine NPs come from another production batch than used for other experiments, but they have similar morphology and size distribution. A concentration of 0.4 mg/mL was used for these test-vials.

As described by Jarvis *et al.* [81] and Anderson *et al.* [13] the pH-dependent stability of nanosized and mesoporous Si is a known phenomenon. As previously mentioned, an increasing pH will increase the dissolution rate compared to neutral solutions due to the increased hydroxyl ion concentration. However, these studies, and several others, show that nano- and microsized Si should dissolve readily also in neutral and slightly acidic solutions. It is also shown that a higher pH induces dissolution rather than being a requirement for dissolution to take place.

The long-term stability of the pristine Si NPs is somewhat surprising in regards to the short dissolution-times reported for particles in the open literature (see Chapter 3). A possible explanation for the increased stability is that non-porous IFE Si NPs are used in the present experiment. Also, the native oxidation layer originating from air exposure could work as a passivation layer for increasing particle stability. The images presented in Figure 5.7, however, underpin how big of an impact the environmental pH has on the dissolution kinetics of nanosized Si. Qualitative studies to investigate how particles dissolve by looking at the size distribution and morphological characteristics are discussed in the sections below.

5.2.1 Dynamic Light Scattering

Intensity weighted size distributions - pristine particles

Figure 5.8 and Figure 5.9 shows the DLS size distributions of pristine IFE Si NPs immersed in acidic-neutral and alkaline buffer solutions, respectively, over a period of 24 hours. These studies are performed to determine the immediate stability properties of the core material intended for use as drug carriers. According to findings in the open literature, this time perspective is appropriate for stability studies as rapid dissolution of as-prepared nanostructured and mesoporous Si might take place.

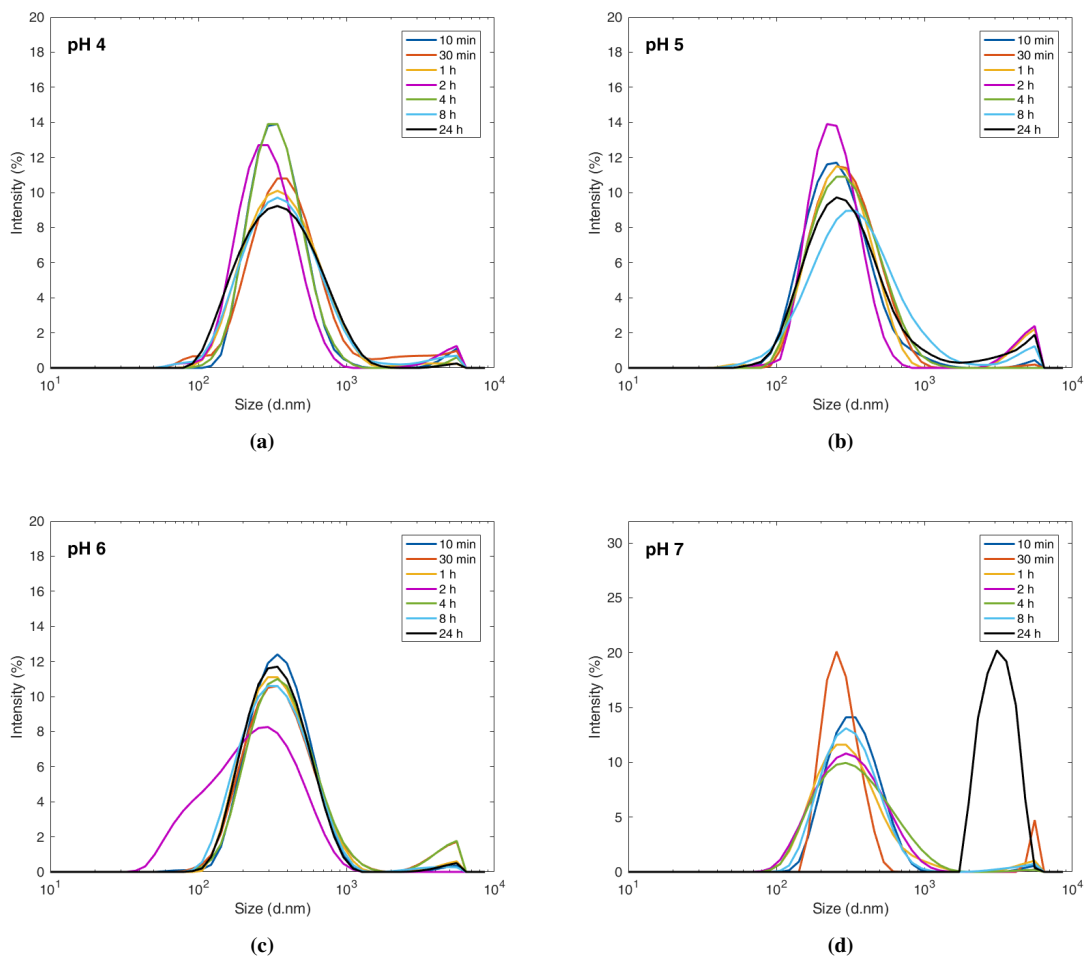


Figure 5.8: DLS intensity size distributions of pristine IFE Si NPs dispersed in acidic buffer solutions at (a) pH 4, (b) pH 5, (c) pH 6 and (d) pH 7 for the indicated durations. Citric acid monohydrate and sodium citrate dihydrate salts are dissolved in DI water at different ratios to get the various pH values.

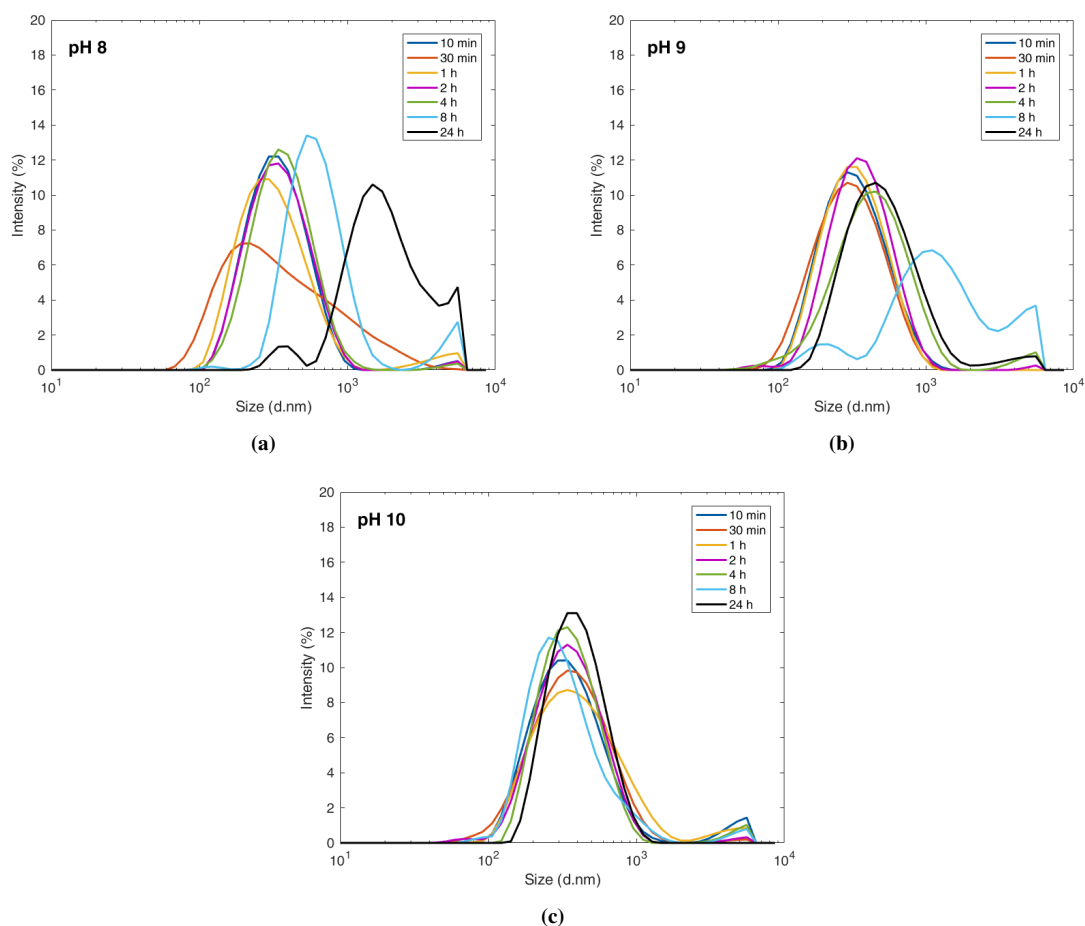


Figure 5.9: DLS intensity size distributions of pristine IFE Si NPs dispersed in alkaline buffer solutions at (a) pH 8, (b) pH 9 and (c) pH 10 for the indicated durations. Ammonium chloride salt and ammonia solution are dispersed in DI water at different ratios to get the various pH values.

As can be seen from Figure 5.8 and Figure 5.9, a major peak at about 250-300 nm is seen across all pH samples. Even in this case, as with the DLS measurements prior to buffer immersion, the hydrodynamic diameters measured by DLS deviates from the core diameter as observed in SEM. However, in this stability study DLS measurements are mainly analyzed for comparative reasons in which this analysis technique serves as a robust foundation.

It can also be seen in Figure 5.8d and 5.9a and b, that a few samples show a much larger average size, *e.g.* the 24 hour immersion in pH 7 and 8, the 24 hour immersion in pH 8, and the 8 hour immersion in pH 9. These obtained data show an increasing tendency to agglomerate after longer immersion times and a lower agglomeration tendency in acidic solutions. The relative height of the peaks within one sample can say something about the

relative particle numbers at that size; however, as shown in Figure 4.2, the intensity height cannot be used to compare particle concentrations of different samples.

For the obtained results for the acidic and neutral buffers in Figure 5.8, the peaks placement along the horizontal axis is approximately constant having a slightly left-shift towards smaller sizes over longer immersion times, while for all the alkaline buffers in Figure 5.9 the peak is clearly right-shifted over time. A decreasing particle size could be a sign of particle material dissolution. An increase in particle size, on the other hand, is a peculiar observation. A similar phenomenon was observed for the porous IFE Si NPs and is therefore discussed in more detail in Section 5.2.3.

The size distributions presented in Figure 5.8 and Figure 5.9 are based on the intensity signal reported from DLS. As this is an indirect measurement technique, small portions of agglomerates might affect the intensity-weighted distribution, which is found present in all the measured samples at about 4-5 μm . Therefore the distributions might not be completely realistic. When considering NPs it is tempting to use number distribution, as it would give a clearer picture of the relative amounts of each particle size. However, low noise fluctuations and intensity errors might result in high errors when converting to number and volume. It is therefore not recommended to over-analyze these distributions, and particularly the width of the peaks is often not reliable. However, comparing relative concentrations of distinct peaks within one population is a more reliable interpretation of the converted results.

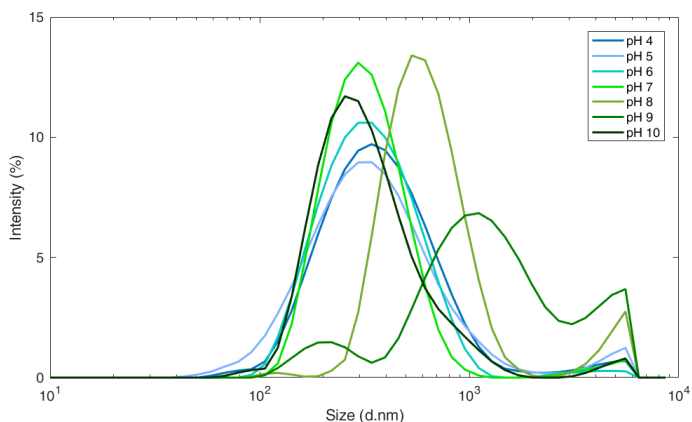


Figure 5.10: DLS size distributions of the 8 hour immersion of pristine IFE Si NP samples to see variations in pH (same data as in Figure 5.9 and Figure 5.8).

In Figure 5.10 the 8 hour size distribution data from the DLS data above, over the entire pH range tested, is presented. No distinct trend is seen across the pH range. However, the particle size seems to be stable in acidic and neutral buffers (pH 4-7), with an increase in pH 8 and 9. A deviation from the increasing size at higher pH is, however, seen in pH 10, which shows smaller sized particles.

Intensity weighted size distributions - porous particles

Figure 5.11 and 5.12 show DLS size distributions of porous IFE Si NPs immersed in acidic-neutral and alkaline buffer solutions, respectively, over a period of 24 hours.

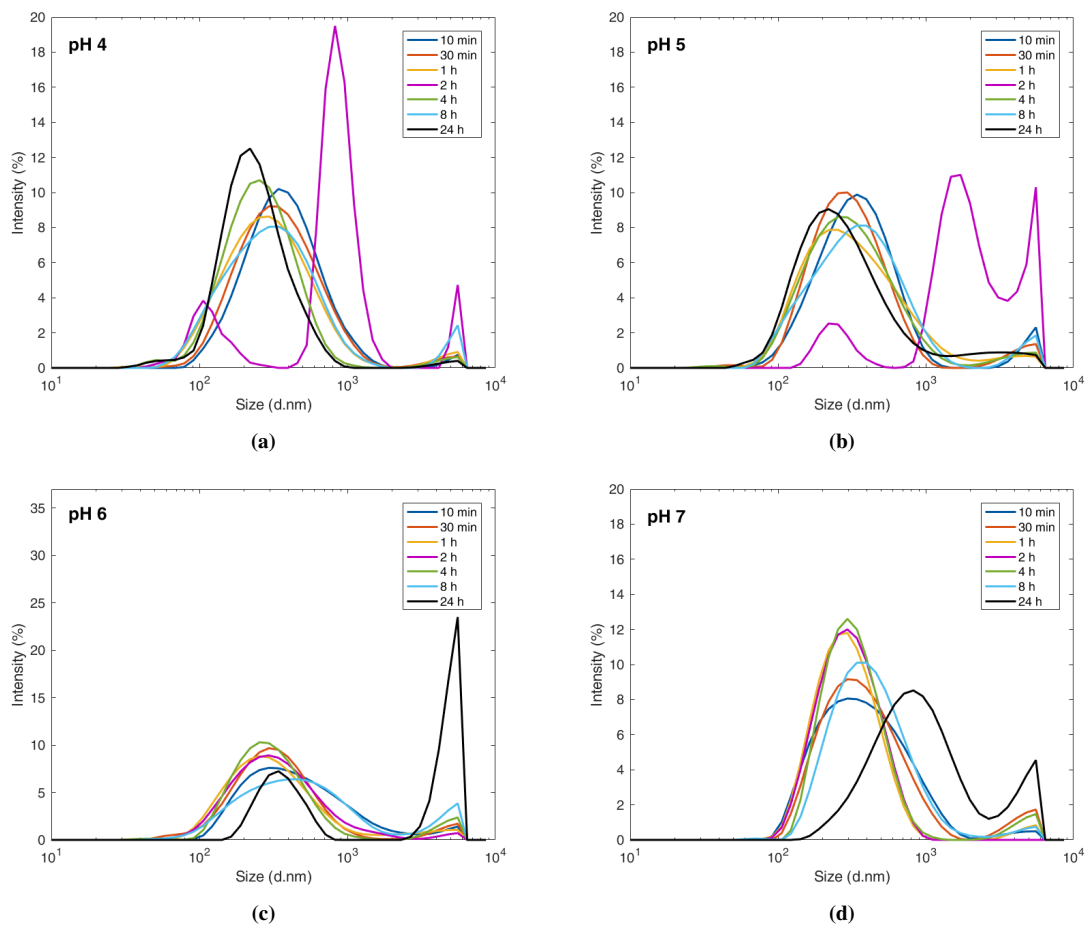


Figure 5.11: DLS intensity size distributions of porous IFE Si NPs dispersed in acidic buffer solutions at (a) pH 4, (b) pH 5, (c) pH 6 and (d) pH 7 for the indicated durations. Citric acid monohydrate and sodium citrate dihydrate salts are dissolved in DI water at different ratios to get the various pH value solutions.

The DLS size distributions of the porous particles are in general showing less stability than pristine particles over 24 hours immersion in buffer solutions. At near-neutral pH (6-8) the size distribution seems to be quite stable, especially when compared to the other pH samples (except for a large agglomerate peak seen in the 24 hour sample in pH 6). For pH 4 and 5 it is the 2 hour sample that deviates from the rest, which possibly is due

to contamination as there is no trend observed to verify the data. Disregarding the 2 hour sample, the remaining samples show a left-shift over time. This shift to smaller sized particles is more evident than what was observed for the pristine particles, see Figure 5.8a and b. For the pH 6 samples, as well as the samples representing an increasing pH, it is rather a right-shift to higher particle size over time that is observed. This is similar to the observations for the alkaline immersion of pristine particles. In general, the main trends observed for the pristine particles are also observed for the porous particles, but they seem to be more distinct for the porous particle samples.

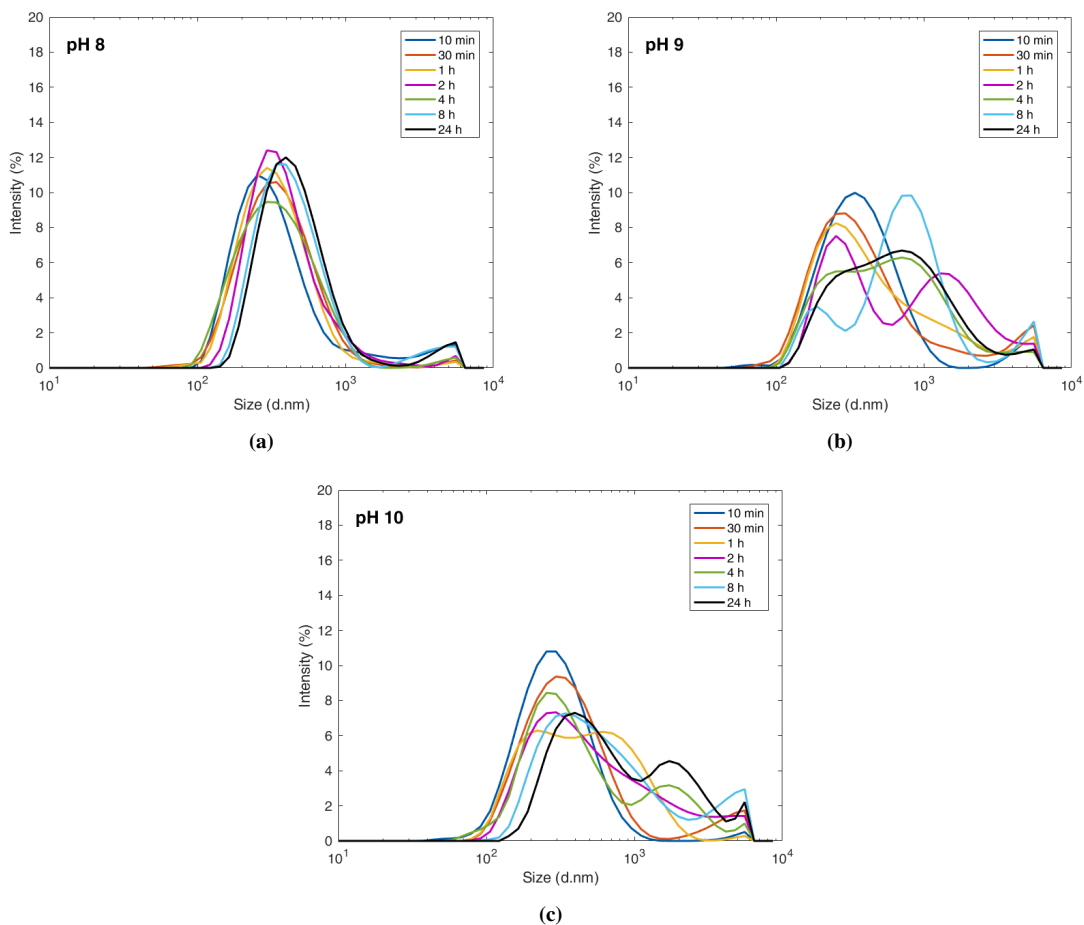


Figure 5.12: DLS intensity size distributions of porous IFE Si NPs dispersed in alkaline buffer solutions at (a) pH 8, (b) pH 9 and (c) pH 10 for the indicated durations. Ammonium chloride salt and ammonia solution are dispersed in DI water at different ratios to get the various pH values.

One main distinction observed in the porous particle samples is the arising of a peak at around 1100 nm connected with the 300 nm peak. This indicates that larger particles

are arising after 1 hour in pH 10 and after 2 hours in pH 9. Due to higher concentration of hydroxy ions in pH 10, which may lead to higher dissolution rates, it is reasonable to expect faster arising of instability changes. However, the 1100 nm peak is higher in the pH 9 samples, which is counter-intuitive for the explanation of pH dependence on stability/dissolution.

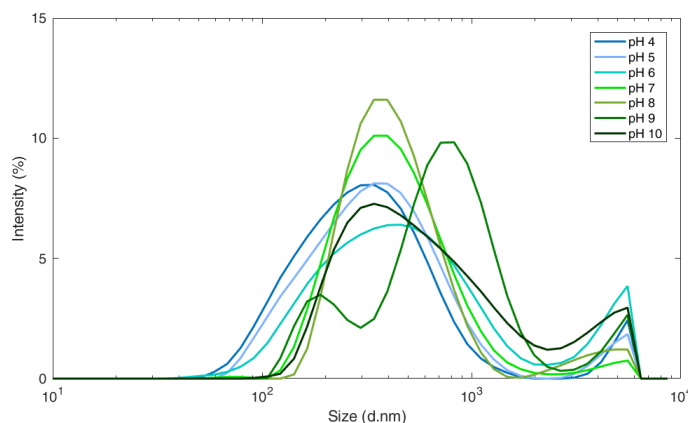


Figure 5.13: DLS size distributions of the 8 hour immersion of IFE pSi NP samples to see variations in pH (same data as in Figure 5.12 and 5.11).

In Figure 5.13 the 8 hour DLS distributions (same data as shown above) across the pH range 4-10 is presented. As can be seen from the figure, there is a clear trend of increasing particle size with increasing pH for the porous particles, as a right-shift of the peaks along the horizontal axis is observed for increasing pH. At pH 9 is an additional peak at larger size arising and at pH 10 do these peaks appear fused, giving rise to one broader peak.

Even though the porous and pristine particles show different behaviour at high pH do the low variations in size over time in the buffer at neutral pH indicate a high degree of stability around pH 7 for both particle types. The *in vivo* pH of blood is maintained around 7.4, which corresponds to a pH where the IFE Si NPs seems to be the most stable. This is beneficial for increasing circulation time of the DDS, but it simultaneously speaks against the bio-elimination predictions. The biodegradability of mesoporous Si is a well-established theory [32], however, the influence of individual environmental factors like pH should be studied in more detail for verification.

From the DLS size distribution data, both the pristine and porous particles seem to be relatively stable compared to the findings in the open literature. Little change in particle size was observed over 24 hours in the present study compared to the results found in the open literature where 100% particle dissolution was reported after 2-4 hours for untreated particles of 100-133 nm size [8], and within a few hours for surface oxidized particles [43, 80]. Moreover, an increase in particle size is remarkable to see, particularly at high pH, as dissolution was observed visually for pristine IFE Si NPs over 24 hours.

Overall, it is clear that the pristine and porous IFE Si NPs have different behaviours in acidic and alkaline buffers in terms of chemical stability, with regard to both dissolution

and agglomeration. This could be due to different degradation rates, as previously discussed, which again could be due to different degradation mechanisms. Moreover, there is a chance that the observed behaviors are salt-dependent rather than pH-dependent as one salt combination was utilized for creating the acidic buffers and another to create the alkaline buffers. This argument is, however, not supported by the fact that pH 7 and 8, created by different salt solutions, are showing a similar behavior for both pristine and porous particles.

Z-average

Figure 5.14 shows the Z-averages over the time immersed in either acidic and alkaline buffers for both pristine and porous particles. Samples with extensive agglomerates above $1\ \mu\text{m}$ hydrodynamic diameter have been removed from this data for clearer identification of trends within the remaining samples. The same plots with this data are included in Appendix B, Figure B2.

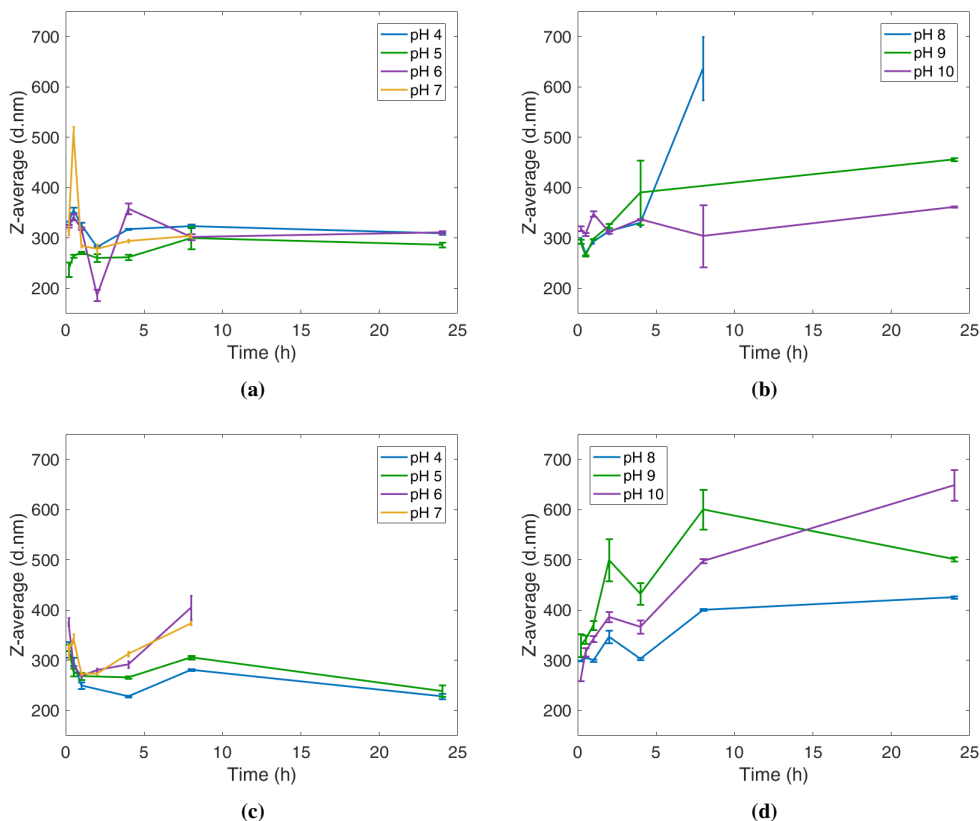


Figure 5.14: Z-average values of pristine (a) and porous (b) IFE Si NPs immersed in acidic buffers, pH 4-7, and pristine (c) and porous (d) IFE Si NPs in alkaline buffers, pH 8-10, measured using DLS. Averages are plotted with standard deviations of n=3 replica measurements.

The pristine particles seem to have a more consistent Z-average value compared to the porous particles over the immersion time in both acidic and alkaline media, as seen in Figure 5.14. Particularly, the acidic samples of pristine particles seem to have a relatively stable size over a period of 24 hours, except for some variations in pH 6 and 7 before reaching 8 hours immersion. For the porous particles in acidic solution the size is observed to change over a period of 24 hours, *i.e.* it gradually decreases within the first hour to start increasing until 8 hours has passed to again start decreasing. This indicates the instability of the porous particles also in acidic solutions. In the alkaline buffers a near continuous increase in hydrodynamic diameter was observed for the porous particles, but to a lesser extent for the pristine particles. This size increase seems to be related to pH, except for the sample in pH 10 for the pristine particles where the size is barely changing and only slightly increased after 24 hours immersion.

As seen in the DLS size distributions of both pristine and porous particles, and also confirmed by the corresponding Z-average plots, immersion in alkaline buffers over time resulted in a gradual increase in the particles' hydrodynamic diameter. This increase in diameter is an indicator of pH-dependent particle instability, which was particularly evident for the porous particles. Figure 5.15 shows the Z-average of porous particles after 8 hour immersion in buffers over the pH range measured (same data as above), along with a linear regression line to the Z-average data. The R^2 value of 75% shows a relatively good correlation between the data and the linear model, and the slope indicates a diameter increase of 44 nm for each pH value increase. Calibration data for DLS measurements using different sample concentrations, seen in Figure 4.2 show a slight increase in Z-average values for decreased concentration. However, this was only a vague trend, and not observed in literature. Other possible mechanisms behind the size increase are discussed in detail in Section 5.2.3.

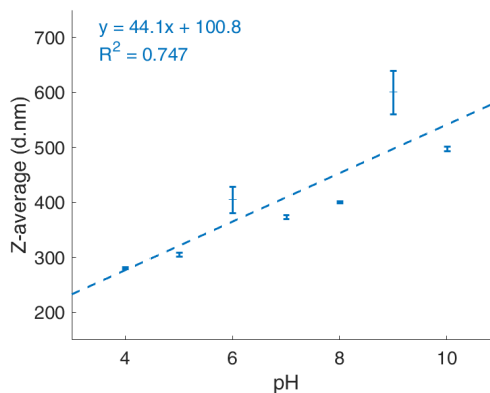


Figure 5.15: Z-average of porous IFE Si NPs in the pH range 4-10 with a simple two-variable linear regression.

Polydispersity index

The polydispersity index, as a measure of the size distribution heterogeneity, over time in acidic, neutral and alkaline buffers of pristine and porous IFE Si NPs are shown in Figure 5.16. These plots also disregard the highly agglomerated samples identified, excluded from the Z-average plots. Complete PDI plots are found in Figure B3 (Appendix).

The PDI of the pristine particles is more stable in both acidic and alkaline solutions, comparing to the porous particles. The pristine particles have a PDI close to or below 0.3, which is the pharmaceutical requirement [98], in most pHs tested. In this perspective it is

clear that the stability of pristine particles is generally closer than the porous particles in meeting the requirements when stored in both acidic and alkaline solutions over 24 hours. The porous particles, however, seem to have a PDI above 0.3 at various time points after immersion in basic solution as well as for the entire time period monitored after 30 minute immersion in pH 9-10. To retain the size distribution quality the particles should not be stored in highly alkaline solutions. However, pH 8 seems to be the best for retaining a low PDI for the porous particles.

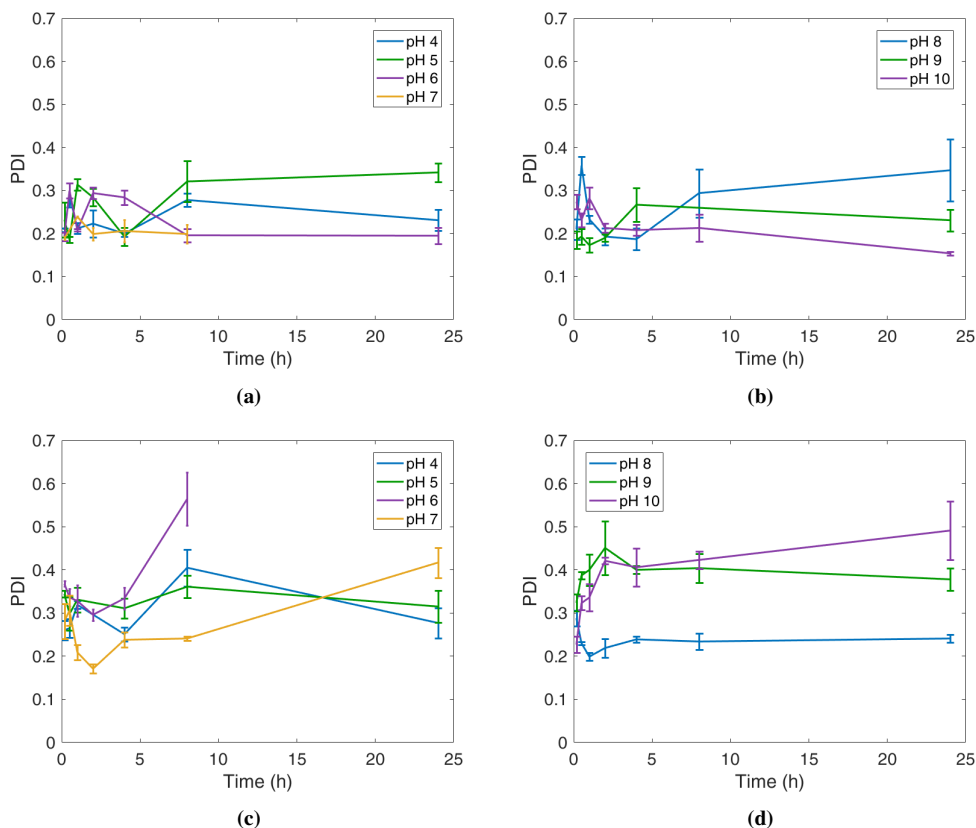


Figure 5.16: PDI values of pristine (a) and porous (b) IFE Si NPs immersed in acidic-neutral buffers, pH 4-7, and pristine (c) and porous (d) IFE Si NPs in alkaline buffers, pH 8-10, measured using DLS. Averages are plotted with standard deviations of n=3 replica measurements.

The variations in PDI generally indicate instability of the particles, as well as an inhomogeneous dissolution profile of the particles, which can be due to specific particle properties. This was more evident in the porous particles that were found to have a higher PDI also before stability studies. Increasing PDI, as mentioned, might also indicate a tendency for agglomerates to form.

5.2.2 Scanning Electron Microscopy

Figure 5.17, Figure 5.18, Figure 5.19 and Figure 5.20 show SEM images of stability-study samples of IFE Si NPs with pristine particles in the first two figures and porous particles in the two latter. Only the samples immersed in buffers over 8 hours, also measured using DLS, were imaged, giving an overview of the trends in morphological change.

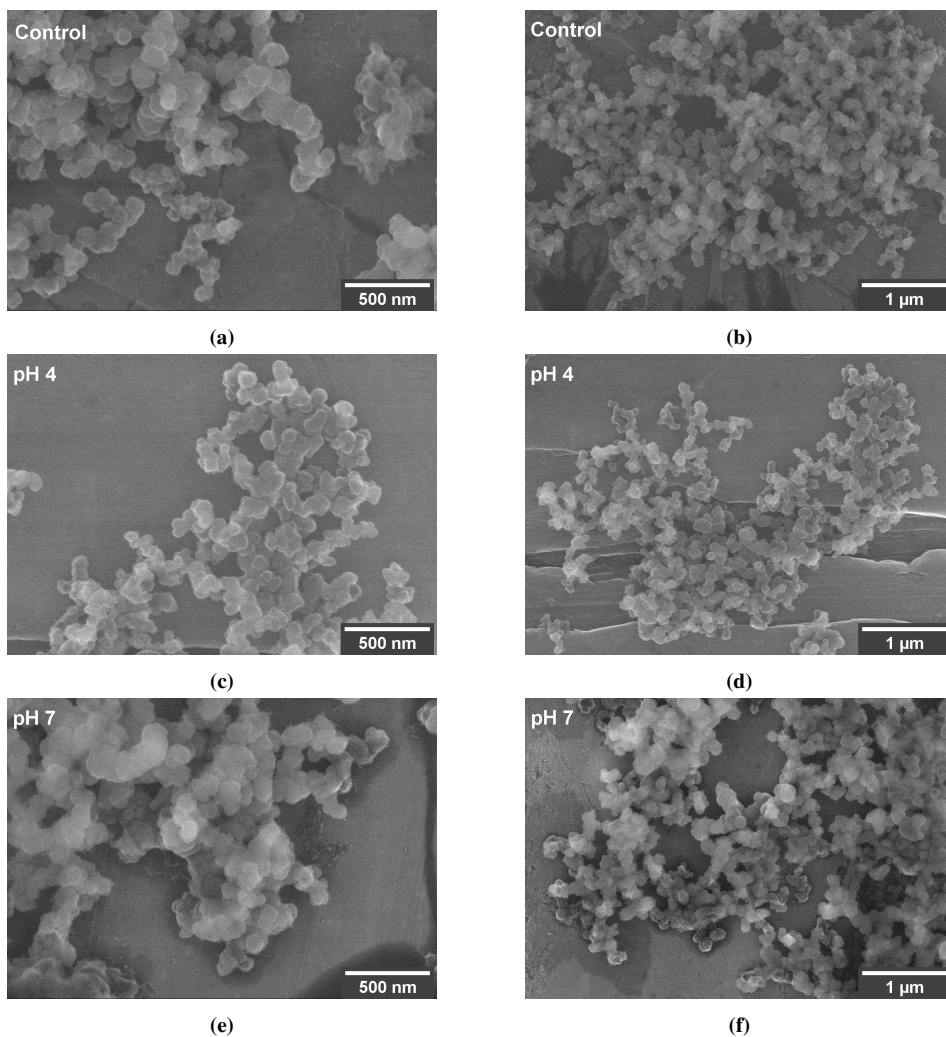


Figure 5.17: SEM micrographs of pristine IFE Si NPs control samples (a)-(b), after 8 hour immersion in acidic solution of pH 4 (c)-(d), and in neutral solution of pH 7 (e)-(f).

As can be seen from Figure 5.17, the pristine particles have after immersion in acidic and neutral solutions retained morphology and size compared to the control. In Figure 5.18a slight structural change can be seen with appearance of fused structures in Figure

5.18c and f, as well as a sheet-like structure covering for some of the particles in Figure 5.18e. The formation of these structures seems to increase with increasing pH, which could explain the increasing particle size observed in DLS measurements at high pH.

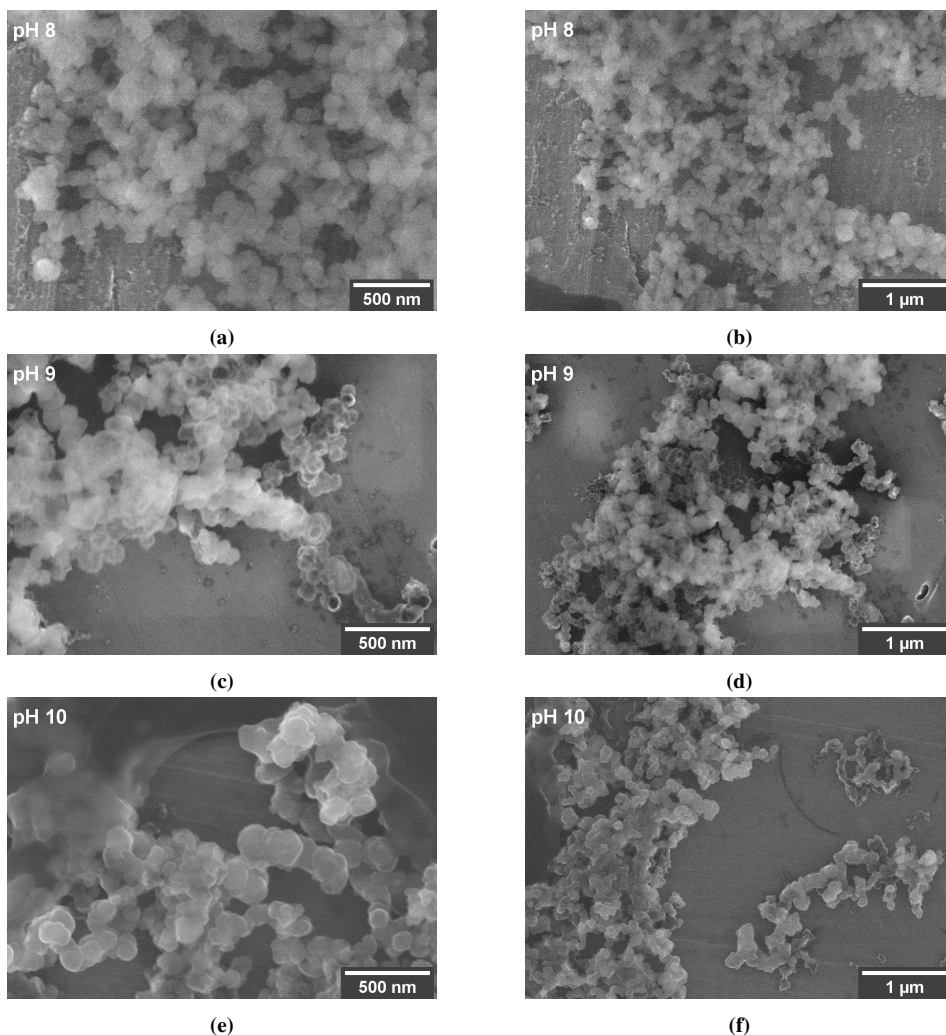


Figure 5.18: SEM micrographs of pristine IFE Si NPs after 8 hour immersion in alkaline solutions of pH 8 (a)-(b), pH 9 (c)-(d) and 10 (e)-(f).

Similar to the pristine particles, the porous particles also show little visible morphological changes after immersion in acidic and neutral buffers, see Figure 5.19, and after exposure to alkaline solutions the particles seem to have a gradual loss of integrity, see Figure 5.20. However, as can be seen from Figure 5.20c, in pH 8 most particles have retained their spherical particle shape, while some are more fused together as seen in Figure 5.20b (difficulties with focusing on the pH 8 sample made high resolution images difficult

to obtain). In Figure 5.20f it can be seen that the particles in pH 9 show a higher degree of formation of micron-sized clusters, with the particles' outline still visible in SEM. After immersion in pH 10 large chunks had formed so that individual particles were barely visible. However, not all particles tend to fuse to the same degree as individual particles were also seen in pH 10, see Figure 5.20i. Irregular structures, seemingly not created by particles merging yet connected to the particle structure, were also observed in the pH 10 solution, see Figure 5.20g. These structures might be formed during particle synthesis, or they might be formed during particle immersion in high pH.

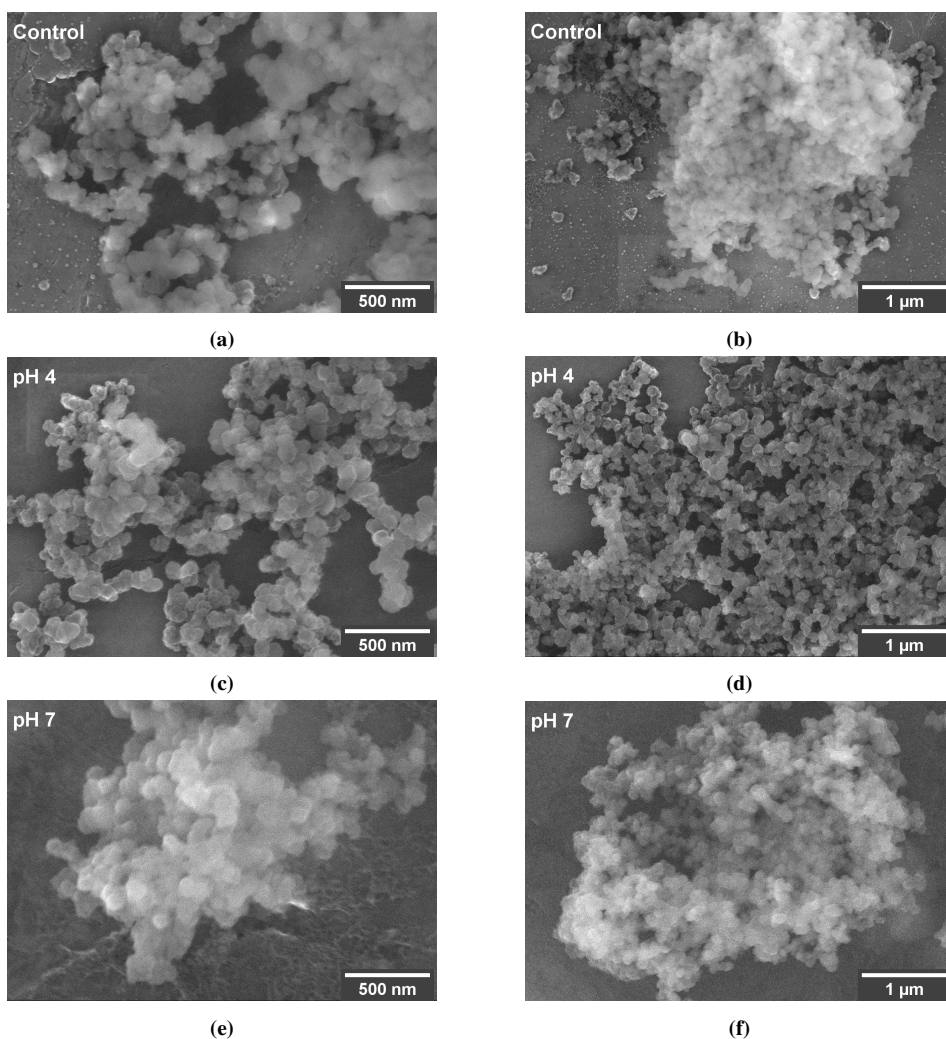


Figure 5.19: SEM micrographs of porous IFE Si NPs control (a)-(b), after 8 hours immersion in acidic solution of pH 4 (c)-(d) and immersed in neutral solution of pH 7 (e)-(f).

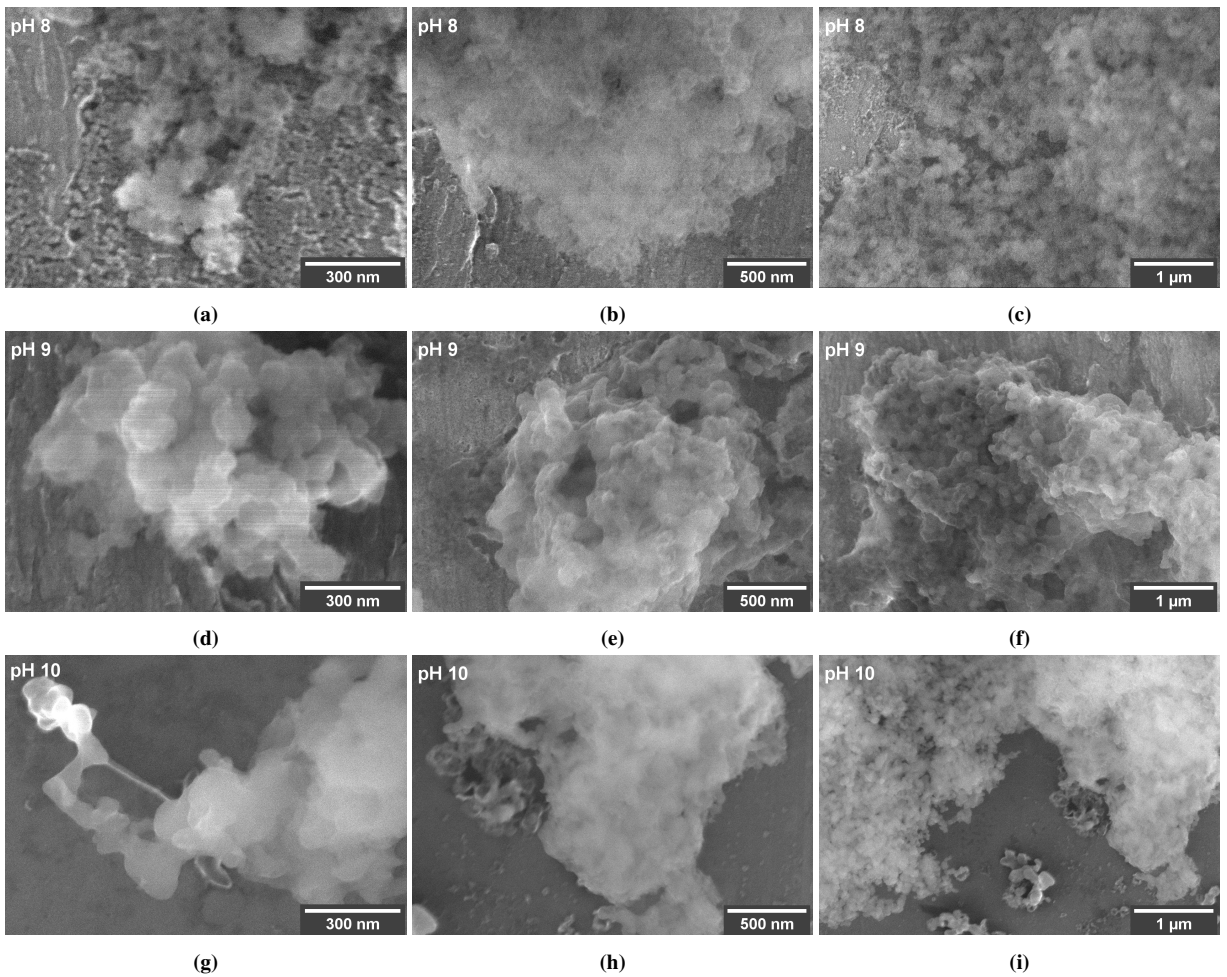


Figure 5.20: SEM micrographs of porous IFE Si NPs after 8 hours immersion in pH 8 (a)-(c), pH 9 (d)-(f) and pH 10 (g)-(i) buffer solutions.

Most of the SEM observations in the recent study correspond well with the increasing particle size observed in DLS for particles in pH 8-10 buffer solutions. The additional peak for larger particles seen in DLS of pH 9-10 immersed particles is likely due to the formation of the fused particle clusters observed in SEM.

In both the SEM and DLS observations, it is clear that altering one property, by porification of the IFE particles, have great impact on the stability behavior of the particles. The different stability profiles for the two Si NP samples underpin the theory that stability and dissolution kinetics are highly particle-dependent, and that other properties like crystallinity, size and surface modifications might also have a striking impact on stability.

5.2.3 Possible explanations for stability study observations

The observed trends with an increasing particle size upon immersion in alkaline solutions are not intuitively correlated to the increased dissolution rate predicted for exposure to high pH as previously discussed based on literature observations. In other words, a decreasing particle size is therefore expected upon dissolution, which would be in agreement with the observations made by previous studies [76, 77]. However, these studies use microsized particles where the morphological changes might be very different from the nanosized ones. Additional observations of the irregular structures seen in SEM of samples in high pH and little morphological and size change in neutral and acidic pH raise questions if the biodegradability theory holds for the IFE Si NPs presently studied. Moreover, there are various possible explanations for the increasing size phenomena observed.

The term agglomeration is mentioned several times above as a description of large particles created by individual particles clustering together. The term cluster or clustering will herein be used as a general term for individual particles coming together to create larger formations. Another term in colloidal science is used for similar observations as agglomeration, which has a slightly different meaning: aggregation. These terms are often used interchangeably and sometimes even assigned the opposite meaning, which has caused confusion. It is useful to distinguish these two terms for a more accurate description of the state of cluster formation and on a basis of the forces involved to understand how to avoid them taking place. In accordance with the ISO 14887, the following definitions will be used to separate the two terms [61]:

- **Agglomeration** is a cluster of loosely attached particles, caused by weak physical interactions and van der Waals forces. The non-covalent bonding is reversible and an agglomerate can be readily dispersed. The loose arrangement has a total surface area similar to the sum of the area of the primary particles involved [61].
- **Aggregation** is a cluster of more firmly attached particles by covalent bonds. An aggregate is formed in an irreversible manner and the surface area is smaller than the sum of the area of the primary particles [61].

DLS is probably not a useful technique for distinguishing agglomerates from aggregates as it is simply an evaluation of size, but ultrasonication of each sample was performed prior to DLS for the purpose of breaking up agglomerates. Thus, the observed size increase was more likely to be due to the more firmly attached aggregates. The fused clusters observed at high pH in SEM also seem to be rigidly bonded, most likely explained by aggregation. Another technique that could be useful for determining the degree of aggregation is nitrogen adsorption specific surface area measurement, as the surface area is reduced by the formation of aggregation to a much higher extent than for agglomerations.

Similar to the experimental results in the present study is the increasing hydrodynamic diameter results reported for mesoporous silica nanoparticles under stability studies by Lin *et al.* [78]. DLS measurements showed in this case a gradual increase over 10 days immersion in PBS, which is explained by aggregation by the authors. Furthermore, the amount of free orthosilicic acid was monitored, showing the degradation of nanoparticles simultaneously as the gradual size increase. Data obtained from DLS stability measurements of the IFE Si NPs, as emphasized above, are comparable to the data obtained by

Lin *et al.* [78], and aggregation of particles may therefore also be a reasonable explanation for the present data. However, the aggregation theory does not explain the gradual pH-dependent size increase or higher instability of porous particles compared to pristine particles. It is therefore interesting and useful to develop an understanding of the influence of these factors.

Other terms in colloidal science used to describe the states of particle clustering's are flocculation, coalescence and coagulation. All these terms are used to describe processes that change the size distribution of particles from a large number of small particles to a smaller number of larger particles. Such terms are often used to describe the nucleation and growth processes of materials for which the driving force is a reduction in the surface area that will reduce the overall energy of the system [61]. Surface area reduction is likely to also be the driving force post-NP synthesis when suspended in liquid solutions. Highly fused particles, as observed particularly for the porous particles in high pH, might be explained by extending the scale beyond aggregation with tight cluster formations where individual particles lose their integrity. A term descriptive of these phenomena is coalescence, conventionally used to describe dense structures characterized by the disappearance of the boundary between individual particles, in which the driving force is lowering of the system energy by elimination of an interface [101]. This may be an adequate description of the process giving rise to the structures seen in the SEM images of pristine and porous particles in high pH presented in Figure 5.18 and Figure 5.20. However, coalescence is mostly used to describe merging of droplets in a liquid-liquid (emulsion) or gas-liquid (foam) colloid solution. It is questionable whether this will apply to Si as a solid but the term is also used to describe growth Si particles under high temperature synthesis [102], so it might be sufficiently descriptive. Figure 5.21 illustrates aggregation, agglomeration and coalescence processes of Si NPs in solutions, as well as a different hypothesis described in the following paragraphs.

Another well-established term in colloidal science, Ostwald ripening, is also possibly part of the explanation of the observed behavior with increasing particle size over immersion time in buffer solutions. As previously discussed an increasing pH will increase the dissolution rate of porous silicon structures. The increasing dissolution rate, observed in the open literature [78], can thus be correlated to the increasing particle size observed in the present study. In other words, the one possible explanation of how increasing dissolution rate can result in larger particles is an Ostwald ripening like process with mass transfer through dissolution and subsequent deposition of silica (SiO_2) structures from dissolved silicon species. Ostwald ripening is the theory of larger particles growing at the expense of smaller particles as they dissolve in a two-phase system. The resulting structures are similar to those formed by coalescence, as illustrated in Figure 5.21. The driving force of this mass exchange, as with the colloid phenomena mentioned above, is reduction of the large surface energy of NPs. The local radius of curvature and ratio of surface area to volume accounts for the particles' surface energy. The decrease in total surface area drives morphological changes based on the curvature dependence of the chemical potential, causing surface atoms to flow from regions of higher to lower curvature, given that the atoms are able to diffuse through the matrix [103]. A variety of materials are reported to undergo Ostwald ripening in solution, including organic, polymeric and inorganic materials such as silver, platinum and oxides [104, 105]. This process is mostly observed

for sub-100 nm particles, and the growth-shrinkage process is more likely to be evident in smaller particles. However, Ostwald ripening is said to be practically always present when NPs are dispersed in solution and the phenomenon is also reported to take place in up to 200 nm particles [106].

Piletska *et al.* [107] reported a mechanism for creating biomimetic imprints of SiO_2 by exploiting the Ostwald ripening process of 12 nm SiO_2 particles in PBS solution of pH 7.2. The authors hypothesized that under kinetically favorable conditions surface silanol groups at highly curved SiO_2 surfaces will dissolve preferentially to release silicic acid that drives a sol-gel formation onto solid templates giving the deposited structures antibody-like properties. This process was confirmed experimentally with a particle diameter growth rate of 30-50 nm over 4 to 6 hours [107]. A similar process is thought to take place in any SiO_2 or Si structure in aqueous solution because of unstable surface silanol groups that dissolve into silicic acid. This process is highly dependent on the dissolution rate of the initial SiO_2 particles and the solubility of the intermediate species, *i.e.* silicic acid. In this case the dissolution rate will be highly dependent on the starting material properties such as crystallinity, impurity content and surface passivation and curvature. The solubility of silicic acid is also highly dependent on the medium temperature, pH and content of various ions [108].

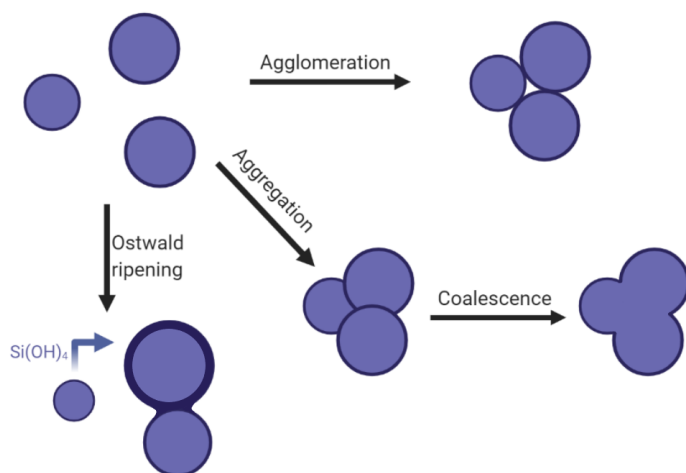


Figure 5.21: Schematic illustration of agglomeration, aggregation, coalescence and Ostwald ripening by silica (SiO_2) deposition from dissolved orthosilicic acid (Si(OH)_4) taking place in colloid Si NP solutions. Blue represents Si and dark blue represents silica SiO_2 shells.

Belton *et al.* [109] describes the formation process of amorphous SiO_2 NPs from dissolved orthosilicic acid based on the following principles. Orthosilicic acid has low solubility in water at room temperature, typically around 100 ppm or 1 mM, but remains stable as long as its concentration remains below the solubility limit. Above this concentration the orthosilicic acid will undergo spontaneous condensation reactions to lower its concentration in solution. Multiple condensation reactions generate various linear and

cyclic structures that eventually cluster and form an amorphous silica gel or aggregate network. Energy minimized structures are formed to maximize the number of Si-O-Si bonds and form novel nuclei or, following the principles of Ostwald ripening, re-deposit onto the larger particles already present [109].

The silica Ostwald ripening process and SiO₂ formation by dissolved orthosilicic acid described by Piletska *et al.* [107] and Belton *et al.* [109], respectively, might together explain how a similar process takes place in the case of Si NP colloidal solutions. Ostwald ripening of Si NPs has not previously been reported experimentally, as far as the present author knows. The tendency of Si to form oxides in aqueous solutions is inevitably a part of the explanation. Oxidation of surface Si, dissolution into orthosilicic acid and subsequent precipitation of an amorphous SiO₂ network on the surface of larger Si particles or aggregates, whichever is the most energetically favourable, could be a reasonable explanation for the experimental observations. Increasing Si dissolution in high pH would speed up the process of SiO₂ deposition, even though orthosilicic acid would readily form other Si species in alkaline solutions. Irregular non-spherical structures as clearly seen in Figure 5.20g can also be explained by the deposition of Si-containing species, in line with the similar structures observed in the experiments of Piletska *et al.*, which has been explained by SiO₂ deposition [107]. The absence of peaks at smaller particle size in the DLS measurements, as well as decreasing average size seen for porous particles in acidic solutions, speaks against the Ostwald ripening theory. However, DLS results only show an instantaneous image of a quenched reaction that might have reached a metastable equilibrium. The reason why this phenomenon takes place in the porous particles to a higher extent than in the pristine particles may be due to the higher surface area available for dissolution as well as higher density of surface dislocations and small radius of local curvature around pores.

A combination of the aforementioned colloid processes is likely to be the cause of Si NP size increase in alkaline solutions. Experimental techniques that could be used for investigating these hypotheses include BET for distinguishing between agglomerates and aggregates, EDS to quantify the thickness of the silica layer and XRD to see if an increasing amount of particle structure is amorphous in order to investigate the silica deposition theory.

5.2.4 Implications of stability observations in biomedical applications

The key findings in the present stability studies of the IFE Si NPs include observations of increased hydrodynamic diameter upon immersion in alkaline buffer solutions, supplemented by fused particle structures and clusters disclosed by SEM. Colloid processes like particle aggregation and/or Ostwald ripening due to SiO₂ deposition of dissolved Si species are believed to be the explanations of the observed cluster formations, which might have implications for the drug delivery application regardless of the underlying mechanism. The findings in the present study are important for discovering the properties of the carrier material, which might affect the drug delivery process *in vivo*, as well as in terms of drug administration. Intravenous injections require a liquid solution in which colloid processes have to be taken into account. Stability properties might also be utilized for triggered drug release upon carrier dissolution tuned to specific pH environments. High stability is conventionally regarded as a requirement for pharmaceutical applications, however,

materials with self-eliminating properties such as Si have been given increasing attention.

The formation of fused structures might arise from dissolved Si, as discussed above, in which porous IFE Si NPs seem to dissolve much faster than pristine. This is in accordance with the findings in literature (Chapter 3), and can be utilized for directing drug release that is highly interconnected with degradation of the carrier. For example, one might tailor release to the alterations in pH through the gastrointestinal tract upon oral administration. The particles are likely to be stable in the acidic environments in the stomach while dissolving in the more alkaline environments in the intestines. Inflamed and malignant tissue has been reported to have pH deviating from that in healthy tissue, in which pH-dependent dissolution might also occur.

It is important to point out that the implications outlined must be seen in light of a discussion of the relevance of the methodology used for stability studies. The stationary and confined glass vials used in the present study, that are easily handled and allowing for the obtained changes to be observed, could be one reason to why the particle merging takes place. High concentrations of IFE Si NPs, above 1 mg/mL, could be reasonable for liquid samples prior to administration but are unlikely for *in vivo* aspects. Furthermore, particles might undergo similar reactions and form merged clusters *in vivo* but the highly complex and dynamic environment (particularly in the circulatory system) might disturb this process. The relevance of the pH range studied compared to biological systems can also be discussed. The size alterations observed in the present study were most evidently seen at pH of 10, exceeding the biological pH range. However, a similar size increase was observed for pristine particles from pH 8 and for porous particles from pH 7, and above, which are highly relevant, as the body remains a near-neutral pH of 7.4 in the blood. As the processes observed were pH-dependent, observing reactions in pH 10 might be an extreme model for predicting what might happen over time in lower hydroxyl concentrations, as well as giving a clearer indication for what colloid processes are taking place.

5.2.5 Comparison of DLS and SEM for stability studies

The two characterization techniques used for the stability studies were, as previously discussed, SEM and DLS, which have their respective benefits and limitations for this purpose. They are both used to assess structural changes with DLS measuring hydrodynamic diameter and SEM visualizing primary particles and morphological changes. It is reasonable to compare the two techniques on basis of the stability study results. The main limitations and benefits (bold) are summarized in Table 5.2.

DLS is a quick and feasible method with automated set-up that gives quantitative data with stable statistical analysis of the entire particle sample population. SEM, on the other hand, requires more time and a higher level of skill to obtain high quality results as it is manually driven. The graphical information obtained from SEM is restricted to a tiny fraction of the entire population, but it gives more intuitive and detailed results. SEM is a versatile method used for many types of samples and materials, while DLS is only used for colloids of particles typically below 10 μm . Dry samples are required for SEM and liquid colloid samples are required for DLS. Whether this is beneficial or not depends on the native environment of the sample, as well as if drying or dispersing affects the particle properties and causes agglomerations or degradation. DLS gives no structural information except for hydrodynamic diameter, based on a series of assumptions like particles having

a spherical shape, which is reasonable for the IFE particles. It should be pointed out that it is a highly averaging technique with poor resolution due to polydispersity and cannot separate aggregates from individual particles, which is easily distinguished in SEM. Unlike the direct measurements obtained from SEM, DLS is an indirect technique for measuring particle size resulting in very different measurements of absolute particle size. For the same particles DLS gives a 300-370 nm diameter whereas SEM gives a 80-100 nm in the case of primary particles, where the direct SEM measurements are more likely to give a realistic value. However, for comparative purposes DLS is a good option for comparative purposes as it is a sensitive technique that measure alterations not immediately apparent in SEM such as a size increase of the pristine particles over time in a high pH of 8-10.

Table 5.2: Limitations and benefits (bold) of using SEM and DLS for evaluation of the stability studies.

SEM	DLS
Direct	Indirect
Manually operated	Automated
Give images	Give statistical hydrodynamic diameter information
High resolution	Low resolution
Dry sample	Liquid colloid sample
Includes a small part of the particle population	Includes the entire particle population
Detailed	Averaging
Can distinguish aggregates from primary particles	Cannot distinguish aggregates from primary particles
	Mathematical assumptions

Several benefits and limitations were identified for both techniques, including that they give very different data. DLS and SEM are complementary techniques, and for appropriate samples one would benefit from using both. As in the stability studies conducted in the present study, DLS was used for identification of trends, while SEM was used to visualize the samples to observe in detail what mechanisms are possibly taking place to cause these trends.

5.3 *In vitro* cytotoxicity studies

In vitro cytotoxicity studies were performed for pre-clinical assessment of the *in vitro* toxicity profile of the IFE Si NPs as function of NP concentration, incubation time and cell line. The effect of particle surface chemistry is often discussed in literature; however, the structure-dependent cytotoxicity in regards to IFE Si NP porosity is also assessed in the present study by comparing data from pristine and porous particles. AlamarBlue cell viability assays were accompanied by bright field microscopy images as a quality control and to assess changing cell morphology as another indicator of cell health.

5.3.1 AlamarBlue assay

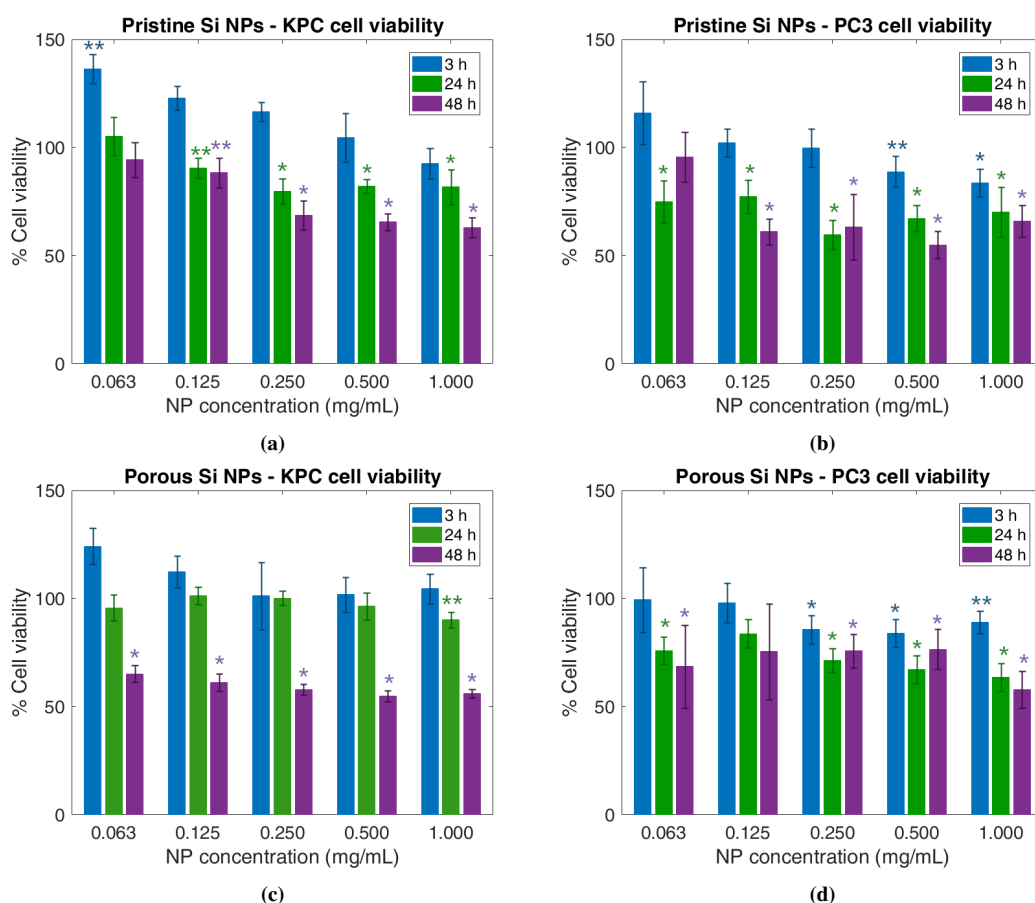


Figure 5.22: *In vitro* cytotoxicity studies of pristine IFE Si NPs, sterilized by autoclave treatment, exposed to (a) KPC and (b) PC3 cell lines, and porous Si NPs exposed to (c) KPC and (d) PC3 cells, for periods of 3, 24 and 48 hours. The %CV mean is plotted as the mean and standard deviations of $n=8$ replications. * $P < 0.01$, ** $P < 0.05$ when comparing to control samples (without NPs).

In Figure 5.22 the %CV results from the AlamarBlue assay of both pristine and porous IFE Si NPs, sterilized by autoclaving, to both KPC and PC3 cells, is presented. Cell viability was measured after 3 hours exposure to NPs, for assessing immediate cytotoxicity, and after 24 and 48 hours exposure for assessing cytotoxicity induced by IFE Si NPs over longer time periods.

As can be seen from the figure, low immediate toxicity is observed for both the pristine and porous IFE Si NPs in the case of both the KPC and PC3 cell lines. Generally, cell toxicity increases for increasing concentrations of particles, as well as increasing incubation time, as would be expected. The pristine particles showed a concentration-dependent toxicity profile with low immediate toxicity and less variation in toxicity between 24 and 48 hours compared to the 3 to 24 hour step, particularly for the lower concentrations below 250 $\mu\text{g}/\text{mL}$ in KPC cells. NP concentration of 250 $\mu\text{g}/\text{mL}$ seems to be a threshold value for the pristine particles in which lower concentrations show less toxicity, while at higher concentrations the %CV response seems to be no longer concentration nor time dependent within the 48 hour period tested. The porous particles show a more time-dependent toxicity profile rather than concentration-dependent, with no such threshold value observed. However, immediate toxicity of porous particles was observed for PC3 cells at concentrations of 250 $\mu\text{g}/\text{mL}$ and above. Contrary to the toxicity profile of the pristine particles in KPC cells the porous particles show a similar viability pattern after 3 and 24 hours incubation, with an increased toxicity after 48 hours. The porous particles show small changes in cytotoxicity for PC3 cells even over 48 hours incubation up to at least 500 $\mu\text{g}/\text{mL}$ NP concentration, with a small decline in %CV at 1 mg/mL.

The cytotoxicity response is similar for the two cell lines. The KPC cell line shows, however, a slightly higher level of cell viability after 3 hours exposure to NPs. The levels of %CV above 100, seen for the KPC cells and for the PC3 cells treated with pristine particles at low concentrations, can be due to various reasons. A possible explanation can be that low concentration of particles promotes cell growth over a short time perspective, or it might simply be due to statistical variations. Natural variations of cytotoxicity responses between cell lines may also be due to the variations in metabolism or cellular respiration processes, as the AlamarBlue assay measures cell metabolism as the health indicator. Two different cell lines are used for quality assurance of the viability data, with the expectation that different cell lines give different assay results. In this regards it should be mentioned that KPC is a pancreatic cancer cell line with mouse origin, while PC3 is a human derived prostate cancer cell line. They are both originating from aggressive forms of cancer with increased metabolism compared to healthy cells. Higher viability, generally seen in the KPC cell line, may naturally derive from higher levels of metabolic activity as KPC cells are found to have an average doubling time of about 16 hours [110] while the number of PC3 cells is doubled after typically 27 hours [111]. A larger variation over time is also typically seen for high metabolism cells as the response is more effectively decreased upon cell death.

The toxic responses of the IFE Si NPs might be due to the hydrophobic properties observed for both pristine and porous particles. The immediate slight toxic response of porous particles to PC3 cells might be due to the immediate contact between cells and the particles that have extremely high surface area and thus increased hydrophobic properties, compared to pristine particles. Hydrophobic NPs have an increased tendency to bind cell

membranes which might cause blockage of proteins and receptors affecting vital signalling pathways and interactions with the environment. However, this is a small effect comparing to the long-term toxic effects of porous particles in KPC cells. This latter effect might be due to similar interactions with cell membranes, or it might be explained by the increasing tendency for cellular uptake over time. This phenomena is also typically observed for hydrophobic NPs, inducing oxidative stress, autophagy and apoptosis, which might be more evident in certain cell lines [66].

The different responses seen for the pristine and porous particles is likely to be partly due to the difference in stability properties, as observed above. In other words, the increased aggregation of porous particles could decrease the surface area of the particles, decreasing the disruptive cell membrane interactions. Increased degradation might also decrease the amount of particles interacting with cells. The pristine particles also display hydrophobic properties, though to a lower degree than the porous particles. The increased toxic effects of pristine particles, compared to porous, might be explained by higher amounts of material in each particle, causing increased cell membrane blockage.

5.3.2 Bright field microscopy images

Micrographs of control samples of PC3 and KPC cells (no particles added) are included in Figure 5.23 for comparative purposes to be able to distinguish alterations in cell shape and size upon addition of NPs. PC3 and KPC are both adherent cell lines growing on dish bottom surfaces but with highly distinct morphologies. KPC cells are small in size and high in number after 48 hour incubation compared to PC3 cells. The KPC cells form a confluent layer of cells filling the entire dish bottom. Individual PC3 cells were easier distinguished with their circular shape with some elongated cells.

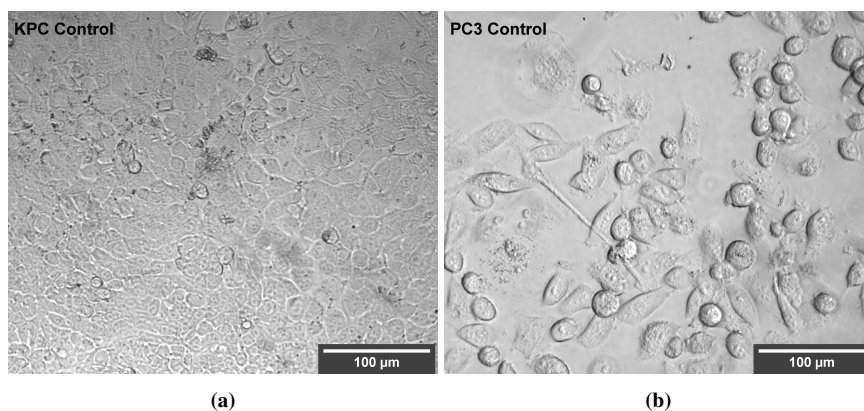


Figure 5.23: Bright field optical microscopy micrographs of control samples of (a) KPC and (b) PC3 cells used in *in vitro* cytotoxicity studies after 48 hour incubation.

In Figure 5.24 and Figure 5.25 are bright field optical microscopy images of KPC and PC3 cells for visual examination of alterations in cell shape and size upon the addition of autoclaved pristine and porous IFE Si NPs at concentrations 0.0625-1 mg/mL after 48

hours presented. These images are secured from the same samples used for the viability measurements presented in Figure 5.22.

The micrographs in Figure 5.24 confirm the low toxicity of KPC cells with a slight concentration dependence seen for the pristine particles. The addition of both particle types seems to break up the confluent cell layer, with larger areas uncovered by cells at higher particle concentrations. Large sections are still covered by cells mainly unaffected in shape and size by particle addition, as far as visible beneath the black particle aggregates. At NP concentrations of 250 $\mu\text{g}/\text{mL}$ and 1 mg/mL , both pristine and porous, circular cells are observed above the confluent layer. These are unhealthy, dead or dying cells showing increased cell death at higher particle concentrations.

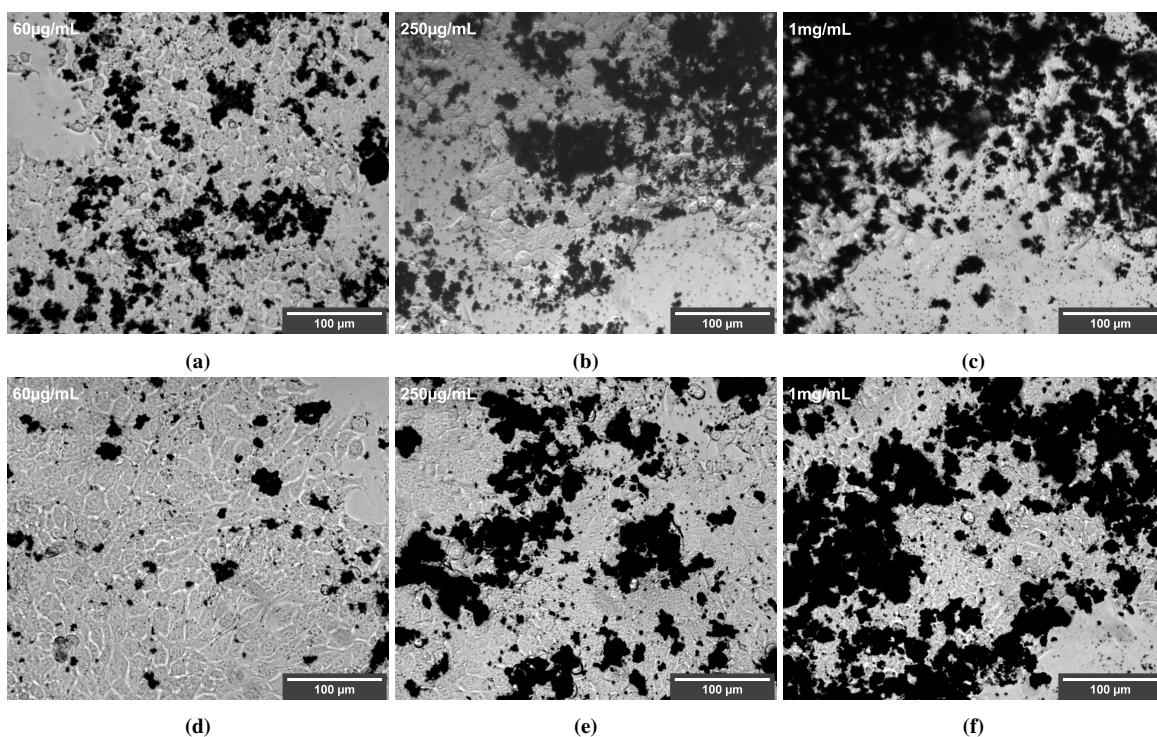


Figure 5.24: Bright field optical micrographs of *in vitro* cytotoxicity studies of IFE Si NPs sterilized by autoclave treatment and incubated with KPC cells over 48 hours. (a)-(c) Pristine particles at 0.0625, 0.250 and 1 mg/mL , respectively, and (d)-(f) corresponding concentrations of porous particles.

These observations seem to correlate with the AlamarBlue assay results, where the concentrations imaged have a similar %CV of about 60-70, except for the 62.5 $\mu\text{g}/\text{mL}$ pristine sample with about 90% CV which also seem to show higher cell density in the corresponding microscopy image. Such images might, however, not be fully representative for the entire cell population tested, only showing a small region of the entire plate well.

IFE Si NPs, both pristine and porous, tend to aggregate on top of cells as the clear

regions without cells contain less particles as well as smaller particles. When comparing (a)-(c) to (d)-(f) in Figure 5.24, it is clear that a higher density of particles is observed in the pristine samples compared to the porous samples. This might be because of faster degradation of porous particles, or it might be that pristine particles have an increased tendency to stick to the cell surface even after the PBS washing steps. This observation supports the idea that particle interaction with cell membranes physically block vital cell functions that induce cell death. It also indicates that hydrophobicity is not the only factor of importance in determining NP induced cell death, as porous particles are observed to have higher degree of hydrophobicity.

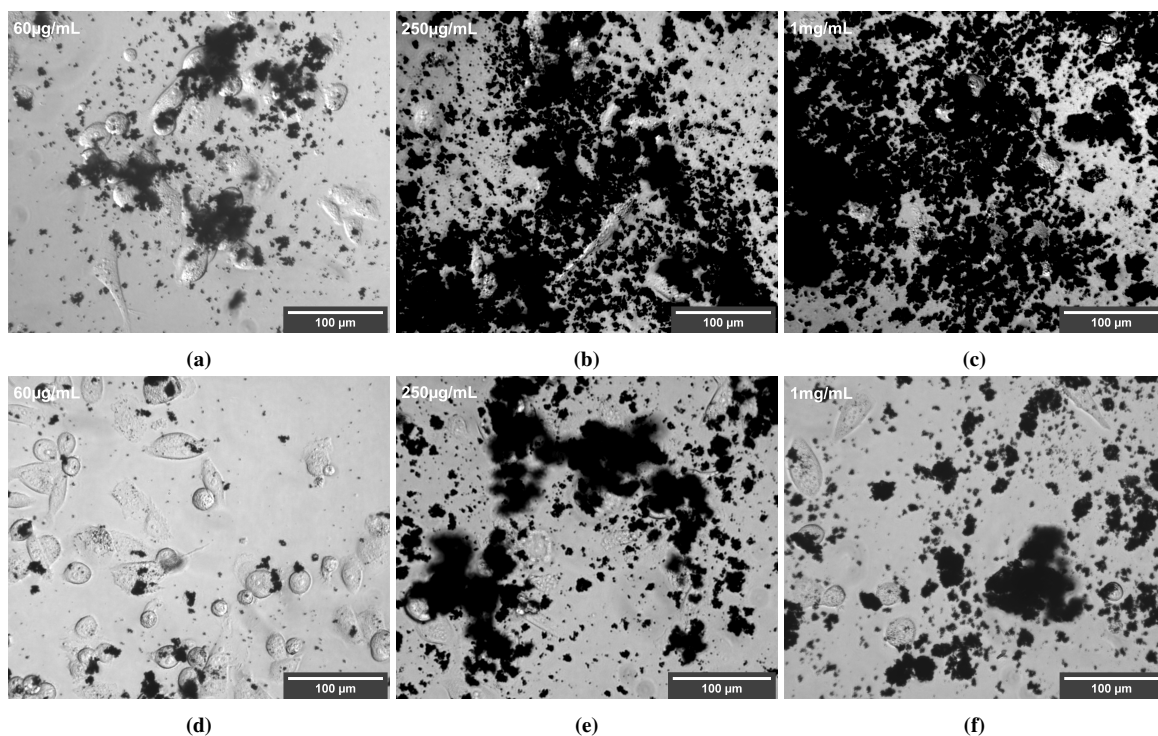


Figure 5.25: Bright field optical microscopy images of *in vitro* cytotoxicity studies of IFE Si NPs sterilized by autoclave treatment and incubated with PC3 cells over 48 hours. (a)-(c) Pristine particles at 0.0625, 0.250 and 1 mg/mL, respectively. (d)-(f) Corresponding concentrations of porous particles.

The PC3 cells exposed to IFE Si NPs in Figure 5.25 generally seems to show a lower density of cells comparing to the PC3 control where the Visible cells seem to have retained size and shape. As observed in the KPC cells, a higher coverage of pristine particles compared to porous is seen also in the PC3 cells. This might give rise to the concentration-dependent toxicity seen in the AlamarBlue assay for the pristine particles. The porous samples seem to have higher cell density, corresponding to higher viability at higher NP concentrations, which also corresponds with the AlamarBlue assay results showing less

toxicity of porous particles.

As for the KPC cells, the particles tend to cluster around cells, which might be inducing the mechanism for cell death by physical blockage of cell-cell interactions and other interactions with the environment. The PC3 cells are larger than the KPC in size, thus having larger surface area for NPs to bind. Also, with the KPC cells having fewer and possibly more sensitive direct cell-cell interactions, NP clustering might induce a higher degree of cell death.

Conclusively, from the AlamarBlue cell viability studies, it is seen that IFE Si NPs show low cytotoxicity to both KPC and PC3 cells. Incubation time has a larger effect on toxicity than concentration for porous particles, while concentration-dependent cytotoxicity is seen for pristine particles. From optical microscopy images it is observed that particles tend to cluster onto the cells' membranes, with pristine particles showing an increased tendency to do so. This particle clustering, and the resulting physical blocking layer created around cells, is likely part of the explanation of IFE Si NP-induced cytotoxicity.

5.3.3 Impact of particle sterilization process

Sterilization of materials for medical usage is required to avoid introducing infectious microbes to the patient. Thus, gaining insights into how various sterilization processes affect the viability assay results is important. As previously elaborated, three means of sterilization were attempted, *i.e.* 1) heat by 121°C autoclaving IFE Si NPs in PBS solution, 2) chemical by ethanol wash, and 3) filtration. For practical considerations, and the fact that autoclaving is a tool widely used in medicine and biomedical research, it was the most feasible sterilization process tested in the present study. Few processing steps and a prepared solution ready to use just after automated autoclaving, also gave the most realistic viability assay results, see Figure 5.22.

In the case of ethanol wash, ethanol immersion had to be followed by centrifugation and the washing require multiple pipetting steps that might cause loss of material, as well as increasing the chance of contamination post-sterilization (the particles underwent ethanol washing following the procedure outlined in Section 4.5.1). Micrographs of cells incubated with the ethanol treated particles are seen in Figure 5.26. As can be seen in the figure, low survival of KPC cells were found even at 125 $\mu\text{g}/\text{mL}$ (higher concentration samples looked similar) and of PC3 cells at 500 $\mu\text{g}/\text{mL}$, as there was virtually no cells left in these samples after 48 hours incubation time. This is in huge contrast to the confluent layer of cells in the control KPC sample presented in Figure 5.23a, as well as the micrographs of similar studies of the autoclaved particles in Figure 5.24, and might be due to the cytotoxicity of ethanol residues on the particles. The PC3 cells are clearly more resistant to the influence of the particles as more cells were observed at a particle concentration of 125 $\mu\text{g}/\text{mL}$. Contrary to the autoclaved particles, more healthy cells are seen in the samples treated with pristine compared to porous particles. However, a higher degree of particle clustering is seen for the pristine particles, which is in good agreement with the observations made for the autoclaved particles.

In 5.26c and d, it seems like the cells, in addition to the clustering around them, takes up both particle types, or alternatively are clustering on top of the cell. Uptake of NPs is a common mechanism previously observed in many cell types [66], and might cause

toxic effects at high concentrations. Particle clusters covering larger portions of the cells' surface is another likely way of inducing cell death, as previously described.

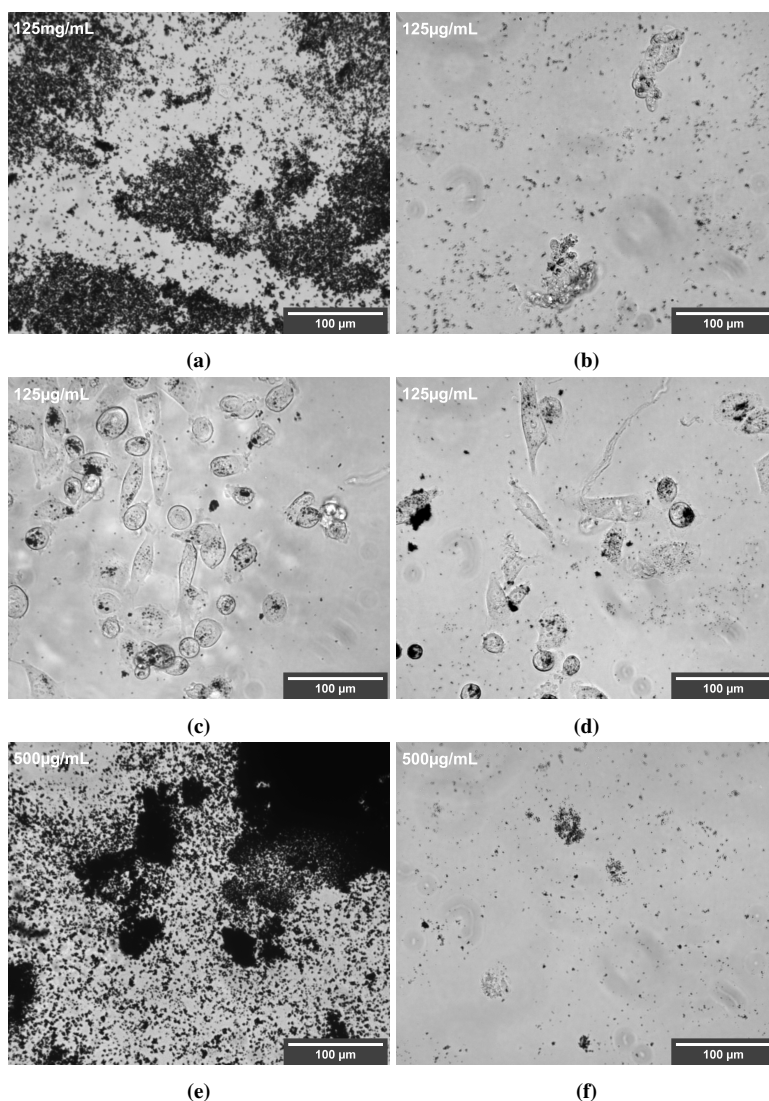


Figure 5.26: Bright field optical micrographs of cells exposed to pristine and porous IFE Si NPs, sterilized by ethanol wash, in *in vitro* cytotoxicity studies. KPC cells treated with 125 µg/mL of (a) pristine and (b) porous Si NPs. PC3 cells treated with 125 µg/mL of (c) pristine and (d) porous IFE Si NPs and 500 µg/mL of (e) pristine and (f) porous IFE Si NPs. All images are taken after 48 hours incubation time with NPs.

The AlamarBlue assay was also followed with the ethanol washed particles. %CV calculations gave unreasonably high results up to 1000%, with increasing trends seen for

increasing particle concentration in some samples. This peculiar observation does not correspond with the low cell density seen in micrographs presented in Figure 5.26. Increasing %CV was more evident for the pristine particles, which might be due to NP-assay interference (discussed in Section 5.3.4 below). Or, it might be due to insufficient sterilization leading to bacterial contamination, as microbial metabolism is also measured in the AlamarBlue assay. Substantially decreased %CV following increasing NP concentrations is also observed for some samples (as in the micrographs in Figure 5.26), that might be caused by residual ethanol among the particles. Ethanol entrapment inside the porous structures, poses a particular challenge for this sterilization technique. The AlamarBlue viability assay results of the ethanol washed particles are included in Appendix C, Figure C1.

Filtration is another conventional method for sterilizing NPs. Filters with pores of $0.2\ \mu\text{m}$ are required for sterilization with removal of both bacteria and viruses. Particles of similar size might get clogged in the filter, so filters of $0.45\text{--}5\ \mu\text{m}$ openings were used for filtration of the IFE Si NPs used in the present study. The images seen in Figure 5.27 show that all filters tested got clogged and the filtered solution after $0.45\ \mu\text{m}$ filtration turned out nearly transparent as a tiny pellet as very few particles were filtered through (the loss of NPs was assumed to be $>90\%$). This is likely due to the hydrophobicity of the particles, showing that as-prepared IFE Si NPs and porous IFE Si NPs are not suitable for sterilization by filtration in a PBS solvent. Furthermore, hydrophobicity is not a desirable property for *in vivo* applications, and a hydrophilic coating would be appropriate for further development of IFE Si NPs as drug carriers.

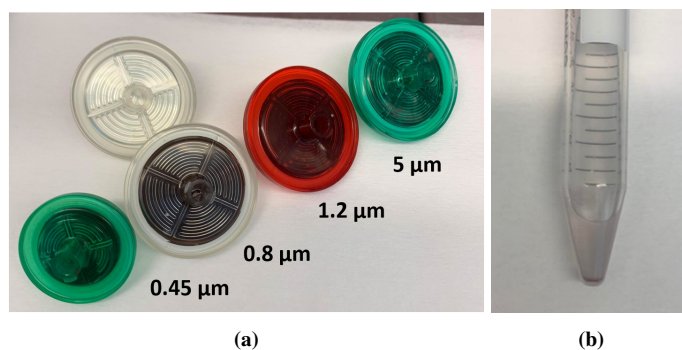


Figure 5.27: Filters after filtration attempts of IFE Si NPs dissolved in PBS. (a) Clogged filters of 0.45, 0.8 (pristine IFE Si NPs), 1.2 and $5\ \mu\text{m}$ (porous IFE Si NPs) pore size. A clean $0.8\ \mu\text{m}$ filter is included in the upper left corner for comparative reasons. (b) Filtrate residual after $0.45\ \mu\text{m}$ filtration of porous IFE Si NPs.

In the present study the sterilization impact on viability assay results was assessed, and it was concluded that characterization of the particle properties should be performed after sterilization to give information on the particles as they are upon administration. For further *in vitro* or *in vivo* studies, it would be necessary to understand how various sterilization techniques affect the various particle properties as well as how that in turn might affect the results of biological studies.

5.3.4 Nanoparticle - viability assay interference

NP interference with the components of viability assays has been discussed in the open literature, and it has been established that the interference is not universal but depends on the nature of both the assay components and the NP [69, 112, 113]. Some metal NPs have shown to interfere with the reduction process of the AlamarBlue component into a fluorescent state. The high surface area of NPs makes them excellent catalysts for chemical reactions [114]. Particles with reducing properties might therefore interfere with the viability results in assays relying on reduction-oxidation principles. The AlamarBlue assay uses such a reduction principle, however, Si NPs are fortunately found not to interfere with the AlamarBlue components at concentrations below 0.01 mg/mL in literature. However, one should be aware that Si NPs were found to interfere with BCA protein assays and catalase assays [69].

It is a well-known fact that pSi has been shown to have intrinsic luminescent properties with emission in the near infrared range upon excitation below 520 nm [6]. These properties might interfere with viability assays using fluorescent tracers, but the excitation and emission wavelengths do not correspond with the specific excitation and emission wavelengths of the AlamarBlue assay (560 and 590 nm). As observed in the micrographs presented in Figure 5.24, Figure 5.25 and Figure 5.26, the IFE particles remain in the sample even after multiple washes with PBS, which means that they have the opportunity of interfering with the AlamarBlue assay components.

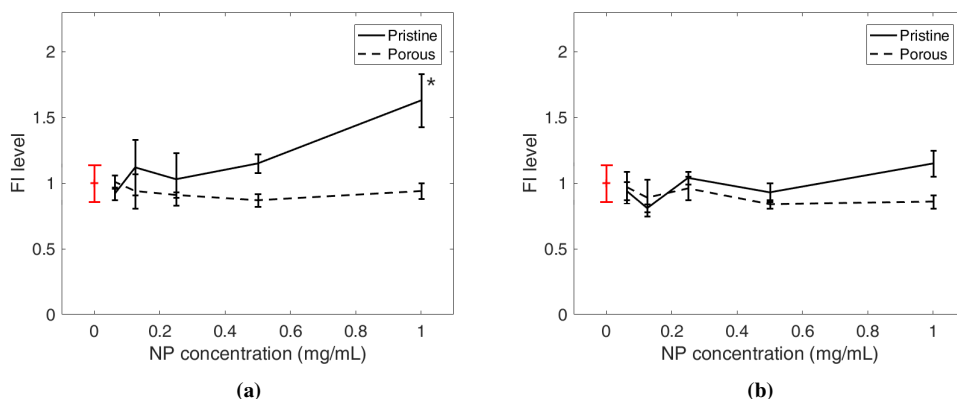


Figure 5.28: Assay interference tests between (a) IFE Si NPs and Alamar blue. Fluorescence intensity (FI) level standardized to samples not added NPs. (b) IFE Si NPs in cell culture media without AlamarBlue, assessing FI of NPs, standardized to FI of only cell culture medium. Red marks statistical average and standard deviation of control samples (no NPs). The results are plotted as averages with standard deviations of at least $n=4$ samples. * $P < 0.05$ compared to control.

Control experiments of IFE Si NPs dissolved in a cell culture media with and without AlamarBlue assay components were conducted to assess the NP-assay interference and the possibility of intrinsic fluorescence at the wavelength of AlamarBlue assay detection. The results, presented in Figure 5.28, show that there is no intrinsic fluorescence at that

particular wavelength, as well as no quenching of fluorescence, revealing no significant interference with the AlamarBlue assay components **except** for the pristine particles at 1 mg/mL. At all NP concentrations above 63 $\mu\text{g/mL}$ a higher fluorescence intensity (FI) level is seen for the pristine particles comparing to the porous particles. This difference is believed not to be a result of intrinsic luminescence. Improved catalytic activity of pristine particles at high NP concentration might, however, be part of the explanation for the observed phenomenon of Si NP-assay interference.

These interference control experiments were performed using IFE Si NPs sterilized by ethanol washing, which might be part of the explanation for the increased viability signals observed for high NP concentrations after ethanol wash. These results might, however, not be trustworthy for assay interference of autoclaved particles. One should carefully select appropriate viability assays suitable for toxicity testing of the nanomaterial in question. Moreover, the addition of analytes such as cells may highly modify the degree of NP interference, and testing for interference by measuring the addition of NP to assay reagents may not be adequate [69]. To accurately obtain trustworthy viability data and to study controls for assay interference, several different cell viability assays measuring various cell health indicators should be conducted in parallel.

Summary and Conclusion

In the present study, the stability and biocompatibility properties of the porous and non-porous IFE Si NPs intended for drug delivery purposes have been studied. Si has been shown to be a highly versatile material giving the possibility to exploit several different technologies for "smart" DDS. A novel Si NP synthesis route using a free space reactor and a highly effective catalytic porosification process has been used for the production of the particles allowing for high-scale synthesis and clinical usage.

The overall aim of the present study has been to assess the IFE Si NPs by characterizing them with an emphasis on the pH-dependent stability and induced *in vitro* cytotoxicity. In other words, assessing the particles suitability as a carrier material for drug delivery. The obtained results are presented in four parts, *i.e.* 1) literature review of pSi and Si NP dissolution stability, 2) characterization of the IFE Si NPs, 3) experimental pH-dependent stability studies of the IFE Si NPs, and 4) *in vitro* cytotoxicity studies of the IFE particles.

The literature review revealed stability dependence on a range of particle properties such as size, crystallinity and porosity, as well as surface modifications and the nature of the media in which particles are immersed. A pH-dependent dissolution was observed with increasing amounts of dissolved Si when increasing the media pH. The IFE Si NPs characterization data disclosed an average particle diameter of 80 and 100 nm for the porous and pristine particles, respectively. According to literature, the nanoscale size indicate fast dissolution, *i.e.* within hours, however, high crystallinity and a native oxide layer identified by XRD and EDS would indicate a slower dissolution process for the IFE particles.

The pH stability studies of the IFE Si NPs showed increasing hydrodynamic diameter, measured by DLS, over 24 hours after immersion in buffer solutions with increasing pH. This increase in size over time was observed for pH as low as 8 and 7 for pristine and porous particles, respectively. For the porous particles, a near-linear dependence was observed between increasing Z-average and pH. SEM images showed larger fused structures of particles in increasing pH. This was seen for pristine particles after 8 hours of immersion

in pH 10 and for porous particles in pH 8-10. Possible colloid phenomena that can explain these observations include agglomeration, aggregation, coalescence and/or deposition of dissolved silicon-containing species in an Ostwald ripening-like manner. The latter theory supports the established increase in the Si dissolution rate at high pH, which is in good agreement with what was found in literature. Regardless of the mechanism, the findings are interesting for drug delivery applications as it might give complications for the *in vivo* drug delivery process, as well as for colloid solutions for intravenous administration. In the case of pH-dependent dissolution, a mechanism for stimuli-responsive drug release has been presented.

In vitro biocompatibility studies with optical microscopy observations and AlamarBlue assay results show low cytotoxicity of the IFE Si NPs to KPC and PC3 cell lines with a minimum of 50% cell viability of up to 1 mg/mL NP exposure over 48 hours of incubation time. Different toxicity profiles were observed for the two particle types, with pristine particles showing concentration-dependent toxicity and porous particles showing a time-dependent toxic response. Moreover, the porous particles generally showed a lower degree of toxicity. The observed hydrophobicity of the particles is believed to be the reason for them clustering to the cell surface, which might also be involved in the mechanism inducing toxicity. These results are for particles sterilized by autoclaving, and higher cytotoxicity was observed for ethanol-washed particles, for which pristine Si NPs were also shown to interfere with the AlamarBlue assay components at concentrations of 1 mg/mL. Autoclaving was shown to be the most successful sterilization route for the IFE Si NPs when comparing to filtration and ethanol wash. It is, however, yet unknown whether these sterilization techniques affect the particle properties.

Compared to several other NP drug carrier materials, Si has several advantages such as biodegradability and non-toxicity. In the present study it has been verified that the novel synthesis method adapted for the IFE particles is a promising method for drug delivery applications in terms of stability and *in vitro* toxicity. The porous particles showed superior properties in terms of cytotoxicity and have decreasing stability at increasing pH, compared to the pristine particles, that might be useful for dissolution-driven drug release. In addition, the mesoporous structure is ideal for loading of an API. The structure-dependent stability and biocompatibility results obtained in the present study will aid in tailoring future drug carrier design for various APIs and with various biological interactions and drug release mechanisms, to be used for improved drug treatment for a variety of patients.

CHAPTER 7

Further Work

A few ideas of tasks that were initiated in the present study but unfortunately not sufficiently completed to be included are summarized in the following remarks.

- Establishing a complete set of standard methods useful for characterization of drug carrier particles is an essential step in scaling up production of NPs for clinical usage. DLS, SEM, XRD and DLS have herein been verified as suitable methods for characterizing the IFE Si NPs. XRD and EDS analysis has yet to be performed for the porous and pristine particles, respectively. Suggested additional techniques include quantification of porosity by specific surface area measurements using nitrogen adsorption analysis (BET) and verification of surface chemistry upon modification using Fourier Transform infrared spectroscopy (FTIR).
- Zeta potential measurements of the IFE Si NPs in buffer solutions was initiated but not completed due to technical problems. Electrostatic forces between particles, measured as the zeta potential, is thought to be important for colloidal stability. Zeta potential is altered by the medium pH, thus apparently highly relevant for the pH-dependent stability studies presently conducted. It should however, be pointed out that the zeta potential is as much dependent on the dispersion media as the nature of the particles, and in high salt concentrations (like 100 mM used herein and in physiological conditions of 150 mM) zeta potential is no longer applicable. One can therefore discuss if it gives useful information for NPs in biomedical applications [60]. Establishment of an appropriate procedure for zeta potential measurement could, however, give valuable information of specified colloidal systems of interest.
- To supplement the DLS particle diameter change measurements in view of the stability studies with a direct analysis method, automated image analysis of SEM micrographs using algorithms for particle counting and size measurement was initi-

ated. Challenges associated with low contrast images and algorithm development, however, created difficulties in completing the task.

Based on the experimental studies performed in the present study, several research questions have been raised that might form the basis of an extension of the work. Verification of the mechanism of the particle growth at high pH could be investigated by nitrogen adsorption surface area measurements to test the aggregation hypothesis, and by elemental composition analysis as well as crystallography measurements of the deposited structures to test the amorphous silica deposition and the aggregation hypotheses. Following the findings from the literature review, it would be interesting to study dissolution kinetics of the IFE Si NPs by ICP or MBA methods, as well as assessing how stability is affected by various particle properties, temperature and the presence of salts and/or other compounds present in biological systems. Compared to the spatially confined containers used for stability studies in the present study, a setup with concentration control or dynamic environments might give a more realistic model for *in vivo* stability studies. Furthermore, an extension to the stability studies is to identify how stability affects drug release kinetics and quantify the differences for drugs loaded by covalent bonding, entrapment in pores or physically adsorbed onto the particle surface. This is, however, another huge research area as such properties highly depend on the properties of the individual drug molecules that in most cases are highly specific, but it would give valuable information about the versatility of the IFE Si NPs as drug carriers.

The mechanisms behind the observations of the cell viability studies might be studied using molecular biological techniques, which might disclose both how particle attachment affect the cell viability and what cellular mechanisms are behind the cytotoxicity profile of the IFE Si NPs. Studying how different particle properties affect cytotoxicity and how various sterilization techniques affect particle properties are yet other interesting approaches to understand the underlying mechanisms.

Exploring chemical modification possibilities of Si is an interesting next phase both for functionalization and stability purposes, and to tune cytotoxic responses. Seen from both the stability and cytotoxicity studies reported herein, the creation of particle assemblages is a major challenge of unmodified particles, partly due to their hydrophobic behavior. Hydrophilicity is also obtained by chemical modification of the particle surfaces. Furthermore, for exploiting the vast opportunities in nanomedicine, such as targeting and stimuli-responsive release, surface modification of drug carriers is inevitable. A natural next phase towards developing a complete drug carrier of the IFE Si NPs includes therefore establishing different surface modification processes, which will allow for creating novel technologies. The study of how stability, as well as cytotoxicity and *in vivo* accumulation is affected by these alterations are also of high priority. Multi-phase clinical trials are then required in order to get a complete pharmaceutical formulation of Si NPs approved for clinical usage.

References

- [1] Daniel Fine, Alessandro Grattoni, Randy Goodall, Shyam S Bansal, Ciro Chiappini, Sharath Hosali, Anne L van de Ven, Srimeenkashi Srinivasan, Xuewu Liu, Biana Godin, et al. “Silicon micro-and nanofabrication for medicine”. In: *Advanced healthcare materials 2.5* (2013), pp. 632–666.
- [2] Youssef W Naguib and Zhengrong Cui. “Nanomedicine: The promise and challenges in cancer chemotherapy”. In: *Nanomaterial*. Springer, 2014, pp. 207–233.
- [3] Nazila Kamaly, John C He, Dennis A Ausiello, and Omid C Farokhzad. “Nanomedicines for renal disease: current status and future applications”. In: *Nature Reviews Nephrology 12.12* (2016), pp. 738–753.
- [4] MG Krukemeyer, V Krenn, F Huebner, W Wagner, and R Resch. “History and possible uses of nanomedicine based on nanoparticles and nanotechnological progress”. In: *Journal of Nanomedicine & Nanotechnology 6.1* (2015).
- [5] You Han Bae and Kinam Park. “Targeted drug delivery to tumors: myths, reality and possibility”. In: *Journal of controlled release 153.3* (2011), p. 198.
- [6] Leigh T Canham. “Silicon quantum wire array fabrication by electrochemical and chemical dissolution of wafers”. In: *Applied physics letters 57.10* (1990), pp. 1046–1048.
- [7] Leigh T Canham. “Bioactive silicon structure fabrication through nanoetching techniques”. In: *Advanced Materials 7.12* (1995), pp. 1033–1037.
- [8] Ji-Ho Park, Luo Gu, Geoffrey Von Maltzahn, Erkki Ruoslahti, Sangeeta N Bhatia, and Michael J Sailor. “Biodegradable luminescent porous silicon nanoparticles for in vivo applications”. In: *Nature materials 8.4* (2009), pp. 331–336.
- [9] Chang-Fang Wang, Mirkka P Sarparanta, Ermei M Mäkilä, Maija LK Hyvönen, Pirjo M Laakkonen, Jarno J Salonen, Jouni T Hirvonen, Anu J Airaksinen, and Hélder A Santos. “Multifunctional porous silicon nanoparticles for cancer therapeutics”. In: *Biomaterials 48* (2015), pp. 108–118.

REFERENCES

- [10] Bárbara Herranz-Blanco, Dongfei Liu, Ermei Mäkilä, Mohammad-Ali Shahbazi, Eloy Ginestar, Hongbo Zhang, Vladimir Aseyev, Vimalkumar Balasubramanian, Jarno Salonen, Jouni Hirvonen, et al. “On-Chip Self-Assembly of a Smart Hybrid Nanocomposite for Antitumoral Applications”. In: *Advanced functional materials* 25.10 (2015), pp. 1488–1497.
- [11] Alejandra Nieto, Huiyuan Hou, Sang Woong Moon, Michael J Sailor, William R Freeman, and Lingyun Cheng. “Surface engineering of porous silicon microparticles for intravitreal sustained delivery of rapamycin”. In: *Investigative ophthalmology & visual science* 56.2 (2015), pp. 1070–1080.
- [12] Byungji Kim, Hong-Bo Pang, Jinyoung Kang, Ji-Ho Park, Erkki Ruoslahti, and Michael J Sailor. “Immunogene therapy with fusogenic nanoparticles modulates macrophage response to *Staphylococcus aureus*”. In: *Nature communications* 9.1 (2018), pp. 1–13.
- [13] SHC Anderson, H Elliott, DJ Wallis, LT Canham, and JJ Powell. “Dissolution of different forms of partially porous silicon wafers under simulated physiological conditions”. In: *physica status solidi (a)* 197.2 (2003), pp. 331–335.
- [14] Simo Näkki, Jussi Rytönen, Tuomo Nissinen, Cristina Florea, Joakim Riikonen, Paul Ek, Hongbo Zhang, Hélder A Santos, Ale Närvänen, Wujun Xu, et al. “Improved stability and biocompatibility of nanostructured silicon drug carrier for intravenous administration”. In: *Acta biomaterialia* 13 (2015), pp. 207–215.
- [15] Hanne Flåten Andersen, Werner Filtvedt, Jan Petter Mæhlen, Trygve Tveiterås Mongstad, Martin Kirkengen, and Arve Holt. “Production of Silicon Particles for High-Capacity Anode Material Yielding Outstanding Production Capacity”. In: *ECS Transactions* 62.1 (2014), pp. 97–105.
- [16] Kurt W Kolasinski, Nathan J Gimbar, Haibo Yu, Mark Aindow, Ermei Mäkilä, and Jarno Salonen. “Regenerative electroless etching of silicon”. In: *Angewandte Chemie International Edition* 56.2 (2017), pp. 624–627.
- [17] Merriam-Webster.com Dictionary. *Stability*. URL: <https://www.merriam-webster.com/dictionary/stability> (visited on 08/06/2020).
- [18] Jan Fallingborg. “Intraluminal pH of the human gastrointestinal tract.” In: *Danish medical bulletin* 46.3 (1999), p. 183.
- [19] Oleg A Andreev, Donald M Engelman, and Yana K Reshetnyak. “Targeting acidic diseased tissue: New technology based on use of the pH (Low) Insertion Peptide (pHLIP)”. In: *Chimica oggi* 27.2 (2009), p. 34.
- [20] Wujin Sun, Quanyin Hu, Wenyan Ji, Grace Wright, and Zhen Gu. “Leveraging physiology for precision drug delivery”. In: *Physiological reviews* 97.1 (2017), pp. 189–225.
- [21] Susan Hua and Sherry Y Wu. “Advances and challenges in nanomedicine”. In: *Frontiers in pharmacology* 9 (2018), p. 1397.
- [22] Keith B Hartman and Lon J Wilson. “Carbon nanostructures as a new high-performance platform for MR molecular imaging”. In: *Bio-Applications of Nanoparticles*. Springer, 2007, pp. 74–84.

-
- [23] Roman A Perez, Rajendra K Singh, Tae-Hyun Kim, and Hae-Won Kim. “Silica-based multifunctional nanodelivery systems toward regenerative medicine”. In: *Materials Horizons* 4.5 (2017), pp. 772–799.
- [24] Hamsa Jaganathan and Biana Godin. “Biocompatibility assessment of Si-based nano- and micro-particles”. In: *Advanced drug delivery reviews* 64.15 (2012), pp. 1800–1819.
- [25] Sazan M Haidary, Emma P Corcoles, and Nihad K Ali. “Nanoporous silicon as drug delivery systems for cancer therapies”. In: *Journal of Nanomaterials* 2012 (2012).
- [26] Conroy Sun, Jerry SH Lee, and Miqin Zhang. “Magnetic nanoparticles in MR imaging and drug delivery”. In: *Advanced drug delivery reviews* 60.11 (2008), pp. 1252–1265.
- [27] Alessandro Bertucci, Kang-Hoon Kim, Jinyoung Kang, Jonathan M Zuidema, Seo Hyeon Lee, Ester J Kwon, Dokyoung Kim, Stephen B Howell, Francesco Ricci, Erkki Ruoslahti, et al. “Tumor-Targeting, MicroRNA-Silencing Porous Silicon Nanoparticles for Ovarian Cancer Therapy”. In: *ACS applied materials & interfaces* 11.27 (2019), pp. 23926–23937.
- [28] Yapei Wang, James D Byrne, Mary E Napier, and Joseph M DeSimone. “Engineering nanomedicines using stimuli-responsive biomaterials”. In: *Advanced drug delivery reviews* 64.11 (2012), pp. 1021–1030.
- [29] Tatsuo Saga. “Advances in crystalline silicon solar cell technology for industrial mass production”. In: *NPG Asia Materials* 2.3 (2010), pp. 96–102.
- [30] Jillian M Buriak. “Organometallic chemistry on silicon surfaces: Formation of functional monolayers bound through Si–C bonds”. In: *Chemical Communications* 12 (1999), pp. 1051–1060.
- [31] Merriam-Webster.com Dictionary. *Biocompatibility*. URL: <https://www.merriam-webster.com/dictionary/biocompatibility> (visited on 07/30/2020).
- [32] Karina S Pérez, David Warther, Ma Estela Calixto, Antonio Méndez-Blas, and Michael J Sailor. “Harnessing the Aqueous Chemistry of Silicon: Self-Assembling Porous Silicon/Silica Microribbons”. In: *ACS applied materials & interfaces* 11.30 (2019), pp. 27162–27169.
- [33] Jarno Salonen and Ermei Mäkilä. “Thermally carbonized porous silicon and its recent applications”. In: *Advanced Materials* 30.24 (2018), p. 1703819.
- [34] Beniamino Sciacca, Sara D Alvarez, Francesco Geobaldo, and Michael J Sailor. “Bioconjugate functionalization of thermally carbonized porous silicon using a radical coupling reaction”. In: *Dalton Transactions* 39.45 (2010), pp. 10847–10853.
- [35] Rabah Boukherroub, JTC Wojtyk, Danial DM Wayner, and David J Lockwood. “Thermal hydrosilylation of undecylenic acid with porous silicon”. In: *Journal of the Electrochemical Society* 149.2 (2002), H59–H63.
- [36] Seo Hyeon Lee, Jae Seung Kang, and Dokyoung Kim. “A mini review: Recent advances in surface modification of porous silicon”. In: *Materials* 11.12 (2018), p. 2557.
-

- [37] Daniela F Enache, Eugenia Vasile, Claudia Maria Simonescu, Daniela Culita, Eugeniu Vasile, Ovidiu Oprea, Andreea Madalina Pandele, Anca Razvan, Florina Dumitru, and Gheorghe Nechifor. "Schiff base-functionalized mesoporous silicas (MCM-41, HMS) as Pb (II) adsorbents". In: *RSC advances* 8.1 (2018), pp. 176–189.
- [38] Dokyoung Kim, Jinmyoung Joo, Youlin Pan, Alice Boarino, Yong Woong Jun, Kyo Han Ahn, Barry Arkles, and Michael J Sailor. "Thermally induced silane dehydrocoupling on silicon nanostructures". In: *Angewandte Chemie* 128.22 (2016), pp. 6533–6537.
- [39] Jung-Woo Park, Young Jun Park, and Chul-Ho Jun. "Post-grafting of silica surfaces with pre-functionalized organosilanes: new synthetic equivalents of conventional trialkoxysilanes". In: *Chemical Communications* 47.17 (2011), pp. 4860–4871.
- [40] J Salonen, Leena Laitinen, Ann Marie Kaukonen, J Tuura, M Björkqvist, T Heikkilä, K Vähä-Heikkilä, Jouni Hirvonen, and V-P Lehto. "Mesoporous silicon microparticles for oral drug delivery: loading and release of five model drugs". In: *Journal of controlled release* 108.2-3 (2005), pp. 362–374.
- [41] Sazan M Haidary, Awaz B Mohammed, Emma P Córcoles, Nihad K Ali, and MR Ahmad. "Effect of coatings and surface modification on porous silicon nanoparticles for delivery of the anticancer drug tamoxifen". In: *Microelectronic Engineering* 161 (2016), pp. 1–6.
- [42] Sazid Hussain, Jinmyoung Joo, Jinyoung Kang, Byungji Kim, Gary B Braun, Zhi-Gang She, Dokyoung Kim, Aman P Mann, Tarmo Mölder, Tambat Teesalu, et al. "Antibiotic-loaded nanoparticles targeted to the site of infection enhance antibacterial efficacy". In: *Nature biomedical engineering* 2.2 (2018), pp. 95–103.
- [43] Biana Godin, Ciro Chiappini, Srimeenakshi Srinivasan, Jenolyn F Alexander, Kenji Yokoi, Mauro Ferrari, Paolo Decuzzi, and Xuewu Liu. "Discoidal porous silicon particles: fabrication and biodistribution in breast cancer bearing mice". In: *Advanced functional materials* 22.20 (2012), pp. 4225–4235.
- [44] PK Sudeep, Zachariah Page, and Todd Emrick. "PEGylated silicon nanoparticles: synthesis and characterization". In: *Chemical communications* 46 (2008), pp. 6126–6127.
- [45] Jamie H Warner, Akiyoshi Hoshino, Kenji Yamamoto, and Richard D Tilley. "Water-soluble photoluminescent silicon quantum dots". In: *Angewandte Chemie International Edition* 44.29 (2005), pp. 4550–4554.
- [46] Luigi Russo, Francesco Colangelo, Raffaele Cioffi, Iliaria Rea, and Luca De Stefano. "A mechanochemical approach to porous silicon nanoparticles fabrication". In: *Materials* 4.6 (2011), pp. 1023–1033.
- [47] İlker Doğan and Mauritius CM van de Sanden. "Gas-Phase Plasma Synthesis of Free-Standing Silicon Nanoparticles for Future Energy Applications". In: *Plasma Processes and Polymers* 13.1 (2016), pp. 19–53.

-
- [48] Trygve Mongstad, Hallgeir Klette, Ørnulf Nordseth, Thomas J Preston, Guro M Wyller, and Werner O Filtvedt. “New technologies for silicon production from monosilane; Pilot testing and on-line process monitoring aiding the development”. In: *Silicon Chem. Sol. Ind. XIII* (2016), pp. 1–10.
- [49] WO Filtvedt, H Klette, S Sørensen, and J Filtvedt. “Low cost/high quality silicon production by centrifuge CVD reactor upscaled and hot harvest”. In: *EU PVSEC* (2015).
- [50] Kurt W Kolasinski. “Silicon nanostructures from electroless electrochemical etching”. In: *Current Opinion in Solid State and Materials Science* 9.1-2 (2005), pp. 73–83.
- [51] Jarno Salonen and Vesa-Pekka Lehto. “Fabrication and chemical surface modification of mesoporous silicon for biomedical applications”. In: *Chemical Engineering Journal* 137.1 (2008), pp. 162–172.
- [52] Mingyuan Ge, Jiepeng Rong, Xin Fang, Anyi Zhang, Yunhao Lu, and Chongwu Zhou. “Scalable preparation of porous silicon nanoparticles and their application for lithium-ion battery anodes”. In: *Nano Research* 6.3 (2013), pp. 174–181.
- [53] Luis M Bimbo, Mirkka Sarparanta, Hélder A Santos, Anu J Airaksinen, Ermei Mäkilä, Timo Laaksonen, Leena Peltonen, Vesa-Pekka Lehto, Jouni Hirvonen, and Jarno Salonen. “Biocompatibility of thermally hydrocarbonized porous silicon nanoparticles and their biodistribution in rats”. In: *ACS nano* 4.6 (2010), pp. 3023–3032.
- [54] Wei Li, Yunzhan Li, Zehua Liu, Nattha Kerdsakundee, Ming Zhang, Feng Zhang, Xueyan Liu, Tomás Bauleth-Ramos, Wenhua Lian, Ermei Mäkilä, et al. “Hierarchical structured and programmed vehicles deliver drugs locally to inflamed sites of intestine”. In: *Biomaterials* 185 (2018), pp. 322–332.
- [55] Inez N Lees, Haohao Lin, Christie A Canaria, Christian Gurtner, Michael J Sailor, and Gordon M Miskelly. “Chemical stability of porous silicon surfaces electrochemically modified with functional alkyl species”. In: *Langmuir* 19.23 (2003), pp. 9812–9817.
- [56] Dokyoung Kim, Jonathan M Zuidema, Jinyoung Kang, Youlin Pan, Lianbin Wu, David Warther, Barry Arkles, and Michael J Sailor. “Facile surface modification of hydroxylated silicon nanostructures using heterocyclic silanes”. In: *Journal of the American Chemical Society* 138.46 (2016), pp. 15106–15109.
- [57] Paul C Hiemenz and Raj Rajagopalan. *Principles of Colloid and Surface Chemistry, revised and expanded (Chapter 1)*. CRC press, 2016.
- [58] Evert Johannes Willem Verwey, Jan Theodoor Gerard Overbeek, and K Van Nes. *Theory of the stability of lyophobic colloids: the interaction of sol particles having an electric double layer*. Elsevier Publishing Company, 1948.
- [59] Barry W Ninham. “On progress in forces since the DLVO theory”. In: *Advances in colloid and interface science* 83.1-3 (1999), pp. 1–17.
-

- [60] Jingkun Jiang, Günter Oberdörster, and Pratim Biswas. “Characterization of size, surface charge, and agglomeration state of nanoparticle dispersions for toxicological studies”. In: *Journal of Nanoparticle Research* 11.1 (2009), pp. 77–89.
- [61] Gary Nichols, Stephen Byard, Mark J Bloxham, Joanne Botterill, Neil J Dawson, Andrew Dennis, Valerie Diart, Nigel C North, and John D Sherwood. “A review of the terms agglomerate and aggregate with a recommendation for nomenclature used in powder and particle characterization”. In: *Journal of pharmaceutical sciences* 91.10 (2002), pp. 2103–2109.
- [62] Jörg Stetefeld, Sean A McKenna, and Trushar R Patel. “Dynamic light scattering: a practical guide and applications in biomedical sciences”. In: *Biophysical reviews* 8.4 (2016), pp. 409–427.
- [63] *Dynamic light scattering. Common terms defined*. MRK1764-01. Malvern Instruments Worldwide. Feb. 2011.
- [64] Meenakshi Arora. “Cell culture media: a review”. In: *Mater methods* 3.175 (2013), p. 24.
- [65] Hainan Sun, Jianbo Jia, Cuijuan Jiang, and Shumei Zhai. “Gold nanoparticle-induced cell death and potential applications in nanomedicine”. In: *International journal of molecular sciences* 19.3 (2018), p. 754.
- [66] Hainan Sun, Cuijuan Jiang, Ling Wu, Xue Bai, and Shumei Zhai. “Cytotoxicity-Related Bioeffects Induced by Nanoparticles: The Role of Surface Chemistry”. In: *Frontiers in Bioengineering and Biotechnology* 7 (2019), p. 414.
- [67] Terry L Riss, Richard A Moravec, Andrew L Niles, Sarah Duellman, Hélène A Benink, Tracy J Worzella, and Lisa Minor. “Cell viability assays”. In: *Assay Guidance Manual [Internet]*. Eli Lilly & Company and the National Center for Advancing Translational Sciences, 2016.
- [68] Joseph R. Lakowicz. *Principles of Fluorescence Spectroscopy*. 3rd edition. Springer US, 2006.
- [69] Kimberly J Ong, Tyson J MacCormack, Rhett J Clark, James D Ede, Van A Ortega, Lindsey C Felix, Michael KM Dang, Guibin Ma, Hicham Fenniri, Jonathan GC Veinot, et al. “Widespread nanoparticle-assay interference: implications for nanotoxicity testing”. In: *PLoS One* 9.3 (2014), e90650.
- [70] Melissa A Vetten, Clarence S Yah, Tanusha Singh, and Mary Gulumian. “Challenges facing sterilization and depyrogenation of nanoparticles: effects on structural stability and biomedical applications”. In: *Nanomedicine: Nanotechnology, Biology and Medicine* 10.7 (2014), pp. 1391–1399.
- [71] Martin Wilson - Leica Microsystems. *Introduction to Widefield Microscopy*. 2017. URL: <https://www.leica-microsystems.com/science-lab/introduction-to-widefield-microscopy/> (visited on 07/14/2020).
- [72] David Ferdinand Boltz and Melvin Guy Mellon. “Determination of phosphorus, germanium, silicon, and arsenic”. In: *Analytical Chemistry* 19.11 (1947), pp. 873–877.

-
- [73] Cristiane X Galhardo and Jorge C Masini. “Spectrophotometric determination of phosphate and silicate by sequential injection using molybdenum blue chemistry”. In: *Analytica Chimica Acta* 417.2 (2000), pp. 191–200.
- [74] A Lopez Molinero, L Martinez, A Villareal, and JR Castillo. “Silicon determination by inductively coupled plasma atomic emission spectrometry after generation of volatile silicon tetrafluoride”. In: *Talanta* 45.6 (1998), pp. 1211–1217.
- [75] Rae Hyung Kang, Seo Hyeon Lee, Sangrim Kang, Jinyoung Kang, Junho K Hur, and Dokyoung Kim. “Systematic Degradation Rate Analysis of Surface-Functionalized Porous Silicon Nanoparticles”. In: *Materials* 12.4 (2019), p. 580.
- [76] Jonathan O Martinez, Ciro Chiappini, Arturas Ziemys, Ari M Faust, Milos Kojic, Xuewu Liu, Mauro Ferrari, and Ennio Tasciotti. “Engineering multi-stage nanovectors for controlled degradation and tunable release kinetics”. In: *Biomaterials* 34.33 (2013), pp. 8469–8477.
- [77] Biana Godin, Jianhua Gu, Rita E Serda, Rohan Bhavane, Ennio Tasciotti, Ciro Chiappini, Xuewu Liu, Takemi Tanaka, Paolo Decuzzi, and Mauro Ferrari. “Tailoring the degradation kinetics of mesoporous silicon structures through PEGylation”. In: *Journal of biomedical materials research Part A* 94.4 (2010), pp. 1236–1243.
- [78] Yu-Shen Lin, Nardine Abadeer, and Christy L Haynes. “Stability of small mesoporous silica nanoparticles in biological media”. In: *Chemical Communications* 47.1 (2011), pp. 532–534.
- [79] Feng Wang, Timothy J Barnes, and Clive A Prestidge. “Controlling and Predicting the Dissolution Kinetics of Thermally Oxidised Mesoporous Silicon Particles: Towards Improved Drug Delivery”. In: *Pharmaceutics* 11.12 (2019), p. 634.
- [80] Nick K Hon, Zory Shaposhnik, Eric D Diebold, Fuyuhiko Tamanoi, and Bahram Jalali. “Tailoring the biodegradability of porous silicon nanoparticles”. In: *Journal of Biomedical Materials Research Part A* 100.12 (2012), pp. 3416–3421.
- [81] Karyn L Jarvis, Timothy J Barnes, and Clive A Prestidge. “Surface chemistry of porous silicon and implications for drug encapsulation and delivery applications”. In: *Advances in colloid and interface science* 175 (2012), pp. 25–38.
- [82] Mengjia Wang, Philip S Hartman, Armando Loni, Leigh T Canham, Nelli Bodiford, and Jeffery L Coffey. “Influence of surface chemistry on the release of an antibacterial drug from nanostructured porous silicon”. In: *Langmuir* 31.22 (2015), pp. 6179–6185.
- [83] Q Shabir, A Pokale, A Loni, DR Johnson, LT Canham, R Fenollosa, M Tymczenko, I Rodr guez, F Meseguer, Ana Cros, et al. “Medically biodegradable hydrogenated amorphous silicon microspheres”. In: *Silicon* 3.4 (2011), pp. 173–176.
- [84] Luis M Bimbo, Ermei M kil , Timo Laaksonen, Vesa-Pekka Lehto, Jarno Salonen, Jouni Hirvonen, and H lder A Santos. “Drug permeation across intestinal epithelial cells using porous silicon nanoparticles”. In: *Biomaterials* 32.10 (2011), pp. 2625–2633.
-

- [85] Adi Tzur-Balter, Zohar Shatsberg, Margarita Beckerman, Ester Segal, and Natalie Artzi. “Mechanism of erosion of nanostructured porous silicon drug carriers in neoplastic tissues”. In: *Nature communications* 6 (2015), p. 6208.
- [86] Fang Chen and Yingchun Zhu. “Chitosan enclosed mesoporous silica nanoparticles as drug nano-carriers: Sensitive response to the narrow pH range”. In: *Microporous and Mesoporous Materials* 150 (2012), pp. 83–89.
- [87] Dongfei Liu, Hongbo Zhang, Bárbara Herranz-Blanco, Ermei Mäkilä, Vesa-Pekka Lehto, Jarno Salonen, Jouni Hirvonen, and Hélder A Santos. “Microfluidic Assembly of Monodisperse Multistage pH-Responsive Polymer/Porous Silicon Composites for Precisely Controlled Multi-Drug Delivery”. In: *Small* 10.10 (2014), pp. 2029–2038.
- [88] Qiaohua Qiu, Zhenzhen Quan, Hongnan Zhang, Xiaohong Qin, Rongwu Wang, and Jianyong Yu. “pH-triggered sustained drug release of multilayer encapsulation system with hollow mesoporous silica nanoparticles/chitosan/polyacrylic acid”. In: *Materials Letters* 260 (2020), p. 126907.
- [89] Miguel A Gosálvez, I Zubel, and Eeva Viinikka. “Wet etching of silicon”. In: *Handbook of Silicon Based MEMS Materials and Technologies*. Elsevier, 2010, pp. 447–480.
- [90] Frank K Crundwell. “On the mechanism of the dissolution of quartz and silica in aqueous solutions”. In: *ACS omega* 2.3 (2017), pp. 1116–1127.
- [91] Yuki Kobayashi, Shinsuke Matsuda, Kentaro Imamura, and Hikaru Kobayashi. “Hydrogen generation by reaction of Si nanopowder with neutral water”. In: *Journal of Nanoparticle Research* 19.5 (2017), p. 176.
- [92] S Litvinenko, S Alekseev, V Lysenko, A Venturello, F Geobaldo, L Gulina, G Kuznetsov, V Tolstoy, V Skryshevsky, E Garrone, et al. “Hydrogen production from nano-porous Si powder formed by stain etching”. In: *international journal of hydrogen energy* 35.13 (2010), pp. 6773–6778.
- [93] Hasliza Bahruji, Michael Bowker, and Philip R Davies. “Photoactivated reaction of water with silicon nanoparticles”. In: *International journal of hydrogen energy* 34.20 (2009), pp. 8504–8510.
- [94] Weilie Zhou, Robert Apkarian, Zhong Lin Wang, and David Joy. “Fundamentals of scanning electron microscopy (SEM)”. In: *Scanning microscopy for nanotechnology*. Springer, 2006, pp. 1–40.
- [95] H Stanjek and W Häusler. “Basics of X-ray Diffraction”. In: *Hyperfine Interactions* 154.1-4 (2004), pp. 107–119.
- [96] John C Russ. *Fundamentals of Energy Dispersive X-Ray Analysis: Butterworths Monographs in Materials*. Butterworth-Heinemann, 2013.
- [97] Invitrogen Molecular Probes. “AlamarBlue® cell viability reagent, Protocol summary”. In: (2008).

-
- [98] M Danaei, M Dehghankhold, S Ataei, F Hasanzadeh Davarani, R Javanmard, A Dokhani, S Khorasani, and MR Mozafari. “Impact of particle size and polydispersity index on the clinical applications of lipidic nanocarrier systems”. In: *Pharmaceutics* 10.2 (2018), p. 57.
- [99] R Bisaro, Ji Magariño, N Proust, and K Zellama. “Structure and crystal growth of atmospheric and low-pressure chemical-vapor-deposited silicon films”. In: *Journal of applied physics* 59.4 (1986), pp. 1167–1178.
- [100] Christian Bohling and Wolfgang Sigmund. “Self-limitation of native oxides explained”. In: *Silicon* 8.3 (2016), pp. 339–343.
- [101] Kari EJ Lehtinen and Michael R Zachariah. “Effect of coalescence energy release on the temporal shape evolution of nanoparticles”. In: *Physical Review B* 63.20 (2001), p. 205402.
- [102] Jason Holm and Jeffrey T Roberts. “Sintering, coalescence, and compositional changes of hydrogen-terminated silicon nanoparticles as a function of temperature”. In: *The Journal of Physical Chemistry C* 113.36 (2009), pp. 15955–15963.
- [103] Peter W Voorhees. “The theory of Ostwald ripening”. In: *Journal of Statistical Physics* 38.1-2 (1985), pp. 231–252.
- [104] Søren Bredmose Simonsen, Ib Chorkendorff, Søren Dahl, Magnus Skoglundh, Jens Sehested, and Stig Helveg. “Ostwald ripening in a Pt/SiO₂ model catalyst studied by in situ TEM”. In: *Journal of catalysis* 281.1 (2011), pp. 147–155.
- [105] Stuart T Gentry, Shane F Kendra, and Mark W Bezpalko. “Ostwald ripening in metallic nanoparticles: stochastic kinetics”. In: *The Journal of Physical Chemistry C* 115.26 (2011), pp. 12736–12741.
- [106] Neus G Bastús, Joan Comenge, and Victor Puntes. “Kinetically controlled seeded growth synthesis of citrate-stabilized gold nanoparticles of up to 200 nm: size focusing versus Ostwald ripening”. In: *Langmuir* 27.17 (2011), pp. 11098–11105.
- [107] Elena Piletska, Heersh Yawer, Francesco Canfarotta, Ewa Moczko, Katarzyna Smolinska-Kempisty, Stanislav S Piletsky, Antonio Guerreiro, Michael J Whitcombe, and Sergey A Piletsky. “Biomimetic silica nanoparticles prepared by a combination of solid-phase imprinting and Ostwald ripening”. In: *Scientific reports* 7.1 (2017), pp. 1–9.
- [108] A Lazaro, MC Van de Griend, HJH Brouwers, and JW Geus. “The influence of process conditions and Ostwald ripening on the specific surface area of olivine nano-silica”. In: *Microporous and mesoporous materials* 181 (2013), pp. 254–261.
- [109] David J Belton, Olivier Deschaume, and Carole C Perry. “An overview of the fundamentals of the chemistry of silica with relevance to biosilicification and technological advances”. In: *The FEBS journal* 279.10 (2012), pp. 1710–1720.
- [110] Kerast. *KPCY Mouse Pancreatic Cancer Cell Lines*. URL: <https://www.kerast.com/productgroup/884/kpcy-mouse-pancreatic-cancer-cell-lines> (visited on 07/25/2020).
-

REFERENCES

- [111] SIB Swiss Institute of Bioinformatics. *Cellosaurus PC-3 (CVCL0035)*. 2012. URL: https://web.expasy.org/cellosaurus/CVCL_0035 (visited on 07/25/2020).
- [112] Alexandra Kroll, Mike Hendrik Pillukat, Daniela Hahn, and Jürgen Schnekenburger. “Interference of engineered nanoparticles with in vitro toxicity assays”. In: *Archives of toxicology* 86.7 (2012), pp. 1123–1136.
- [113] Ivana Vinković Vrček, Ivan Pavičić, Tea Crnković, Darija Jurašin, Michal Babič, Daniel Horák, Marija Lovrić, Lejla Ferhatović, Marija Ćurlin, and Srećko Gajović. “Does surface coating of metallic nanoparticles modulate their interference with in vitro assays?” In: *RSC advances* 5.87 (2015), pp. 70787–70807.
- [114] Qi-Long Zhu and Qiang Xu. “Immobilization of ultrafine metal nanoparticles to high-surface-area materials and their catalytic applications”. In: *Chem* 1.2 (2016), pp. 220–245.

Appendix

A Si NP stability & drug interactions

Literature search methodology - Si NP stability

A variety of research articles on the topic of porous and non-porous silicon nano- and microparticles was studied and crucial parameters for characterization, stability and drug interaction were identified. Porous Si NPs intended for drug delivery and other biomedical applications was the main focus. Google Scholar was the main search engine used for identifying relevant literature and key words like "nanoparticles", "drug delivery", "surface modifications", "functionalization", "stability/degradation/dissolution" and "biomedical applications" were used in different combinations with "porous silicon". Subscription access to scientific articles was given via the NTNU network library.

It was found that studies involving particle synthesis, processing, stability studies and characterization gave information on porous silicon in mainly two categories, *i.e.* drug interactions and material characterization. Drug interactions included drug loading degree and release profiles in various media, while material characterization included particle measurements like size, morphology, surface charge and area, as well as surface chemistry. Characterization parameters are related to inherent carrier material properties that are defined as quantitative parameters for easy comparison. On the other hand, drug interactions highly depend on the physical and chemical properties of the API in question and how strongly it associates with the carrier material. Also, drug release data must be compared to similar properties for the drug molecules without carrier to give valuable information. For simplicity, and to give a focused quality review in line with experimental work, a focus on characterization data and stability studies from literature was chosen for further discussion. The identified drug interaction properties can be found in Table A1.

REFERENCES

Table A1: Drug interactions found in literature studies. TOPSi = thermally oxidized pSi, TCPSi = thermally carbonized pSi, UnTHCPSi = undecylenic acid thermally hydrocarbonized pSi. t_{50} and t_{100} is the time at which 50% and 100% of the drug is released from the particle (estimated from drug release curves). Alexa488-DBCO-DOTA = dibenzocyclooctyl(DBCO)-PEG4-amine functionalized and Alexa Fluor 488-labeled. iRGD = tumor-homing peptide.

Author year	PSi particle size	Surface modifications	Loaded drug	Loading efficiency	Release profile (PBS, 37 °C)	Estimated t_{50} & t_{100} (PBS, 37 °C)
Kim et al. [56]	200 nm	Air oxidation & cyclic silanes	Lyzosome	41%	30-40% re-released after 72 h	NA
Salonen et al. [40]	20 μm	TCPSi	Ibuprofen	30.4%	20% release after 350 min	t_{50} =20-25 min,
			Antipyrine	53.4%		t_{100} =100min
			Griseofluvin	16.5%		t_{50} =25 min,
			Ranitidine	13.2%		t_{100} >100 min
			Furosemide	41.3%		t_{50} =15 min,
Wang et al. [9]	223 nm	TOPSi + Alexa488-DBCO-DOTA	Ibuprofen	7.9%	Max 70% re-release after 360 min	t_{50} =1-5 min, t_{100} >360 min
	203 nm	UnTHCPSi + Alexa488-DBCO-DOTA+iRGD	Antipyrine	27.3%		
Nieto et al. [11]	43x70x25 μm	undecylenic acid	Sorafenib	28.2%	- -	- -
		1-dodecene	Rapamycin	27.0%		
		methoxy (dimethyl) octysilane	Rapamycin	22%	Max 60% re-release after 32 days	t_{50} =18 days, t_{100} >32 days
			Rapamycin	17%	Max 2.5% re-released after 32 days	t_{50}, t_{100} >32 days
			Rapamycin	28%	Max 14% re-released after 32 days	t_{50}, t_{100} >32 days

Author year	PSi particle size	Surface modifications	Loaded drug	Loading efficiency	Release profile (in PBS at 37 °C)	Estimated t_{50} & t_{100} (in PBS at 37 °C)
Haidary et al. [41]	36.7 μm		Tamoxifen		100% released after 6 h	$t_{50}=3.5$ h, $t_{100}=6$ h
		Undecylenic acid	Tamoxifen		30.7% released after 6 h	$t_{50}, t_{100} >6$ h
		Chitosan	Tamoxifen		73.4% released after 6 h	$t_{50}=3.5$ h, $t_{100} >6$ h
		Silica xerogel	Tamoxifen		100% released after 3 h	$t_{50}=2.2$ h, $t_{100}=3$ h
		Chitosan + silica xerogel	Tamoxifen		34.6% released after 6 h	$t_{50}, t_{100} >6$ h

B Supplementary DLS material

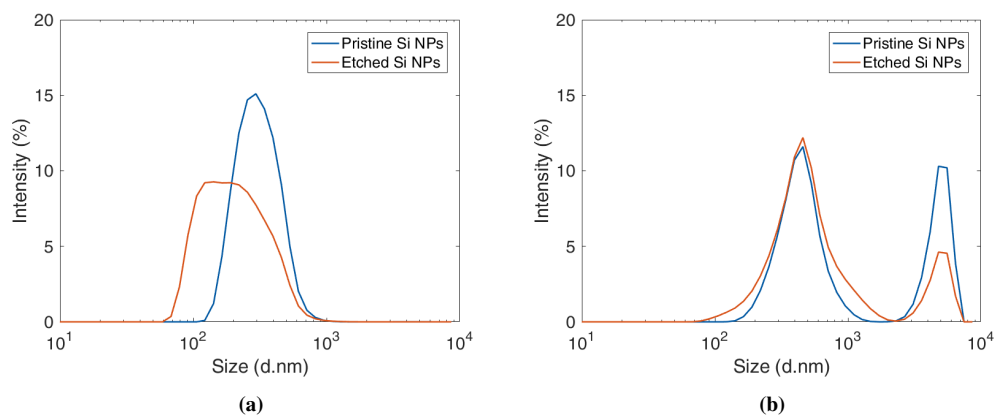


Figure B1: (a) Number and (b) volume distributions of pristine and etched Si NPs measured by DLS.

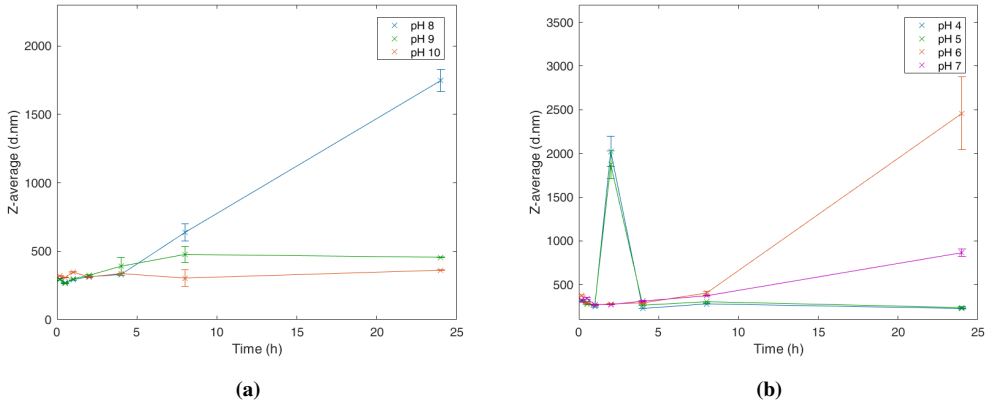


Figure B2: Z-average values of Si NPs including the "outlier" agglomerates above $1 \mu\text{m}$ hydrodynamic diameter found in (a) pristine alkaline and (b) porous acidic samples. Similar Figures without outliers are shown in Figure 5.14.

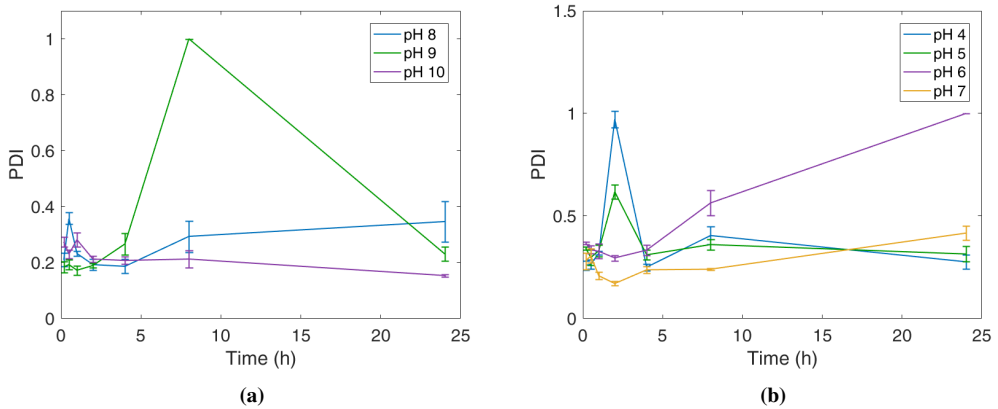


Figure B3: PDI values of Si NPs including the "outlier" agglomerates above $1 \mu\text{m}$ hydrodynamic diameter found in (a) pristine alkaline and (b) porous acidic samples. Similar Figures without outliers are shown in Figure 5.16.

C AlamarBlue assay results for ethanol washed Si NPs

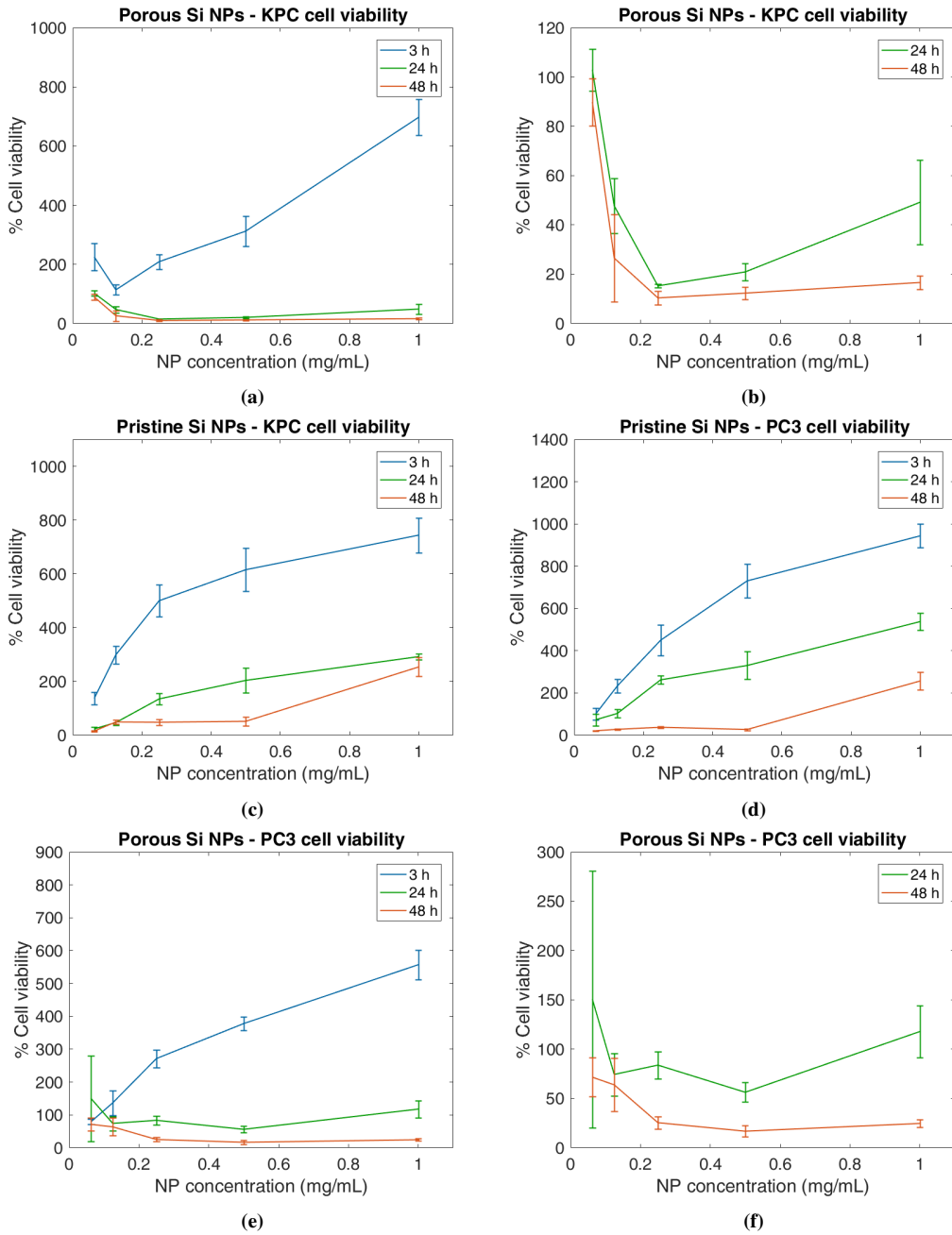


Figure C1: *In vitro* cytotoxicity studies (Alamar blue) of Si NPs sterilized by ethanol treatment. The %CV mean is plotted with standard deviations of n=8 replications.

